# The influence of the inertially dominated outer region on the rheology of a dilute dispersion of low-Reynolds-number drops or rigid particles

GANESH SUBRAMANIAN[1]†, DONALD L. KOCH[2],
JINGSHENG ZHANG[3] AND CHAO YANG[3]

[1]Engineering Mechanics Unit, Jawaharlal Nehru Centre for Advanced Scientific Research, Jakkur, Bangalore 560064, India

[2]School of Chemical and Biomolecular Engineering, Cornell University, Ithaca, NY 14853, USA

[3]Institute of Process Engineering, Chinese Academy of Sciences, Beijing 100190, China

We calculate the rheological properties of a dilute emulsion of neutrally buoyant nearly spherical drops at $O(\phi Re^{3/2})$ in a simple shear flow ($\boldsymbol{u}^\infty = \dot{\gamma} x_2 \boldsymbol{1}_1$, $\dot{\gamma}$ being the shear rate) as a function of the ratio of the dispersed- and continuous-phase viscosities ($\lambda = \hat{\mu}/\mu$). Here, $\phi$ is the volume fraction of the dispersed phase and $Re$ is the micro-scale Reynolds number. The latter parameter is a dimensionless measure of inertial effects on the scale of the dispersed-phase constituents and is defined as $Re = \dot{\gamma} a^2 \rho/\mu$, $a$ being the drop radius and $\rho$ the common density of the two phases. The analysis is restricted to the limit $\phi, Re \ll 1$, when hydrodynamic interactions between drops may be neglected, and the velocity field in a region around the drop of the order of its own size is governed by the Stokes equations at leading order. The dominant contribution to the rheology at $O(\phi Re^{3/2})$, however, arises from the so-called outer region where the leading-order Stokes approximation ceases to be valid. The relevant length scale in this outer region, the inertial screening length, results from a balance of convection and viscous diffusion, and is $O(aRe^{-1/2})$ for simple shear flow in the limit $Re \ll 1$. The neutrally buoyant drop appears as a point-force dipole on this scale. The rheological calculation at $O(\phi Re^{3/2})$ is therefore based on a solution of the linearized Navier–Stokes equations forced by a point dipole. The principal contributions to the bulk rheological properties at this order arise from inertial corrections to the drop stresslet and Reynolds stress integrals. The theoretical calculations for the stresslet components are validated via finite volume simulations of a spherical drop at finite $Re$; the latter extend up to $Re \approx 10$.

Combining the results of our $O(\phi Re^{3/2})$ analysis with the known rheology of a dilute emulsion to $O(\phi Re)$ leads to the following expressions for the relative viscosity ($\mu_e$), and the non-dimensional first ($N_1$) and second normal stress differences ($N_2$) to $O(\phi Re^{3/2})$: $\mu_e = 1 + \phi[(5\lambda + 2)/(2(\lambda+1)) + 0.024 Re^{3/2}(5\lambda+2)^2/(\lambda+1)^2]$; $N_1 = \phi[-Re4(3\lambda^2 + 3\lambda + 1)/(9(\lambda+1)^2) + 0.066 Re^{3/2}(5\lambda+2)^2/(\lambda+1)^2]$ and $N_2 = \phi[Re 2(105\lambda^2 + 96\lambda + 35)/(315(\lambda+1)^2) - 0.085 Re^{3/2}(5\lambda+2)^2/(\lambda+1)^2]$.

† Email address for correspondence: sganesh@jncasr.ac.in

Thus, for small but finite $Re$, inertia endows an emulsion with a non-Newtonian rheology even in the infinitely dilute limit, and in particular, our calculations show that, aside from normal stress differences, such an emulsion also exhibits a shear-thickening behaviour. The results for a suspension of rigid spherical particles are obtained in the limit $\lambda \to \infty$.

**Key words:** emulsions, particle/fluid flow, rheology

## 1. Introduction

In an earlier paper (see Vivek Raja, Subramanian & Koch 2010), we have analysed, to $O(\phi Re)$, the effect of inertia on the rheology of a dilute emulsion of neutrally buoyant nearly spherical drops of viscosity $\hat{\mu}$ subjected to an ambient flow that varies over length scales large compared with the size of a single drop. Here, $\phi$ is the drop volume fraction and $Re = \dot{\gamma} a^2 \rho / \mu$ is the micro-scale Reynolds number based on the drop radius $(a)$ and the shear rate $(\dot{\gamma})$ in the ambient flow; $Re$ is thus a dimensionless measure of the importance of inertial forces at the micro-scale in a suspending fluid with density $\rho$ and viscosity $\mu$. Such a calculation has already been performed for a suspension of rigid particles (for instance, see Lin, Peery & Schowalter 1970; Stone, Brady & Lovalenti 2000), and leads to normal stress differences in simple shear flow, implying that an inertial suspension is non-Newtonian even in the absence of interparticle interactions. For an emulsion, inertial effects again lead to normal stress differences at $O(\phi Re)$. A dilute emulsion, unlike a suspension, remains non-Newtonian even in the Stokesian limit on account of drop deformation due to viscous stresses (see Schowalter, Chaffey & Brenner 1968; Frankel & Acrivos 1970). However, the simulations of Li & Sarkar (2005) and the subsequent analysis of Vivek Raja *et al.* (2010) showed that even a small amount of inertia qualitatively alters emulsion rheology in simple shear by changing the signs of the normal stress differences. In the aforementioned instances, the inertial correction to the rheology arises from the $O(Re)$ modification of the flow field around an isolated drop or particle, immersed in an ambient linear flow, in a region around it of the order of its own size. Since the Stokes equations remain a valid leading-order approximation in this region, the $O(\phi Re)$ correction to the inertialess rheology may be obtained from a regular perturbation expansion about the Stokes limit.

In this paper, we consider the next inertial correction to the rheology of a dilute emulsion subjected to a simple shear flow. This contribution is $O(\phi Re^{3/2})$, and has a singular character. There have been earlier attempts to calculate the rheological properties of an inertial suspension in simple shear, to $O(\phi Re^{3/2})$, by the same sets of authors referred to above in the context of the $O(\phi Re)$ calculation. Lin *et al.* (1970) were the first to investigate the effect of micro-scale inertia on the rheology of a suspension of rigid particles in simple shear, and obtained results to $O(\phi Re^{3/2})$ via the traditionally matched asymptotic expansions approach. Later, Stone *et al.* (2000) redid the calculation using a more concise formulation in Fourier space based on the generalized reciprocal theorem, and in the process, also extended the rheological results at $O(\phi Re)$ to an arbitrary ambient linear flow. Although the two theories agreed at $O(\phi Re)$ for simple shear flow, there remained a discrepancy at $O(\phi Re^{3/2})$ that has not yet been resolved. The discrepancy is a particularly important one, since the first inertial correction to the suspension shear viscosity is $O(\phi Re^{3/2})$, the effects

of inertia at $O(\phi Re)$ being restricted to normal stress differences. The rheology of an inertial suspension has also been the subject of recent numerical calculations. Mikulencak & Morris (2004) computed the stationary flow around both fixed and torque-free spheres in a simple shear flow for a range of $Re$ (0–100) using finite element methods. For a torque-free sphere, a comparison of the inertial corrections to the computed angular velocity and the shear component of the stresslet, both of which are $O(Re^{3/2})$ in the limit of small $Re$, appeared to validate the results of Stone *et al.* (2000). A favourable comparison with the theoretical predictions was also obtained for the other stresslet components; these are $O(Re)$, however, and as already mentioned, the two theories are in agreement at this order. Kulkarni & Morris (2008) have recently used a lattice Boltzmann method to simulate a suspension undergoing simple shear flow in a wall-bounded domain at finite $Re$, thereby extending the rheology of an inertial suspension to higher volume fractions when interparticle interactions become important. The bulk rheological properties were correlated to the anisotropy of the finite-$Re$ microstructure.

Here, we show that the aforementioned theoretical calculations for the bulk stress are incomplete since they neglect the contributions of the Reynolds stresses at $O(\phi Re^{3/2})$; furthermore, the results for the $O(Re^{3/2})$ correction to the stresslet are only partially correct. The computations of Mikulencak & Morris (2004) are again restricted to obtaining the stresslet at finite $Re$ in the infinitely dilute limit and do not include the results for the Reynolds stresses. We derive the complete $O(\phi Re^{3/2})$ contributions to the viscosity and normal stress differences of a dilute emulsion of neutrally buoyant spherical drops in simple shear flow as a function of the viscosity ratio $\lambda\,(=\hat{\mu}/\mu)$; the correct results for a dilute suspension are then obtained in the limit $\lambda \to \infty$. The bulk stress in simple shear flow (a viscometric flow) of an incompressible homogeneous emulsion is completely characterized by the shear viscosity $(\mu_e)$ and the first $(N_1)$ and second normal stress differences $(N_2)$. The analysis in this paper, together with the results for the inertial corrections at $O(\phi Re)$ (see Vivek Raja *et al.* 2010), yields the following expressions for the three viscometric coefficients, correct to $O(\phi Re^{3/2})$:

$$\mu_e = 1 + \phi \left[ \frac{(5\lambda + 2)}{2(\lambda + 1)} + 0.024 Re^{3/2} \frac{(5\lambda + 2)^2}{(\lambda + 1)^2} \right] + O(\phi Re^2, \phi^2), \tag{1.1}$$

$$N_1 = \phi \left[ -Re \frac{4(3\lambda^2 + 3\lambda + 1)}{9(\lambda + 1)^2} + 0.066 Re^{3/2} \frac{(5\lambda + 2)^2}{(\lambda + 1)^2} \right] + O(\phi Re^2, \phi^2), \tag{1.2}$$

$$N_2 = \phi \left[ Re \frac{2(105\lambda^2 + 96\lambda + 35)}{315(\lambda + 1)^2} - 0.085 Re^{3/2} \frac{(5\lambda + 2)^2}{(\lambda + 1)^2} \right] + O(\phi Re^2, \phi^2), \tag{1.3}$$

where the shear viscosity and the normal stress differences have been non-dimensionalized by $\mu$ and $\mu\dot{\gamma}$, respectively. The above expressions may be combined with those that result from drop deformation due to viscous forces alone (see Schowalter *et al.* 1968), and this is done in §6 in order to compare with simulation results; note that the calculations here are restricted to the infinitely dilute limit, and the isotropic part of the dispersed-phase stress tensor is therefore not considered.

Micro-scale inertia at $O(\phi Re)$ only contributes to the normal stresses with $N_1$ being negative and $N_2$ being positive (see (1.2) and (1.3)). The $O(\phi Re^{3/2})$ analysis yields the first correction to the shear viscosity and predicts a shear-thickening rheology. Simulations (see Kulkarni & Morris 2008) showed that this prediction

is robust and the shear-thickening persists at higher $Re$ up until $\phi \approx 0.2$. At these volume fractions, there is a significant contribution due to the anisotropic pair microstructure; the results for the pair distribution function, $g(r)$, show the development of an increasingly strong anisotropy along the compressional quadrant with an increase in $Re$, consistent with a shear-thickening behaviour. At higher volume fractions, and for $Re < O(1)$, the shear-thinning rheology characteristic of a flow-aligning microstructure, arising from a balance of hydrodynamic and Brownian (or interparticle) forces in a Stokesian suspension, begins to dominate. The shear viscosity therefore exhibits a non-monotonic behaviour with increasing $Re$. It is of interest to note that while shear-thickening in the absence of inertia relies on the formation of multi-particle structures, mediated by lubrication interactions, at the highest shear rates (see Brady & Morris 1997), inertia leads to shear-thickening even in the absence of interparticle interactions. The enhancement of the microstructural anisotropy at finite $Re$ also implies that the finite $Re$ contributions to $N_1$ and $N_2$, arising from pair interactions, are both negative. Thus, the pair interaction contribution to $N_2$, in particular, has a sign opposite to the single-particle contribution (see (1.3)), implying a reversal in sign with increasing $\phi$ for a fixed $Re$; this is confirmed by simulations of Kulkarni & Morris (2008). The $O(Re^{3/2})$ analysis, in the limit $\lambda \to \infty$, leads to the following angular velocity of a torque-free rigid spherical particle: $\Omega_p = -\frac{1}{2}\mathbf{1}_z + 0.054 Re^{3/2}$; inertia causes the particle to slow down, which is again a robust prediction. Numerical computations show this to be true at higher $Re$ both in two (Kossack & Acrivos 1974) and three dimensions (Mikulencak & Morris 2004). Computations by Mikulencak & Morris indicated that the angular velocity of a sphere continues to decay roughly in proportion to $Re^{-0.1}$ for large $Re$, so that broad features of the velocity field around the particle become rather insensitive to the torque-free constraint for $Re \gg 1$. A similar effect of fluid inertia leads to a complete arrest of rotation, at a finite $Re$, for cylindrical particles with an anisotropic cross-section (see Ding & Aidun 2000).

The most relevant numerical calculation for comparison with the present analysis is that of Li & Sarkar (2005). The authors have simulated the effect of micro-scale inertia on the rheology of an infinitely dilute emulsion with unit viscosity ratio. A comparison with their results was initiated by Vivek Raja *et al.* (2010), wherein a discrepancy with the $O(\phi Re)$ theory was found even at the smallest Reynolds numbers. It was suggested therein that such a discrepancy might arise, in part, due to the neglect of higher-order inertial corrections. The inclusion of the $O(Re^{3/2})$ inertial corrections, and additional contributions that arise from drop deformation, allow a more comprehensive comparison in this paper. Since rheological information from numerical computations has been restricted to only a pair of viscosity ratios (both the stresslet and Reynolds stress contributions for a unit viscosity ratio, Li & Sarkar 2005, and only the stresslet coefficients for an infinite viscosity ratio, Mikulencak & Morris 2004), we present new results for the stresslet components at finite $Re$, over a range of viscosity ratios, obtained using a control volume formulation with the SIMPLE algorithm. The computations extend up to a Reynolds number of 10 and, together with the analytical predictions, allow the synthesis of correlations for the stresslet contributions to the three viscometric coefficients, in this range of $Re$, and for the different viscosity ratios.

The calculation of the inertial correction at $O(\phi Re^{3/2})$ is a more difficult task than that at $O(\phi Re)$, owing to the non-uniformity of the Stokes approximation for the disturbance velocity field. The Stokes description breaks down for distances larger than the inertial screening length that, for a linear flow, is $O(a Re^{-1/2})$ in the

limit $Re \ll 1$ (Lin *et al.* 1970). In the so-called outer region $(r \gtrsim aRe^{-1/2})$, inertial and viscous forces remain comparable and the disturbance fields are governed by the linearized Navier–Stokes equations instead. As argued by Stone *et al.* (2000) and Vivek Raja *et al.* (2010), the above non-uniformity affects the bulk stress calculation at $O(\phi Re^{3/2})$. The increased mathematical difficulty related to solving the linearized Navier–Stokes equations also implies that an analysis, at $O(\phi Re^{3/2})$, for an arbitrary linear flow is a formidable undertaking. The structure of the disturbance field in the outer region depends crucially on the topology of the imposed flow. In contrast, in the inertialess limit, a drop always induces a disturbance flow that is similar in structure, but opposite in sense, to the ambient rate of strain. The analysis in this paper is thus restricted to simple shear flow. A second difficulty arises because an arbitrary steady linear flow is not an exact solution of the Navier–Stokes equations. Steady linear flows that satisfy the Navier–Stokes equations are devoid of vortex stretching. Inclusion of the latter necessitates either an unsteadiness on a time scale of $O(\dot{\gamma}^{-1})$ or higher-order terms in the spatial variation (see Stone *et al.* 2000; Vivek Raja *et al.* 2010). Since the outer velocity field relaxes on a convective time scale, however, the quasi-steady approximation must break down, at $O(\phi Re^{3/2})$, for the case of an unsteady ambient flow. On the other hand, if the ambient flow must remain steady, the additional nonlinear terms (that balance the vortex stretching at leading order) become comparable with the linearly varying part in the outer region, and a consistent calculation, at $O(\phi Re^{3/2})$, must therefore account for contributions to the outer velocity field arising from such nonlinear corrections. Clearly, unlike the $O(\phi Re)$ analysis detailed in Vivek Raja *et al.* (2010), the $O(\phi Re^{3/2})$ analysis depends on details specific to a particular ambient flow, and is not readily generalizable. Furthermore, the longer length and time scales associated with the disturbance flow in the outer region imply that factors such as a drift velocity arising (due to either inertia or drop deformation) become more important; these may even lead to an inhomogeneous number density field over longer time scales, bringing into question the utility of a rheological calculation based on a homogeneous suspension. However, recent simulations (Wang *et al.* 2009) have shown that, even in unidirectional flows such as those that occur in a pipe or a channel, the balance between a transverse drift and hydrodynamic diffusion leads to a stationary inhomogeneity only on length scales much larger than the inertial screening length. Since any unidirectional flow may be locally approximated as a simple shear flow, the rheological response, to $O(Re^{3/2})$, of a homogeneous suspension subjected to a simple shear flow becomes relevant in these instances. An analysis of micro-scale inertia remains important for reasons other than its rheological relevance, however, and a discussion in this regard appears in the conclusions section.

This paper is organized as follows. In § 2, we obtain the Fourier-transformed velocity field in the outer region that is central to the bulk stress calculation. Then, in § 3, we derive an expression for the bulk stress, accurate to $O(\phi Re^{3/2})$, in a dilute emulsion subjected to simple shear flow. The two principal contributions to the bulk stress, viz. the $O(Re^{3/2})$ correction to the stresslet associated with an isolated neutrally buoyant drop in a simple shear flow, and the corrections to the Reynolds stress integrals at the same order, are obtained in §§ 4 and 5, respectively. Section 6.1 is devoted to a collation and discussion of prior numerical results, particularly those available for an infinitely dilute emulsion of unit viscosity ratio, and their comparison with the present theory. In the light of the general paucity of numerical results, particularly as a function of the viscosity ratio, in § 6.2, we present new results for the finite-$Re$ stresslet components over a wide range of viscosity ratios. The stresslet components

are obtained from a finite volume simulation of a spherical drop centred within a much larger spherical domain outside of which the ambient simple shear flow prevails. While conforming to the theoretical estimates at small $Re$, the computed values extend up to $Re \approx 10$, and thereby allow the development of empirical fits over the range of $Re$ examined. Finally, in §7, we comment on the directions in which the present analysis may be usefully extended, so one may obtain greater insight into the effects of inertia at the micro-scale, and the manner in which these couple with macro-scale flow. The results for an inertial suspension in all the above cases are obtained in a straightforward manner by taking the limit $\lambda \to \infty$.

## 2. The Fourier-transformed velocity field in the outer region

For particles or drops moving in an unbounded fluid domain, the limit of weak inertia is a singular one (for instance, see Proudman & Pearson 1957). The exterior Stokes velocity field for a neutrally buoyant drop in an ambient simple shear flow, obtained by setting $Re = \hat{Re} = 0$ (here, $\hat{Re} = \dot{\gamma} a^2 \rho / \hat{\mu}$ is the Reynolds number based on the dispersed-phase viscosity $\hat{\mu}$), is not a uniformly valid approximation at any finite $Re$ however small. The approximation breaks down for distances from the drop larger than an inertial screening length that, for a simple shear flow, scales as $O(aRe^{-1/2})$. The leading-order velocity field in this outer region satisfies the linearized Navier–Stokes equations instead, the convection by the simple shear being included in a linearized form. It is shown in the next section that the above non-uniformity affects the bulk stress at $O(\phi Re^{3/2})$. Since the drop appears only as a point-force dipole on length scales of the order of the inertial screening length, the stress calculation may be carried out in Fourier space. In what follows, we obtain an expression for the Fourier-transformed outer velocity field.

We scale distances by $a$, velocities by $\dot{\gamma} a$ and stresses by $\mu \dot{\gamma}$, while continuing to use the same notation for the resulting dimensionless variables. Thus, in the outer region, $r \sim O(Re^{-1/2})$, and the relevant scales for the velocity and pressure fields may be derived as follows. Since the Stokes velocity disturbance generated by a force-free torque-free drop is $O(1/r^2)$ for $r \gg 1$, it is only $O(Re)$ for $r \sim O(Re^{-1/2})$. Comparing the viscous and pressure terms, the corresponding disturbance pressure field must be $O(\nabla u) \sim O(Re^{3/2})$. Defining the re-scaled variables in the outer region as $\boldsymbol{r} = Re^{-1/2} \boldsymbol{\rho}$, $\boldsymbol{u}' = Re\, \boldsymbol{u}_o$ and $p' = Re^{3/2} p_o$, one obtains the linearized Navier–Stokes equations and the equation of continuity in the following dimensionless form:

$$\boldsymbol{\Gamma} \cdot \boldsymbol{u}_o + (\boldsymbol{\Gamma} \cdot \boldsymbol{\rho}) \cdot \nabla_{\boldsymbol{\rho}} \boldsymbol{u}_o = -\nabla_{\boldsymbol{\rho}} p_o + \nabla_{\boldsymbol{\rho}}^2 \boldsymbol{u}_o - \frac{4\pi(5\lambda + 2)}{3(\lambda + 1)} \boldsymbol{E} \cdot \nabla \delta(\boldsymbol{\rho}), \qquad (2.1)$$

$$\nabla_{\boldsymbol{\rho}} \cdot \boldsymbol{u}_o = 0, \qquad (2.2)$$

where $\boldsymbol{\Gamma} = \boldsymbol{1}_1 \boldsymbol{1}_2$ is the transpose of the velocity gradient tensor in simple shear flow, and $\boldsymbol{E} = \frac{1}{2}(\boldsymbol{\Gamma} + \boldsymbol{\Gamma}^\dagger)$ is the rate-of-strain tensor, $\lambda$ being the viscosity ratio; here, 1, 2 and 3 correspond, respectively, to the flow, gradient and vorticity directions of the ambient simple shear. We have followed Saffman (1965) in replacing the matching condition (to the inner expansion) by a point-dipole forcing at the origin in (2.1), the constant of proportionality being the familiar stresslet coefficient that characterizes the response of a neutrally buoyant drop in a linear flow in the absence of inertia (see Kim & Karrila 1991; Leal 1992).

The finite size of the drop now being irrelevant, the analysis for the outer velocity field may be conveniently carried out in Fourier space. Using (2.1) and (2.2), we write down the Fourier-transformed equations of continuity and motion. Defining the

Fourier transform as $\hat{f}(k) = \int e^{-ik\cdot\rho} f(\rho)\,d\rho$, one obtains

$$\boldsymbol{\Gamma}\cdot\hat{\boldsymbol{u}}_o - (\boldsymbol{\Gamma}^\dagger\cdot\boldsymbol{k})\cdot\nabla_k\hat{\boldsymbol{u}}_o = i\,k\,\hat{p}_o - k^2\hat{\boldsymbol{u}}_o - \frac{4\pi i(5\lambda+2)}{3(\lambda+1)}\boldsymbol{E}\cdot\boldsymbol{k},\tag{2.3}$$

$$\boldsymbol{k}\cdot\hat{\boldsymbol{u}}_o = 0.\tag{2.4}$$

In the limit $k \gg 1$, convection by the shear flow becomes unimportant at leading order, and the solution of (2.3) and (2.4) reduces to the inertialess disturbance field induced by a point dipole, satisfying

$$i\,k\,\hat{p}^d - k^2\hat{\boldsymbol{u}}^d = \frac{4\pi i(5\lambda+2)}{3(\lambda+1)}\boldsymbol{E}\cdot\boldsymbol{k},\tag{2.5}$$

$$\boldsymbol{k}\cdot\hat{\boldsymbol{u}}^d = 0,\tag{2.6}$$

in Fourier space. Since we are interested in the inertial corrections to the bulk stress in a dilute emulsion, and not the Stokes contribution that leads to the Taylor viscosity (see Schowalter *et al.* 1968; Frankel & Acrivos 1970), it is convenient to remove the singular stresslet contribution from the outer velocity field. In a manner similar to Stone *et al.* (2000), we therefore define $\boldsymbol{u}^*(\rho) = \boldsymbol{u}_o(\rho) - \boldsymbol{u}^d(\rho)$, $p^*(\rho) = p_o(\rho) - p^d(\rho)$, and the equations satisfied by the Fourier-transformed variables, $\hat{\boldsymbol{u}}^*(k)$ and $\hat{p}^*(k)$, may then be obtained from the difference of the equations governing $[\hat{\boldsymbol{u}}_o(k), \hat{p}_o(k)]$ and $[\hat{\boldsymbol{u}}^d(k), \hat{p}^d(k)]$ above. Thus,

$$\boldsymbol{\Gamma}\cdot\hat{\boldsymbol{u}}^* - (\boldsymbol{\Gamma}^\dagger\cdot\boldsymbol{k})\cdot\nabla_k\hat{\boldsymbol{u}}^* = i\,k\,\hat{p}^* - k^2\hat{\boldsymbol{u}}^* - \boldsymbol{\Gamma}\cdot\hat{\boldsymbol{u}}^d + (\boldsymbol{\Gamma}^\dagger\cdot\boldsymbol{k})\cdot\nabla_k\hat{\boldsymbol{u}}^d,\tag{2.7}$$

$$\boldsymbol{k}\cdot\hat{\boldsymbol{u}}^* = 0.\tag{2.8}$$

Furthermore, using the projection operator $(\boldsymbol{I} - \hat{\boldsymbol{k}}\hat{\boldsymbol{k}})$ together with (2.8) to eliminate the pressure from (2.7), one obtains

$$\boldsymbol{\Gamma}\cdot\hat{\boldsymbol{u}}^*\cdot(\boldsymbol{I}-2\hat{\boldsymbol{k}}\hat{\boldsymbol{k}}) - (\boldsymbol{\Gamma}^\dagger\cdot\boldsymbol{k})\cdot\nabla_k\hat{\boldsymbol{u}}^* + k^2\hat{\boldsymbol{u}}^* = -\boldsymbol{\Gamma}\cdot\hat{\boldsymbol{u}}^d\cdot(\boldsymbol{I}-2\hat{\boldsymbol{k}}\hat{\boldsymbol{k}}) + (\boldsymbol{\Gamma}^\dagger\cdot\boldsymbol{k})\cdot\nabla_k\hat{\boldsymbol{u}}^d,\tag{2.9}$$

where $\hat{\boldsymbol{k}} = \boldsymbol{k}/k$ is the unit vector in Fourier space. The terms involving $\hat{\boldsymbol{u}}^d(k)$, rather than the original singular forcing, now act as forcing terms in (2.9). Using the Fourier-transformed stresslet velocity field,

$$\hat{\boldsymbol{u}}^d(k) = -\frac{4\pi i(5\lambda+2)}{3(\lambda+1)}\left(\frac{\boldsymbol{E}\cdot\boldsymbol{k}}{k^2} - \frac{(\boldsymbol{E}:\boldsymbol{k}\boldsymbol{k})\boldsymbol{k}}{k^4}\right),\tag{2.10}$$

(2.9) takes the form

$$\boldsymbol{\Gamma}\cdot\hat{\boldsymbol{u}}^*\cdot(\boldsymbol{I}-2\hat{\boldsymbol{k}}\hat{\boldsymbol{k}}) - (\boldsymbol{\Gamma}^\dagger\cdot\boldsymbol{k})\cdot\nabla_k\hat{\boldsymbol{u}}^* + k^2\hat{\boldsymbol{u}}^* = \frac{4\pi i(5\lambda+2)}{3(\lambda+1)k}[\boldsymbol{\Gamma}\cdot(\boldsymbol{E}\cdot\hat{\boldsymbol{k}} - (\boldsymbol{E}:\hat{\boldsymbol{k}}\hat{\boldsymbol{k}})\hat{\boldsymbol{k}})$$
$$+ (\boldsymbol{\Gamma}^\dagger\cdot\hat{\boldsymbol{k}})\cdot(\boldsymbol{E}-2\hat{\boldsymbol{k}}(\boldsymbol{E}\cdot\hat{\boldsymbol{k}}) + (\boldsymbol{E}\cdot\hat{\boldsymbol{k}})\hat{\boldsymbol{k}} - (\boldsymbol{I}-4\hat{\boldsymbol{k}}\hat{\boldsymbol{k}})(\boldsymbol{E}:\hat{\boldsymbol{k}}\hat{\boldsymbol{k}}))],\tag{2.11}$$

for a general linear flow. Finally, using the expressions for $\boldsymbol{\Gamma}$ and $\boldsymbol{E}$ for simple shear flow, one obtains

$$k_1\frac{\partial\hat{\boldsymbol{u}}^*}{\partial k_2} + \frac{2k_1}{k^2}k\hat{u}_2^* - \hat{u}_2^*\boldsymbol{1}_1 - k^2\boldsymbol{u}^* = \frac{8\pi i(5\lambda+2)}{3(\lambda+1)}\left(-\frac{k_1^2k_2^2}{k^6}\boldsymbol{k} + \frac{k_1^2k_2}{k^4}\boldsymbol{1}_2\right).\tag{2.12}$$

The individual components along the flow, gradient and vorticity directions are given by

$$k_1 \frac{\partial \hat{u}_1^*}{\partial k_2} - k^2 \hat{u}_1^* = -\left(\frac{2k_1^2}{k^2} - 1\right)\hat{u}_2^* - \frac{8\pi i(5\lambda + 2)}{3(\lambda + 1)} \frac{k_1^3 k_2^2}{k^6}, \tag{2.13}$$

$$k_2 \frac{\partial \hat{u}_2^*}{\partial k_2} + \left(\frac{2k_1 k_2}{k^2} - k^2\right)\hat{u}_2^* = \frac{8\pi i(5\lambda + 2)}{3(\lambda + 1)} \frac{k_1^2 k_2(k_1^2 + k_3^2)}{k^6}, \tag{2.14}$$

$$k_1 \frac{\partial \hat{u}_3^*}{\partial k_2} - k^2 \hat{u}_3^* = -\frac{2k_1 k_3}{k^2}\hat{u}_2^* - \frac{8\pi i(5\lambda + 2)}{3(\lambda + 1)} \frac{k_1^2 k_2^2 k_3}{k^6}. \tag{2.15}$$

The equation governing the gradient component, $\hat{u}_2^*$, is decoupled from the others, and may therefore be solved first. Expressions for $\hat{u}_1^*$ and $\hat{u}_3^*$ may then be obtained in terms of $\hat{u}_2^*$. In (2.13)–(2.15), one may identify a 'simple shear flow' in Fourier space too, given by $\hat{\boldsymbol{u}}^{*\infty}(\boldsymbol{k}) = k_1 \boldsymbol{1}_2$. This simple shear flow is orthogonal to the one in physical space ($\boldsymbol{u}^\infty = x_2 \boldsymbol{1}_1$), and the orthogonality arises because the wave vector is oriented normal to the wave fronts, the latter being rotated by the shear flow in physical space. The Fourier-transformed velocity components are convected by this flow, and the characteristics of the above system of first-order differential equations correspond to the streamlines in Fourier space. A characteristic or a streamline is defined by $k_2' = k_2 + k_1 s$, where $s$ is a time-like variable; thus, $k_2$ is the initial position on the streamline, and $(k_2' - k_2)$ is the distance travelled along the streamline in a time $s$ moving with velocity $k_1$. The solutions for the individual components, $\hat{u}_2^*$, $\hat{u}_1^*$ and $\hat{u}_3^*$, may now be written down in terms of $s$ as follows:

$$\hat{u}_2^*(\boldsymbol{k}) = -\frac{8\pi i(5\lambda + 2)}{3(\lambda + 1)k^2} \int_0^\infty ds \frac{k_1^2 (k_1^2 + k_3^2)(k_2 + sk_1) e^{-(k^2 s + k_1 k_2 s^2 + \frac{1}{3}k_1^2 s^3)}}{(k^2 + 2k_1 k_2 s + k_1^2 s^2)^2}, \tag{2.16}$$

$$\hat{u}_1^*(\boldsymbol{k}) = \frac{8\pi i(5\lambda + 2)}{3(\lambda + 1)} \int_0^\infty ds \frac{k_1^3 (k_2 + sk_1)^2 e^{-(k^2 s + k_1 k_2 s^2 + \frac{1}{3}k_1^2 s^3)}}{(k^2 + 2k_1 k_2 s + k_1^2 s^2)^3}$$
$$- \int_0^\infty ds \frac{(k^2 + 2k_1 k_2 s + k_1^2 s^2 - 2k_1^2) e^{-(k^2 s + k_1 k_2 s^2 + \frac{1}{3}k_1^2 s^3)}}{(k^2 + 2k_1 k_2 s + k_1^2 s^2)} \hat{u}_2^*(k_1, k_2 + sk_1, k_3), \tag{2.17}$$

$$\hat{u}_3^*(\boldsymbol{k}) = \frac{8\pi i(5\lambda + 2)}{3(\lambda + 1)} \int_0^\infty ds \frac{k_1^2 k_3 (k_2 + sk_1)^2 e^{-(k^2 s + k_1 k_2 s^2 + \frac{1}{3}k_1^2 s^3)}}{(k^2 + 2k_1 k_2 s + k_1^2 s^2)^3}$$
$$+ \int_0^\infty ds \frac{2k_1 k_3 e^{-(k^2 s + k_1 k_2 s^2 + \frac{1}{3}k_1^2 s^3)}}{(k^2 + 2k_1 k_2 s + k_1^2 s^2)} \hat{u}_2^*(k_1, k_2 + sk_1, k_3). \tag{2.18}$$

Here, the $s$ dependence of $\hat{u}_2^*$ inside the integrals in (2.17) and (2.18) has been made explicit by way of its arguments. The limiting form of the inverse Fourier transforms of (2.16)–(2.18), in the matching region ($1 \ll r \ll Re^{-1/2}$), will be used in §4 to determine the stresslet to $O(Re^{3/2})$. The full expressions enter the Reynolds stress calculation in §5.

## 3. The bulk stress in a dilute emulsion subjected to a simple shear flow

The expression for the non-dimensional bulk stress in an emulsion of neutrally buoyant drops subjected to an ambient linear flow, $\boldsymbol{u}^\infty = \boldsymbol{\Gamma} \cdot \boldsymbol{r}$, is given by

$$\Sigma_{ij} = -p_t \delta_{ij} + 2E_{ij} + \Sigma_{ij}^{(d)}, \tag{3.1}$$

where $p_t$ is an arbitrary isotropic pressure, the second term is the deviatoric stress in the Newtonian suspending fluid, and $\Sigma_{ij}^{(d)}$ is the excess stress due to the dispersed phase. In Vivek Raja *et al.* (2010), it has been shown that the excess stress in a dilute non-interacting emulsion with volume fraction $\phi$ may be written in the following form involving integrals of dynamical quantities related to an isolated drop in simple shear flow:

$$
\Sigma_{ij}^{(d)} = \frac{3\phi}{4\pi} \int_{A_d^+} \left[ \frac{1}{2}(\sigma_{ik}r_j + \sigma_{jk}r_i)n_k - (u_i n_j + u_j n_i) \right] \mathrm{d}A + \frac{3\phi}{4\pi} Re \left( \frac{4\pi}{15} \Gamma_{ik}\Gamma_{jk} \right.
$$
$$
\left. + \int_{V_d} \Gamma_{ik}r_k u_j' \, \mathrm{d}r + \int_{V_d} \Gamma_{jk}r_k u_i' \, \mathrm{d}r - \int_{V-V_d} u_i' u_j' \, \mathrm{d}r \right). \quad (3.2)
$$

Here, $A_d^+$ denotes the external surface of an isolated drop, $V_d$ denotes the volume of the drop and $(V - V_d)$ denotes the exterior (infinite) fluid domain. Only the first term in (3.2), the stresslet integral $(S_{ij})$ survives in the inertialess limit, leading to the familiar Taylor viscosity (Taylor 1932). The remaining terms arise only for non-zero $Re$, and may therefore be termed the direct inertial contributions. Vivek Raja *et al.* (2010) derived the $O(Re)$ correction to the leading-order Stokes velocity field in the inner region using a regular perturbation expansion, and thereby, the correction to the stresslet at the same order. Writing the stresslet as $S_{ij} = S_{ij}^{(0)} + Re \, S_{ij}^{(1)} + \tilde{S}_{ij}^{(2)}$, and using their results, we have

$$
S_{ij}^{(0)} = \frac{(5\lambda + 2)}{(\lambda + 1)} E_{ij}, \quad (3.3)
$$
$$
S_{ij}^{(1)} = \left( \frac{4(3\lambda^2 + 3\lambda + 1)}{9(\lambda + 1)^2} (\Omega_{ik}E_{kj} - E_{ik}\Omega_{kj}) + \frac{(43\lambda^2 + 36\lambda + 8)}{35(\lambda + 1)^2} E_{ik}E_{kj} \right), \quad (3.4)
$$

with $\tilde{S}_{ij}^{(2)}$ denoting the higher-order contributions (that is, smaller than $O(Re)$). Using (3.3) and (3.4), (3.2) takes the form

$$
\Sigma_{ij}^{(d)} = \frac{(5\lambda + 2)}{(\lambda + 1)} E_{ij} - Re \left( \frac{4(3\lambda^2 + 3\lambda + 1)}{9(\lambda + 1)^2} (\Omega_{ik}E_{kj} - E_{ik}\Omega_{kj}) \right.
$$
$$
\left. + \frac{(43\lambda^2 + 36\lambda + 8)}{35(\lambda + 1)^2} E_{ik}E_{kj} \right) + \tilde{S}_{ij}^{(2)} + \frac{3\phi}{4\pi} Re \left( \frac{4\pi}{15} \Gamma_{ik}\Gamma_{jk} + \int_{V_d} \Gamma_{ik}r_k u_j' \, \mathrm{d}r \right.
$$
$$
\left. + \int_{V_d} \Gamma_{jk}r_k u_i' \, \mathrm{d}r - \int_{V-V_d} u_i' u_j' \, \mathrm{d}r \right). \quad (3.5)
$$

The Reynolds stress integrals and $\hat{S}^{(2)}$ in (3.5) remain to be evaluated. At leading order, the Reynolds stresses may be evaluated using the well-known expression for the Stokes disturbance velocity field, $u'^{(0)}(r)u^{(0)} - \Gamma \cdot r$, with $u^{(0)}$ given by (Leal 1992)

$$
u^{(0)}(r) = \Gamma \cdot r - \frac{\lambda}{(\lambda + 1)r^5} E \cdot r - \left( \frac{(5\lambda + 2)}{2(\lambda + 1)r^5} - \frac{5\lambda}{2(\lambda + 1)r^7} \right) r(E:rr). \quad (3.6)
$$

This leads to contributions to the bulk stress at $O(\phi Re)$. Writing the disturbance velocity field as $u' = u'^{(0)} + Re \, u^{(1)}$ in order to formally separate stress contributions arising from the Stokes and inertial parts of the velocity field, the expression for the

dispersed-phase stress becomes

$$
\Sigma_{ij}^{(d)} = \phi \left[ \frac{(5\lambda + 2)}{(\lambda + 1)} E_{ij} - Re \left( \frac{4(3\lambda^2 + 3\lambda + 1)}{9(\lambda + 1)^2} (\Omega_{ik} E_{kj} - E_{ik} \Omega_{kj}) \right. \right.
$$
$$
+ \frac{(43\lambda^2 + 36\lambda + 8)}{35(\lambda + 1)^2} E_{ik} E_{kj} \right) + \frac{3}{4\pi} Re \left( \frac{4\pi}{15} \Gamma_{ik} \Gamma_{jk} + \int_{V_d} \Gamma_{ik} r_k u_j'^{(0)} \, d\boldsymbol{r} \right.
$$
$$
+ \int_{V_d} \Gamma_{jk} r_k u_i'^{(0)} \, d\boldsymbol{r} - \int_{V-V_d} u_i'^{(0)} u_j'^{(0)} \, d\boldsymbol{r} \right) + \tilde{S}_{ij}^{(2)}
$$
$$
+ \frac{3}{4\pi} Re^2 \left( \int_{V_d} \Gamma_{ik} r_k u_j^{(1)} \, d\boldsymbol{r} + \int_{V_d} \Gamma_{jk} r_k u_i^{(1)} \, d\boldsymbol{r} \right)
$$
$$
- \frac{3}{4\pi} Re^2 \left( \int_{V-V_d} u_i'^{(0)} u_j^{(1)} \, d\boldsymbol{r} + \int_{V-V_d} u_i^{(1)} u_j'^{(0)} \, d\boldsymbol{r} \right) - \frac{3}{4\pi} Re^3 \int_{V-V_d} u_i^{(1)} u_j^{(1)} \, d\boldsymbol{r} \right].
$$
$$
\tag{3.7}
$$

The direct inertial contributions have again been evaluated to $O(\phi Re)$ by Vivek Raja *et al.* (2010) and are given by

$$
\frac{3}{4\pi} \left( \frac{4\pi}{15} \Gamma_{ik} \Gamma_{jk} + \int_{V_d} \Gamma_{ik} r_k u_j'^{(0)} \, d\boldsymbol{r} + \int_{V_d} \Gamma_{jk} r_k u_i'^{(0)} \, d\boldsymbol{r} - \int_{V-V_d} u_i'^{(0)} u_j'^{(0)} \, d\boldsymbol{r} \right)
$$
$$
= \left[ \frac{1}{5} \Gamma_{ik} \Gamma_{jk} - \frac{1}{5} (E_{jk} \Gamma_{ik} + E_{ik} \Gamma_{jk}) - \left( \frac{2(5\lambda + 2)^2}{35(\lambda + 1)^2} - \frac{2\lambda(5\lambda + 2)}{35(\lambda + 1)^2} + \frac{3\lambda^2}{35(\lambda + 1)^2} \right) \right.
$$
$$
\times E_{ik} E_{kj} \Big].
$$
$$
\tag{3.8}
$$

Combining (3.8) with (3.7), the dispersed-phase stress takes the form

$$
\Sigma_{ij}^{(d)} = \phi \left[ \frac{(5\lambda + 2)}{(\lambda + 1)} E_{ij} - Re \left( \frac{4(3\lambda^2 + 3\lambda + 1)}{9(\lambda + 1)^2} (\Omega_{ik} E_{kj} - E_{ik} \Omega_{kj}) - \frac{8\lambda}{35(\lambda + 1)^2} E_{ik} E_{kj} \right) \right.
$$
$$
+ \tilde{S}_{ij}^{(2)} + \frac{3}{4\pi} Re^2 \left( \int_{V_d} \Gamma_{ik} r_k u_j^{(1)} \, d\boldsymbol{r} + \int_{V_d} \Gamma_{jk} r_k u_i^{(1)} \, d\boldsymbol{r} \right)
$$
$$
- \frac{3}{4\pi} Re^2 \left( \int_{V-V_d} u_i'^{(0)} u_j^{(1)} \, d\boldsymbol{r} + \int_{V-V_d} u_i^{(1)} u_j'^{(0)} \, d\boldsymbol{r} \right) - \frac{3}{4\pi} Re^3 \int_{V-V_d} u_i^{(1)} u_j^{(1)} \, d\boldsymbol{r} \right].
$$
$$
\tag{3.9}
$$

The validity of a regular perturbation expansion, to $O(Re)$, in a region around the drop of the order of its own size, implies that the correction to the integrals over the drop volume in (3.9) is $O(Re^2)$. The correction to the leading-order estimate for the integral over the unbounded fluid domain is, however, larger than the formal scalings indicated; it is $O(Re^{3/2})$, this being related to the breakdown of the regular perturbation at distances of $O(Re^{-1/2})$. To see this, we note that in a regular perturbation approach, $\boldsymbol{u}^{(1)}$, at $O(Re)$, satisfies the inhomogeneous Stokes equations, $-\nabla p^{(1)} + \nabla^2 \boldsymbol{u}^{(1)} = \boldsymbol{u}^{(0)} \cdot \nabla \boldsymbol{u}^{(0)}$. For $r \gg 1$, $\nabla^2 \boldsymbol{u}^{(1)} \approx (\boldsymbol{\Gamma} \cdot \boldsymbol{r}) \cdot \nabla \boldsymbol{u}'^{(0)}$, with $\boldsymbol{u}'^{(0)} \sim O(1/r^2)$. Thus, $\boldsymbol{u}^{(1)} \sim O(1)$ for $r \gg 1$, the failure to satisfy the far-field decay condition again being a signature of the aforementioned non-uniformity. With $\boldsymbol{u}'^{(0)} \sim O(1/r^2)$ and $\boldsymbol{u}^{(1)} \sim O(1)$, $\int \boldsymbol{u}'^{(0)} \boldsymbol{u}^{(1)} \, dV \sim O(R)$ and $\int \boldsymbol{u}^{(1)} \boldsymbol{u}^{(1)} \, dV \sim O(R^3)$, when integrated over a domain of size $R$. The divergence with domain size is cutoff on using the correct outer solution obtained from the linearized Navier–Stokes equations. Since this cutoff occurs at the inertial screening length ($R \sim O(Re^{-1/2})$), $\int \boldsymbol{u}'^{(0)} \boldsymbol{u}^{(1)} \, dV \sim O(Re^{-1/2})$ and $\int \boldsymbol{u}^{(1)} \boldsymbol{u}^{(1)} \, dV \sim O(Re^{-3/2})$, respectively. As a result, all Reynolds stress integrals over

the exterior fluid domain in (3.9) contribute at $O(\phi Re^{3/2})$. This Reynolds stress contribution has been overlooked in the two earlier calculations referred to in the Introduction, viz. Lin *et al.* (1970) and Stone *et al.* (2000).

Since the dominant contributions to the Reynolds stress integrals arise in the outer region, it is natural to use the outer variable $\boldsymbol{\rho} = Re^{1/2}\boldsymbol{r}$. Writing the disturbance velocity field as $\boldsymbol{u}'(\boldsymbol{r}) = \boldsymbol{u}'^{(0)}(\boldsymbol{r}) + Re\,\boldsymbol{u}^*(\boldsymbol{\rho})$ (the components of $\boldsymbol{u}^*(\boldsymbol{\rho})$ are given in §4; see (4.1)–(4.3); only the Fourier-transformed velocity components, $\hat{u}_i^*(\boldsymbol{k})$, are needed in the Reynolds stress evaluation), the dispersed-phase stress takes the form

$$
\Sigma_{ij}^{(d)} = \phi \left[ \frac{(5\lambda+2)}{(\lambda+1)} E_{ij} - Re \left( \frac{4(3\lambda^2+3\lambda+1)}{9(\lambda+1)^2}(\Omega_{ik}E_{kj} - E_{ik}\Omega_{kj}) - \frac{8\lambda}{35(\lambda+1)^2} E_{ik}E_{kj} \right) \right.
$$
$$
\times \tilde{S}_{ij}^{(2)} - \frac{3}{4\pi} Re^{1/2} \left( \int_{V-V_d} u_i'^{(0)}(\boldsymbol{r})u_j^*(\boldsymbol{\rho})\,\mathrm{d}\boldsymbol{\rho} + \int_{V-V_d} u_i^*(\boldsymbol{\rho})u_j'^{(0)}(\boldsymbol{r})\,\mathrm{d}\boldsymbol{\rho} \right)
$$
$$
\left. - \frac{3}{4\pi} Re^{3/2} \int_{V-V_d} u_i^*(\boldsymbol{\rho})u_j^*(\boldsymbol{\rho})\,\mathrm{d}\boldsymbol{\rho} \right] + O(\phi Re^2). \tag{3.10}
$$

Furthermore, we note that $\boldsymbol{u}'^{(0)}(\boldsymbol{r}) \sim Re\,\boldsymbol{u}^d(\boldsymbol{\rho}) + o(Re)$ in the outer region, $\boldsymbol{u}^d(\boldsymbol{\rho})$ being the singular dipole velocity field expressed in outer variables; and that the volume of the drop $V_d$ is only $O(Re^{3/2})$ in units of the inertial screening length, and may therefore be neglected. Thus, the integrals over $(V - V_d)$ may be extended to include the volume inside the drop with an error of $o(Re^{3/2})$, and one obtains

$$
\Sigma_{ij}^{(d)} = \phi \left[ \frac{(5\lambda+2)}{(\lambda+1)} E_{ij} - Re \left( \frac{4(3\lambda^2+3\lambda+1)}{9(\lambda+1)^2}(\Omega_{ik}E_{kj} - E_{ik}\Omega_{kj}) - \frac{8\lambda}{35(\lambda+1)^2} E_{ik}E_{kj} \right) \right.
$$
$$
\left. + \tilde{S}_{ij}^{(2)} - \frac{3}{4\pi} Re^{3/2} \left( \int \{u_i^d(\boldsymbol{\rho})u_j^*(\boldsymbol{\rho}) + u_i^*(\boldsymbol{\rho})u_j^d(\boldsymbol{\rho}) + u_i^*(\boldsymbol{\rho})u_j^*(\boldsymbol{\rho})\}\,\mathrm{d}\boldsymbol{\rho} \right) \right] + O(\phi Re^2). \tag{3.11}
$$

With the finite size of the drop neglected, the analysis may be done in Fourier space. Using the convolution theorem to transform the Reynolds stress integrals, (3.11) takes the form

$$
\Sigma_{ij}^{(d)} = \phi \left[ \frac{(5\lambda+2)}{(\lambda+1)} E_{ij} - Re \left( \frac{4(3\lambda^2+3\lambda+1)}{9(\lambda+1)^2}(\Omega_{ik}E_{kj} - E_{ik}\Omega_{kj}) - \frac{8\lambda}{35(\lambda+1)^2} E_{ik}E_{kj} \right) \right.
$$
$$
\left. + \tilde{S}_{ij}^{(2)} - \frac{3Re^{3/2}}{32\pi^4} \int \{\hat{u}_i^d(-\boldsymbol{k})\hat{u}_j^*(\boldsymbol{k}) + \hat{u}_i^*(\boldsymbol{k})\hat{u}_j^d(-\boldsymbol{k}) + \hat{u}_i^*(-\boldsymbol{k})\hat{u}_j^*(\boldsymbol{k})\}\,\mathrm{d}\boldsymbol{k} \right] + O(\phi Re^2), \tag{3.12}
$$

with

$$
\hat{\boldsymbol{u}}^d(\boldsymbol{k}) = -\frac{4\pi\mathrm{i}(5\lambda+2)}{3(\lambda+1)} \left( \frac{\boldsymbol{E} \cdot \boldsymbol{k}}{k^2} - \frac{(\boldsymbol{E} : \boldsymbol{kk})\boldsymbol{k}}{k^4} \right) \tag{3.13}
$$

and the components of $\hat{\boldsymbol{u}}^*(\boldsymbol{k})$ being given by (2.16)–(2.18). Since both $\boldsymbol{u}(\boldsymbol{r})$ and $\boldsymbol{u}^d(\boldsymbol{r})$ are odd functions of $\boldsymbol{r}$ in simple shear flow, their transforms are odd functions of $\boldsymbol{k}$,

and (3.12) may be written as

$$\Sigma_{ij}^{(d)} = \phi \left[ \frac{(5\lambda+2)}{(\lambda+1)} E_{ij} - Re\left( \frac{4(3\lambda^2+3\lambda+1)}{9(\lambda+1)^2}(\Omega_{ik}E_{kj} - E_{ik}\Omega_{kj}) - \frac{8\lambda}{35(\lambda+1)^2}E_{ik}E_{kj} \right) \right.$$
$$\left. + \tilde{S}_{ij}^{(2)} + \frac{3Re^{3/2}}{32\pi^4}\left( \int \{\hat{u}_i^d(\boldsymbol{k})\hat{u}_j^*(\boldsymbol{k}) + \hat{u}_i^*(\boldsymbol{k})\hat{u}_j^d(\boldsymbol{k}) + \hat{u}_i^*(\boldsymbol{k})\hat{u}_j^*(\boldsymbol{k})\} \, \mathrm{d}\boldsymbol{k} \right) \right] + O(\phi Re^2).$$

$$(3.14)$$

The stresslet coefficient, $\tilde{\boldsymbol{S}}^{(2)}$, is also $O(Re^{3/2})$, and to see this, we note that, for distances much smaller than an inertial screening length ($\rho \ll 1$), the outer velocity field, corresponding to a point-dipole forcing in simple shear flow, may be written in the following general form:

$$\lim_{\rho \to 0} \boldsymbol{u}_o(\boldsymbol{\rho}) = Re\left[ \boldsymbol{u}^d(\boldsymbol{\rho}) + \sum_{i=0}^{\infty} \boldsymbol{G}^{(i)}(\boldsymbol{\rho}) \right], \qquad (3.15)$$

where $\boldsymbol{G}^{(i)}(\boldsymbol{\rho})$ denotes a homogeneous vector function of degree $i$. Expressed in inner variables using $\boldsymbol{\rho} = Re^{1/2}\boldsymbol{r}$, $\boldsymbol{G}^{(0)}(\boldsymbol{\rho})$ remains unchanged, while succeeding terms are smaller by $O(Re^{1/2})$. Thus, $Re\,\boldsymbol{G}^{(0)}(\boldsymbol{r})$ must match up to the $O(Re)$ correction to the Stokes velocity field, while the term $Re^{3/2}\boldsymbol{G}^{(1)}(\boldsymbol{r})$ determines the next correction in the inner region, and hence, $\tilde{\boldsymbol{S}}^{(2)}$. One may therefore write $\tilde{\boldsymbol{S}}^{(2)} = Re^{3/2}\boldsymbol{S}^{(2)}$, and the resulting dispersed-phase stress is given by

$$\Sigma_{ij}^{(d)} = \phi \left[ \frac{(5\lambda+2)}{(\lambda+1)} E_{ij} - Re\left( \frac{4(3\lambda^2+3\lambda+1)}{9(\lambda+1)^2}(\Omega_{ik}E_{kj} - E_{ik}\Omega_{kj}) - \frac{8\lambda}{35(\lambda+1)^2}E_{ik}E_{kj} \right) \right.$$
$$\left. + Re^{3/2}\left\{ S_{ij}^{(2)} + \frac{3}{32\pi^4}\left( \int \{\hat{u}_i^d(\boldsymbol{k})\hat{u}_j^*(\boldsymbol{k}) + \hat{u}_i^*(\boldsymbol{k})\hat{u}_j^d(\boldsymbol{k}) + \hat{u}_i^*(\boldsymbol{k})\hat{u}_j^*(\boldsymbol{k})\} \, \mathrm{d}\boldsymbol{k} \right) \right\} \right]$$
$$+ O(\phi Re^2). \qquad (3.16)$$

The $O(\phi Re^2)$ correction now includes both the corrections to the stresslet integral and the Reynolds stresses. The $O(Re^{3/2})$ stresslet coefficient, $S^{(2)}$, is calculated in the next section, while the Reynolds stress integrals are evaluated in §5. We also note in passing that the Fourier integrals to be evaluated in the succeeding sections, in order to characterize the $O(Re^{3/2})$ correction, are independent of the viscosity ratio, and therefore remain the same both for a rigid particles and drops. As will be seen, the entire dependence on viscosity ratio, at $O(Re^{3/2})$, appears in a pre-factor of the form $(5\lambda+2)^2/(\lambda+1)^2$.

## 4. The $O(Re^{3/2})$ correction to the stresslet

In this section, we determine the $O(Re^{3/2})$ correction to the stresslet using the limiting form of the outer velocity field in the matching region. The velocity field, $\boldsymbol{u}^*(\boldsymbol{\rho})$, in real space may be obtained formally by inverting the expressions (2.16)–(2.18) derived in §2. In order to obtain the velocity field in the inner region, to $O(Re^{3/2})$, we need only to examine the limiting form of $\hat{\boldsymbol{u}}^*(\boldsymbol{k})$ in the overlap region. With the finite size of the drop being neglected, the overlap region in Fourier space merely corresponds to the limit $k \gg 1$. One expects convection along a Fourier streamline to become unimportant in this limit, reflecting the local nature of the Fourier space forcing for dominant viscosity. This is seen from (2.16)–(2.18), where for $k \to \infty$, the exponential kernel in the integrals becomes increasingly damped, and

the dominant contribution to the integrals is restricted to an asymptotically small interval, $s \sim O(k^{-2})$, along the streamline. Using this estimate, it may be shown that the only $s$-dependence in the integrands that needs to be retained at this order is the one in the exponential kernel now approximated as $e^{-k^2 s}$; the resulting integral over $s$ is trivial: $\int_0^\infty e^{-k^2 s} \, ds = 1/k^2$. Thus, the leading-order approximations for the components of the outer velocity field, $\boldsymbol{u}^*(\boldsymbol{\rho})$, in the overlap region $1 \ll r \ll Re^{-1/2}$, are given by

$$u_2^*(\boldsymbol{\rho}) = -\frac{1}{(2\pi)^3} \frac{8\pi i(5\lambda + 2)}{3(\lambda + 1)} \int d\boldsymbol{k} \, e^{i\boldsymbol{k} \cdot \boldsymbol{\rho}} \frac{k_1^2 k_2(k_1^2 + k_3^2)}{k^8}, \tag{4.1}$$

$$u_1^*(\boldsymbol{\rho}) = \frac{1}{(2\pi)^3} \frac{8\pi i(5\lambda + 2)}{3(\lambda + 1)} \int d\boldsymbol{k} \, e^{i\boldsymbol{k} \cdot \boldsymbol{\rho}} \frac{k_1^3 k_2^2}{k^8}, \tag{4.2}$$

$$u_3^*(\boldsymbol{\rho}) = \frac{1}{(2\pi)^3} \frac{8\pi i(5\lambda + 2)}{3(\lambda + 1)} \int d\boldsymbol{k} \, e^{i\boldsymbol{k} \cdot \boldsymbol{\rho}} \frac{k_1^2 k_2^2 k_3}{k^8}, \tag{4.3}$$

where we have also neglected the integral terms involving $\hat{u}_2^*$ that enter the expressions for $\hat{u}_1^*$ and $\hat{u}_3^*$ since they only contribute at $O(Re^{3/2})$. The above approximate expressions for the leading-order inverse Fourier transforms may further be written in the form

$$u_2^*(\boldsymbol{\rho}) = -\frac{1}{(2\pi)^3} \frac{8\pi i(5\lambda + 2)}{3(\lambda + 1)} \frac{\partial^3}{\partial \rho_1^2 \partial \rho_2} \left[ \frac{\partial^2}{\partial \rho_1^2} + \frac{\partial^2}{\partial \rho_3^2} \right] F(\rho), \tag{4.4}$$

$$u_1^*(\boldsymbol{\rho}) = \frac{1}{(2\pi)^3} \frac{8\pi i(5\lambda + 2)}{3(\lambda + 1)} \frac{\partial^3}{\partial \rho_1^3} \frac{\partial^2}{\partial \rho_2^2} F(\rho), \tag{4.5}$$

$$u_3^*(\boldsymbol{\rho}) = \frac{1}{(2\pi)^3} \frac{8\pi i(5\lambda + 2)}{3(\lambda + 1)} \frac{\partial^2}{\partial \rho_1^2} \frac{\partial^2}{\partial \rho_2^2} \frac{\partial}{\partial \rho_3} F(\rho), \tag{4.6}$$

where $F(\rho)$ is the inverse Fourier transform of $1/k^8$, and satisfies $(\nabla_\rho^2)^4 F = \delta(\boldsymbol{\rho})$. Furthermore, it is seen from equations (4.1)–(4.3) that the velocity field in physical space must be a homogeneous function of $\boldsymbol{\rho}$ of degree zero. This then corresponds to retaining only the particular solution for $F$; thus, one is led to the following sequence: $(\nabla_\rho^2)^4 F = \delta(\boldsymbol{\rho})$, $(\nabla_\rho^2)^3 F = -1/4\pi\rho$, $(\nabla_\rho^2)^2 F = -\rho/8\pi$, and so on, until $F = -\rho^5/96(30\pi)$. Using this in (4.4)–(4.6), and carrying out the differentiations, one finally obtains

$$u_2^*(\boldsymbol{\rho}) = \frac{(5\lambda + 2)}{72(\lambda + 1)} \frac{\rho_2}{\rho^5} \left( \rho_1^2 \rho_2^2 + 4\rho_2^4 + 3\rho_3^4 + 3\rho_1^2 \rho_3^2 + 7\rho_2^2 \rho_3^2 \right), \tag{4.7}$$

$$u_1^*(\boldsymbol{\rho}) = -\frac{(5\lambda + 2)}{72(\lambda + 1)} \frac{\rho_1}{\rho^5} \left( 2\rho_1^4 + 3\rho_3^4 + 5\rho_1^2 \rho_2^2 + 3\rho_2^2 \rho_3^2 + 5\rho_1^2 \rho_3^2 \right), \tag{4.8}$$

$$u_3^*(\boldsymbol{\rho}) = -\frac{(5\lambda + 2)}{72(\lambda + 1)} \frac{\rho_3}{\rho^5} \left( \rho_3^4 + \rho_1^2 \rho_3^2 + \rho_2^2 \rho_3^2 + 3\rho_1^2 \rho_2^2 \right), \tag{4.9}$$

at leading order. Note that the terms above really represent the $O(Re)$ corrections to the leading-order stresslet field, $\boldsymbol{u}^d(\boldsymbol{\rho})$, in the matching region; the latter contribution was subtracted from $\boldsymbol{u}_o(\boldsymbol{\rho})$ when defining $\boldsymbol{u}^*(\boldsymbol{\rho})$ in order to isolate the inertial corrections. For purposes of comparing our results thus far with an earlier analysis in Vivek Raja *et al.* (2010), we now write down the limiting form of the full outer velocity field in the matching region, to $O(Re)$, and expressed in terms of inner variables. One

obtains

$$\lim_{1 \ll r \ll Re^{-1/2}} \boldsymbol{u}'(\boldsymbol{r}) = Re \lim_{\rho \ll 1} \boldsymbol{u}_o(\boldsymbol{\rho}), \tag{4.10}$$

$$= Re(\boldsymbol{u}^d(\boldsymbol{\rho}) + \lim_{\rho \ll 1} \boldsymbol{u}^*(\boldsymbol{\rho})), \tag{4.11}$$

$$= Re \left[ -\frac{5}{2} \frac{\boldsymbol{\rho}(\boldsymbol{E}:\boldsymbol{\rho}\boldsymbol{\rho})}{\rho^5} + \lim_{\rho \ll 1} \boldsymbol{u}^*(\boldsymbol{\rho}) \right], \tag{4.12}$$

$$= -\frac{5}{2} \frac{\boldsymbol{r}(\boldsymbol{E}:\boldsymbol{r}\boldsymbol{r})}{r^5} + Re \frac{(5\lambda+2)}{72(\lambda+1)} \left[ \frac{r_2}{r^5} \left( r_1^2 r_2^2 + 4r_2^4 + 3r_3^4 \right. \right.$$
$$+ 3r_1^2 r_3^2 + 7r_2^2 r_3^2 \right) \boldsymbol{1}_2 - \frac{r_1}{r^5} \left( 2r_1^4 + 3r_3^4 + 5r_1^2 r_2^2 + 3r_2^2 r_3^2 + 5r_1^2 r_3^2 \right) \boldsymbol{1}_1$$
$$\left. - \frac{r_3}{r^5} \left( r_3^4 + r_1^2 r_3^2 + r_2^2 r_3^2 + 3r_1^2 r_2^2 \right) \boldsymbol{1}_3 \right] + O(Re^{3/2}), \tag{4.13}$$

where we have used the expression for the stresslet field in physical space The above expression is identical to the limiting form, for $r \gg 1$, of the velocity field obtained by Vivek Raja *et al.* (2009) via a regular perturbation expansion, to $O(Re)$, in the inner region. The identity of the two expressions for simple shear flow confirms the regular nature of the $O(Re)$ inertial correction. As shown by Vivek Raja *et al.* (2010), the structure of the regular perturbation expansion remains unchanged, to $O(Re)$, even for a general ambient linear flow, implying that the $O(Re)$ inertial correction must continue to have a regular character in this case.

The identity of the results, to $O(Re)$, obtained here and in Vivek Raja *et al.* (2010) implies that despite the regular perturbation expansion being valid only to $O(Re)$, and only in the region $r \ll Re^{-1/2}$, it nevertheless yields the correct inner velocity field to this order. Thus, rather surprisingly (from the perspective of a matched asymptotic expansions approach), a solution of the linearized Navier–Stokes equations in the outer region is not needed at this order. This situation is, however, peculiar to a neutrally buoyant drop in an ambient linear flow, and is not true, for instance, in the simpler case of a drop translating in a quiescent unbounded fluid domain. The difference arises because, in the translation problem, the velocity field at $O(Re)$ (where $Re = aU/\nu$, $U$ being the translation velocity) includes both a particular integral and a homogeneous solution. Although the $O(Re)$ particular integral obtained fails to satisfy the far-field decay condition, in a manner similar to the linear flow case, it does not lead to a drag. Thus, the well-known Oseen correction to the Stokes drag arises from a homogeneous solution forced by the outer velocity field obtained from solving the Oseen equations (valid in the region $r \sim O(Re^{-1})$, this being the inertial screening length for the translation problem). For an ambient linear flow, however, the $O(Re)$ particular solution yields a non-trivial contribution to the stresslet and additional homogeneous contributions are excluded on grounds of symmetry.

A situation similar to that given above, for a translating drop at $O(Re)$, prevails at $O(Re^{3/2})$ in simple shear flow. The inner limit of the outer solution at this order acts as an ambient linear flow for the inner region, and the correction to the stresslet is the familiar inertialess response of a neutrally buoyant drop to this linear flow (arising as a homogeneous solution of the Stokes equations). Thus, at $O(Re^{3/2})$, the outer solution must reduce to the form $Re^{3/2}(\boldsymbol{r} \cdot \boldsymbol{A})$ in the matching region, and the analysis below determines the elements of the velocity gradient tensor $\boldsymbol{A}$. We begin with (2.16),

the expression for $u_2^*(\boldsymbol{\rho})$, which is the least cumbersome:

$$u_2^*(\boldsymbol{\rho}) = -\frac{i(5\lambda + 2)}{3\pi^2(\lambda + 1)} \int d\boldsymbol{k} \frac{e^{i\boldsymbol{k}\cdot\boldsymbol{\rho}}}{k^2} \int_0^\infty ds \frac{k_1^2(k_1^2 + k_3^2)(k_2 + sk_1) e^{-(k^2 s + k_1 k_2 s^2 + \frac{1}{3}k_1^2 s^3)}}{(k^2 + 2k_1 k_2 s + k_1^2 s^2)^2}.$$

(4.14)

As already seen, the leading-order approximation for $u_2^*(\boldsymbol{\rho})$ was obtained as the inverse Fourier transform of $\hat{u}_2^*(\boldsymbol{k})$ in the limit $k \gg 1$, leading to a term of $O(Re)$ in the matching region. However, carrying out such a large-$k$ expansion to second order, in order to isolate the next inertial correction, leads to a divergent integral. In particular, one obtains

$$\lim_{k \gg 1} u_2^*(\boldsymbol{\rho}) \approx -\frac{i(5\lambda + 2)}{3\pi^2(\lambda + 1)} \int d\boldsymbol{k} \frac{e^{i\boldsymbol{k}\cdot\boldsymbol{\rho}}}{k^2} \int_0^\infty ds \frac{k_1^2(k_1^2 + k_3^2)(k_2 + sk_1) e^{-k^2 s}(1 - k_1 k_2 s^2)}{k^4 \left(1 + \dfrac{2k_1 k_2 s}{k^2}\right)^2},$$

(4.15)

$$\approx -\frac{i(5\lambda + 2)}{3\pi^2(\lambda + 1)} \left[ \int d\boldsymbol{k} \frac{k_1^2 k_2(k_1^2 + k_3^2)}{k^8} e^{i\boldsymbol{k}\cdot\boldsymbol{\rho}} + \int d\boldsymbol{k} \frac{k_1^3(k_1^2 + k_3^2)}{k^6} \left(\frac{1}{k^4} - \frac{6k_2^2}{k^6}\right) e^{i\boldsymbol{k}\cdot\boldsymbol{\rho}} + \cdots \right],$$

(4.16)

where the first term leads to the $O(Re)$ correction analysed earlier, while the second term leads to a divergent integral in the limit of small $\boldsymbol{\rho}$. Specifically, for $\rho \ll 1$, this integral takes the form

$$\int d\boldsymbol{k}(1 + i\boldsymbol{k}\cdot\boldsymbol{\rho})\frac{k_1^3(k_1^2 + k_3^2)}{k^6}\left(\frac{1}{k^4} - \frac{6k_2^2}{k^6}\right)$$

$$\approx i \int d\boldsymbol{k}(\boldsymbol{k}\cdot\boldsymbol{\rho})\frac{k_1^3(k_1^2 + k_3^2)}{k^6}\left(\frac{1}{k^4} - \frac{6k_2^2}{k^6}\right) \sim \rho \int \frac{d\boldsymbol{k}}{k^2}, \quad (4.17)$$

where the contribution from the leading-order term in the Fourier exponential yields an odd integrand, and therefore integrates to zero. The divergence arises because of the lack of a reciprocal correspondence between the limits in physical and Fourier space beyond $O(Re)$. In order to obtain a convergent result at the next order, we need to take the limit $\rho \ll 1$ rather than $k \gg 1$. In the latter instance, one may always expand the exponential kernel in the Fourier integrals, thereby obtaining a local relation between a Fourier-transformed velocity component and the corresponding component of the projected point-dipole forcing. However, physically, the singular nature of the $O(Re^{3/2})$ correction implies that convection along a Fourier streamline remains important, and the non-local nature of the forcing in Fourier space must be accounted for beyond $O(Re)$. In other words, the integral along the characteristic coordinate $s$ must be retained in its full form. We therefore proceed a little differently, first extracting the $O(Re)$ correction from the exact expression for the Fourier transform:

$$\lim_{\rho \ll 1} u_2^*(\boldsymbol{\rho}) = -\lim_{\rho \ll 1} \frac{i(5\lambda + 2)}{3\pi^2(\lambda + 1)} \int d\boldsymbol{k} \frac{e^{i\boldsymbol{k}\cdot\boldsymbol{\rho}}}{k^2} \int_0^\infty ds \frac{k_1^2(k_1^2 + k_3^2)(k_2 + sk_1) e^{-(k^2 s + k_1 k_2 s^2 + \frac{1}{3}k_1^2 s^3)}}{(k^2 + 2k_1 k_2 s + k_1^2 s^2)^2},$$

(4.18)

$$= -\frac{\mathrm{i}(5\lambda+2)}{3\pi^2(\lambda+1)}\int\mathrm{d}\boldsymbol{k}\,\frac{k_1^2 k_2\left(k_1^2+k_3^2\right)}{k^8}\,\mathrm{e}^{\mathrm{i}\boldsymbol{k}\cdot\boldsymbol{\rho}} + \lim_{\rho\ll1}\frac{\mathrm{i}(5\lambda+2)}{3\pi^2(\lambda+1)}$$

$$\times\int\mathrm{d}\boldsymbol{k}\,\frac{\mathrm{e}^{\mathrm{i}\boldsymbol{k}\cdot\boldsymbol{\rho}}}{k^2}\left[\frac{k_1^2 k_2\left(k_1^2+k_3^2\right)}{k^6} - \int_0^\infty\mathrm{d}s\,\frac{k_1^2\left(k_1^2+k_3^2\right)(k_2+sk_1)\,\mathrm{e}^{-(k^2 s+k_1 k_2 s^2+\frac{1}{3}k_1^2 s^3)}}{\left(k^2+2k_1 k_2 s+k_1^2 s^2\right)^2}\right],\quad (4.19)$$

where the small $\rho$ limit is a redundant one in the first term, it being a homogeneous function of degree zero. In the second term, one may now expand (only) the Fourier exponential, and thereby, still obtain convergent integrals. Using (4.7) and converting to inner variables, one obtains

$$\lim_{1\ll r\ll Re^{-1/2}} u_2^*(\boldsymbol{r}) = \frac{(5\lambda+2)}{72(\lambda+1)}\frac{r_2}{r^5}\left(r_1^2 r_2^2+4r_2^4+3r_3^4+3r_1^2 r_3^2+7r_2^2 r_3^2\right) - Re^{1/2}\boldsymbol{r}\cdot\frac{(5\lambda+2)}{3\pi^2(\lambda+1)}$$

$$\times\int\mathrm{d}\boldsymbol{k}\,\boldsymbol{k}\,\frac{k_1^2\left(k_1^2+k_3^2\right)}{k^2}\left[\frac{k_2}{k^6} - \int_0^\infty\mathrm{d}s\,\frac{(k_2+sk_1)\,\mathrm{e}^{-(k^2 s+k_1 k_2 s^2+\frac{1}{3}k_1^2 s^3)}}{\left(k^2+2k_1 k_2 s+k_1^2 s^2\right)^2}\right].$$

$$(4.20)$$

Even with the $s$-dependence included, the factor multiplying the Fourier exponential in the integrand of the second term in (4.19) remains an odd function of $\boldsymbol{k}$, and the first non-trivial contribution in (4.20) therefore comes from the term of $O(\boldsymbol{\rho})\equiv O(Re^{1/2}\boldsymbol{r})$ in the limit $\rho\to0$. With the retention of the exact dependence on $s$ in the exponential kernel, the divergence with $k$, for $k\to0$, encountered earlier in (4.16) is no longer a concern. Since $s\sim O(1)$ for $k\sim O(1)$, all the terms in the argument of the exponential kernel become important once $k\sim O(1)$, cutting off the divergence. In fact, it is now seen that the earlier approximate form in (4.16), obtained by Taylor-expanding exponential kernel about $\mathrm{e}^{-k^2 s}$, is only appropriate for $k\to\infty$, and the resulting limiting form ensures convergence in the large $k$ limit instead. Using (4.20), one may now write down the limiting form for the gradient component of the outer velocity field in the matching region. Thus,

$$\lim_{1\ll r\ll Re^{-1/2}} u_{o2}(\boldsymbol{r}) = -\frac{5}{2}\frac{r_2(\boldsymbol{E}:\boldsymbol{rr})}{r^5} + Re\frac{(5\lambda+2)}{72(\lambda+1)}\frac{r_2}{r^5}\left(r_1^2 r_2^2+4r_2^4+3r_3^4+3r_1^2 r_3^2+7r_2^2 r_3^2\right)$$

$$- Re^{3/2}\boldsymbol{r}\cdot\frac{(5\lambda+2)}{3\pi^2(\lambda+1)}\int\mathrm{d}\boldsymbol{k}\boldsymbol{k}\frac{k_1^2\left(k_1^2+k_3^2\right)}{k^2}$$

$$\times\left[\frac{k_2}{k^6} - \int_0^\infty\mathrm{d}s\,\frac{(k_2+sk_1)\,\mathrm{e}^{-(k^2 s+k_1 k_2 s^2+\frac{1}{3}k_1^2 s^3)}}{\left(k^2+2k_1 k_2 s+k_1^2 s^2\right)^2}\right].$$

$$(4.21)$$

Arguments along similar lines applied to the expressions for $u_1^*$ and $u_3^*$, that is,

$$u_1^*(\boldsymbol{\rho}) = \frac{1}{(2\pi)^3}\int\mathrm{d}\boldsymbol{k}\,\mathrm{e}^{\mathrm{i}\boldsymbol{k}\cdot\boldsymbol{\rho}}\left[\frac{8\pi\mathrm{i}(5\lambda+2)}{3(\lambda+1)}\int_0^\infty\mathrm{d}s\,\frac{k_1^3(k_2+sk_1)^2\,\mathrm{e}^{-(k^2 s+k_1 k_2 s^2+\frac{1}{3}k_1^2 s^3)}}{\left(k^2+2k_1 k_2 s+k_1^2 s^2\right)^3}\right.$$

$$\left. - \int_0^\infty\mathrm{d}s\,\frac{\left(k^2+2k_1 k_2 s+k_1^2 s^2-2k_1^2\right)\mathrm{e}^{-(k^2 s+k_1 k_2 s^2+\frac{1}{3}k_1^2 s^3)}}{\left(k^2+2k_1 k_2 s+k_1^2 s^2\right)}\,\hat{u}_2^*(k_1, k_2+sk_1, k_3)\right],$$

$$(4.22)$$

$$u_3^*(\boldsymbol{\rho}) = \frac{1}{(2\pi)^3} \int d\boldsymbol{k} \, e^{i\boldsymbol{k}\cdot\boldsymbol{\rho}} \left[ \frac{8\pi i(5\lambda + 2)}{3(\lambda + 1)} \int_0^\infty ds \, \frac{k_1^2 k_3 (k_2 + sk_1)^2 \, e^{-(k^2 s + k_1 k_2 s^2 + \frac{1}{3} k_1^2 s^3)}}{\left(k^2 + 2k_1 k_2 s + k_1^2 s^2\right)^3} \right.$$

$$\left. + \int_0^\infty ds \, \frac{2k_1 k_3 \, e^{-(k^2 s + k_1 k_2 s^2 + \frac{1}{3} k_1^2 s^3)}}{\left(k^2 + 2k_1 k_2 s + k_1^2 s^2\right)} \hat{u}_2^*(k_1, k_2 + sk_1, k_3) \right], \tag{4.23}$$

yield the corresponding $O(Re^{3/2})$ corrections. The limiting form of the outer velocity field in the matching region may be written down in the following succinct form:

$$\lim_{1 \ll r \ll Re^{-1/2}} \boldsymbol{u}_o(\boldsymbol{r}) = -\frac{5}{2} \frac{\boldsymbol{r}(\boldsymbol{E}:\boldsymbol{rr})}{r^5} + Re \frac{(5\lambda + 2)}{72(\lambda + 1)} \boldsymbol{B}(\boldsymbol{r}) + Re^{3/2} \frac{(5\lambda + 2)}{3\pi^2(\lambda + 1)} (\boldsymbol{r} \cdot \boldsymbol{A}), \tag{4.24}$$

where the components of the vector $\boldsymbol{B}(\boldsymbol{r})$ given by

$$B_1(\boldsymbol{r}) = -\frac{r_1}{r^5} \left( 2r_1^4 + 3r_3^4 + 5r_1^2 r_2^2 + 3r_2^2 r_3^2 + 5r_1^2 r_3^2 \right), \tag{4.25}$$

$$B_2(\boldsymbol{r}) = \frac{r_2}{r^5} \left( r_1^2 r_2^2 + 4r_2^4 + 3r_3^4 + 3r_1^2 r_3^2 + 7r_2^2 r_3^2 \right), \tag{4.26}$$

$$B_3(\boldsymbol{r}) = \frac{r_3}{r^5} \left( r_3^4 + r_1^2 r_3^2 + r_2^2 r_3^2 + 3r_1^2 r_2^2 \right), \tag{4.27}$$

characterize the far-field form of the regular $O(Re)$ correction. It is worth reiterating that $\boldsymbol{B}(\boldsymbol{r})$ is the limiting form, for $r \gg 1$, of the $O(Re)$ velocity field obtained by Vivek Raja *et al.* (2010) via a regular perturbation expansion. The components of $\boldsymbol{A}$ given by

$$A_{11} = \int d\boldsymbol{k} \, k_1^4 \left[ \frac{k_2^2}{k^8} - \int_0^\infty ds \, \frac{(k_2 + sk_1)^2 \, e^{-(k^2 s + k_1 k_2 s^2 + \frac{1}{3} k_1^2 s^3)}}{\left(k^2 + 2k_1 k_2 s + k_1^2 s^2\right)^3} \right]$$

$$- \int d\boldsymbol{k} \, k_1^3 (k_1^2 + k_3^2) \left[ \int_0^\infty ds \, \frac{(k^2 + 2k_1 k_2 s + k_1^2 s^2 - 2k_1^2) \, e^{-(k^2 s + k_1 k_2 s^2 + \frac{1}{3} k_1^2 s^3)}}{\left(k^2 + 2k_1 k_2 s + k_1^2 s^2\right)^2} \right.$$

$$\left. \times \int_0^\infty ds' \, \frac{(k_2 + k_1(s + s')) \, e^{-[k^2 s' + k_1 k_2(s'^2 + 2ss') + \frac{1}{3} k_1^2(s'^3 + 3ss'^2 + 3s^2 s')]}}{\left[k^2 + 2k_1 k_2(s + s') + k_1^2(s + s')^2\right]^2} \right], \tag{4.28}$$

$$A_{12} = \int d\boldsymbol{k} \, \frac{k_1^3 (k_1^2 + k_3^2)}{k^2} \int_0^\infty ds \, \frac{(k_2 + sk_1) \, e^{-(k^2 s + k_1 k_2 s^2 + \frac{1}{3} k_1^2 s^3)}}{\left(k^2 + 2k_1 k_2 s + k_1^2 s^2\right)^2}, \tag{4.29}$$

$$A_{21} = -\int d\boldsymbol{k} \, k_1^3 k_2 \int_0^\infty ds \, \frac{(k_2 + sk_1)^2 \, e^{-(k^2 s + k_1 k_2 s^2 + \frac{1}{3} k_1^2 s^3)}}{\left(k^2 + 2k_1 k_2 s + k_1^2 s^2\right)^3}$$

$$- \int d\boldsymbol{k} \, k_1^2 k_2 (k_1^2 + k_3^2) \left[ \int_0^\infty ds \, \frac{(k^2 + 2k_1 k_2 s + k_1^2 s^2 - 2k_1^2) \, e^{-(k^2 s + k_1 k_2 s^2 + \frac{1}{3} k_1^2 s^3)}}{\left(k^2 + 2k_1 k_2 s + k_1^2 s^2\right)^2} \right.$$

$$\left. \times \int_0^\infty ds' \, \frac{(k_2 + k_1(s + s'))^2 \, e^{-[k^2 s' + k_1 k_2(s'^2 + 2ss') + \frac{1}{3} k_1^2(s'^3 + 3ss'^2 + 3s^2 s')]}}{\left[k^2 + 2k_1 k_2(s + s') + k_1^2(s + s')^2\right]^2} \right], \tag{4.30}$$

$$A_{22} = \int d\mathbf{k} \frac{k_1^2 k_2 (k_1^2 + k_3^2)}{k^2} \left[ \int_0^\infty ds \frac{(k_2 + sk_1)\, e^{-(k^2 s + k_1 k_2 s^2 + \frac{1}{3} k_1^2 s^3)}}{(k^2 + 2k_1 k_2 s + k_1^2 s^2)^2} - \frac{k_2}{k^6} \right], \qquad (4.31)$$

$$A_{33} = \int d\mathbf{k}\, k_1^2 k_3^2 \left[ \frac{k_2^2}{k^8} - \int_0^\infty ds \frac{(k_2 + sk_1)^2\, e^{-(k^2 s + k_1 k_2 s^2 + \frac{1}{3} k_1^2 s^3)}}{(k^2 + 2k_1 k_2 s + k_1^2 s^2)^3} \right]$$

$$- \int d\mathbf{k}\, 2k_1^3 k_3^2 (k_1^2 + k_3^2) \left[ \int_0^\infty ds \frac{e^{-(k^2 s + k_1 k_2 s^2 + \frac{1}{3} k_1^2 s^3)}}{(k^2 + 2k_1 k_2 s + k_1^2 s^2)^2} \right.$$

$$\left. \times \int_0^\infty ds' \frac{(k_2 + k_1(s + s'))\, e^{-[k^2 s' + k_1 k_2 (s'^2 + 2ss') + \frac{1}{3} k_1^2 (s'^3 + 3ss'^2 + 3s^2 s')]}}{\left[ k^2 + 2k_1 k_2 (s + s') + k_1^2 (s + s')^2 \right]^2} \right], \qquad (4.32)$$

$$A_{13} = A_{23} = A_{31} = A_{32} = 0, \qquad (4.33)$$

characterize the singular $O(Re^{3/2})$ correction. Here, the nested characteristic integrals in $A_{11}$, $A_{21}$ and $A_{33}$ arise because both $u_1^*$ and $u_3^*$ involve an integration of $u_2^*$ along a Fourier streamline (see (4.22) and (4.23)), and the latter involves a second characteristic integral.

The disturbance velocity field at $O(Re^{3/2})$, in the inner region, is now readily calculated as the inertialess disturbance field induced by a neutrally buoyant drop subjected to an 'ambient' linear flow given by $u^\infty = Re^{3/2}\{(5\lambda + 2)/[3\pi^2(\lambda + 1)]\}(\mathbf{r} \cdot \mathbf{A})$. Thus, in contrast to the rather cumbersome algebra involved in obtaining the $O(Re)$ inner velocity field, the $O(Re^{3/2})$ analysis only involves knowledge of a well-known Stokes solution (see Leal 1992), once the elements of $\mathbf{A}$ are determined. One may now write the velocity field in the exterior fluid domain, in the inner region, to $O(Re^{3/2})$ as

$$u(r) = u^{(0)}(r) + Re\, u^{(1)}(r) + Re^{3/2} u^{(2)}(r), \qquad (4.34)$$

where

$$u^{(0)}(r) = \boldsymbol{\Gamma} \cdot r - \frac{\lambda}{(\lambda + 1)r^5} \mathbf{E} \cdot r - \left( \frac{(5\lambda + 2)}{2(\lambda + 1)r^5} - \frac{5\lambda}{2(\lambda + 1)r^7} \right) r(\mathbf{E} : rr), \qquad (4.35)$$

$$u^{(2)}(r) = \frac{(5\lambda + 2)}{3\pi^2(\lambda + 1)} \mathbf{A}^\dagger \cdot r - \frac{\lambda(5\lambda + 2)}{6\pi^2(\lambda + 1)^2 r^5} (\mathbf{A} + \mathbf{A}^\dagger) \cdot r$$

$$- \frac{(5\lambda + 2)}{6\pi^2(\lambda + 1)} \left( \frac{(5\lambda + 2)}{2(\lambda + 1)r^5} - \frac{5\lambda}{2(\lambda + 1)r^7} \right) r((\mathbf{A} + \mathbf{A}^\dagger) : rr), \qquad (4.36)$$

and the general form of the regular correction, $u^{(1)}(r)$, derived in Vivek Raja *et al.* (2010), is reproduced here for the exterior fluid domain:

$$u^{(1)}(r) = \frac{1}{(\lambda + 1)} \left[ \left( -\frac{c_1}{4r^{11}} + \frac{c_2}{2r^{10}} - \frac{7c_3}{4r^9} + \frac{c_4}{3r^8} - \frac{c_5}{12r^5} \right)(\boldsymbol{\Gamma} : rr)^2 r + \left( \frac{c_1}{18r^9} - \frac{3c_2}{32r^8} \right. \right.$$

$$+ \frac{c_6}{r^7} - \frac{c_4}{36r^6} - \frac{c_7}{2r^5} + \frac{c_5}{18r^3} \right)(\boldsymbol{\Gamma} : rr)(\boldsymbol{\Gamma} \cdot r) + \left( \frac{c_1}{18r^9} - \frac{3c_2}{32r^8} + \frac{c_8}{r^7} - \frac{c_4}{36r^6} \right.$$

$$+ \frac{c_7}{2r^5} - \frac{c_5}{9r^3} \right)(\boldsymbol{\Gamma} : rr)(\boldsymbol{\Gamma}^\dagger \cdot r) + \left( \frac{c_1}{36r^9} - \frac{3c_2}{32r^8} + \frac{c_9}{r^7} - \frac{5c_4}{36r^6} - \frac{c_{10}}{r^5} + \frac{c_5}{36r^3} \right)$$

$$\times (\boldsymbol{\Gamma} \cdot \boldsymbol{r}) \cdot (\boldsymbol{\Gamma} \cdot \boldsymbol{r})\boldsymbol{r} + \left( \frac{c_1}{18r^9} - \frac{3c_2}{16r^8} + \frac{c_9 + c_{11}}{r^7} - \frac{5c_4}{18r^6} + \frac{c_5}{18r^3} \right) (\boldsymbol{\Gamma} \cdot \boldsymbol{r}) \cdot (\boldsymbol{\Gamma}^\dagger \cdot \boldsymbol{r})\boldsymbol{r}$$

$$+ \left( \frac{c_1}{36r^9} - \frac{3c_2}{32r^8} + \frac{c_{11}}{r^7} - \frac{5c_4}{36r^6} + \frac{c_{10}}{r^5} + \frac{c_5}{36r^3} \right) (\boldsymbol{\Gamma}^\dagger \cdot \boldsymbol{r}) \cdot (\boldsymbol{\Gamma}^\dagger \cdot \boldsymbol{r})\boldsymbol{r}$$

$$+ \left( -\frac{c_1}{126r^7} + \frac{c_2}{32r^6} - \frac{c_{17}}{r^5} + \frac{c_4}{36r^4} - \frac{\lambda+1}{30r^3} + \frac{c_5}{9r} \right) \boldsymbol{\Gamma} \cdot (\boldsymbol{\Gamma} \cdot \boldsymbol{r})$$

$$+ \left( -\frac{c_1}{126r^7} + \frac{c_2}{32r^6} - \frac{c_{18}}{r^5} + \frac{c_4}{36r^4} + \frac{\lambda+1}{30r^3} - \frac{c_5}{18r} \right) \boldsymbol{\Gamma}^\dagger \cdot (\boldsymbol{\Gamma}^\dagger \cdot \boldsymbol{r})$$

$$+ \left( -\frac{c_1}{126r^7} + \frac{c_2}{32r^6} - \frac{c_{12}}{r^5} + \frac{c_4}{36r^4} - \frac{c_7}{6r^3} + \frac{c_5}{9r} \right) \boldsymbol{\Gamma}^\dagger \cdot (\boldsymbol{\Gamma} \cdot \boldsymbol{r})$$

$$+ \left( -\frac{c_1}{126r^7} + \frac{c_2}{32r^6} - \frac{c_{13}}{r^5} + \frac{c_4}{36r^4} + \frac{c_7}{6r^3} - \frac{c_5}{18r} \right) \boldsymbol{\Gamma} \cdot (\boldsymbol{\Gamma}^\dagger \cdot \boldsymbol{r})$$

$$+ \left( -\frac{c_1}{252r^7} + \frac{c_2}{48r^6} - \frac{c_{12} + c_{13}}{2r^5} + \frac{c_4}{18r^4} - \frac{c_5}{36r} \right) (\boldsymbol{\Gamma} : \boldsymbol{\Gamma}^\dagger + \boldsymbol{\Gamma} : \boldsymbol{\Gamma})\boldsymbol{r} \bigg]. \tag{4.37}$$

The constants $c_i$ in (4.37) are functions of the viscosity ratio and have been defined in Vivek Raja *et al.* (2010). For $r \gg 1$, (4.37) reduces to $\boldsymbol{B}(\boldsymbol{r})$ as defined by (4.25)–(4.27).

We again emphasize that the only difference between the Stokes disturbance field and that at $O(Re^{3/2})$ is the ambient linear flow. In the former case, it is the actual imposed flow, $\boldsymbol{\Gamma} \cdot \boldsymbol{r}$, while in the latter case, it is the 'ambient' flow, $[(5\lambda + 2)/3\pi^2(\lambda+1)](\boldsymbol{A}^\dagger \cdot \boldsymbol{r})$, set up by the outer field in the overlap region $\text{overlap}\,(1 \ll r \ll Re^{-1/2})$. The expression for the $O(Re^{3/2})$ correction to the stresslet is immediate. The stresslet for a neutrally buoyant drop in a linear flow, $\boldsymbol{\Gamma} \cdot \boldsymbol{r}$, is $\boldsymbol{S} = (4\pi/3)[(5\lambda + 2)/(\lambda+1)]\boldsymbol{E}$, and for the ambient flow at $O(Re^{3/2})$, this takes the form $Re^{3/2}(2/9\pi)[(5\lambda + 2)^2/(\lambda+1)^2](\boldsymbol{A} + \boldsymbol{A}^\dagger)$. Thus, $\boldsymbol{S}^{(2)}$, which appears in (3.14) for the bulk stress in §3, is given by

$$\boldsymbol{S}^{(2)} = \frac{2}{9\pi} \frac{(5\lambda+2)^2}{(\lambda+1)^2} (\boldsymbol{A} + \boldsymbol{A}^\dagger). \tag{4.38}$$

Combining this result with the $O(Re)$ correction to the stresslet derived for simple shear flow by Vivek Raja *et al.* (2010) (see (3.4) in §3), one obtains the following expression for the stresslet, accurate to $O(Re^{3/2})$:

$$\boldsymbol{S} = \boldsymbol{S}^{(0)} + Re\,\boldsymbol{S}^{(1)} + Re^{3/2}\,\boldsymbol{S}^{(2)}, \quad = \frac{4\pi(5\lambda+2)}{3(\lambda+1)}\boldsymbol{E} - Re \left[ \frac{16\pi(3\lambda^2 + 3\lambda + 1)}{27(\lambda+1)^2} \right.$$

$$\left. \times (\boldsymbol{\Omega} \cdot \boldsymbol{E} - \boldsymbol{E} \cdot \boldsymbol{\Omega}) + \frac{4\pi(43\lambda^2 + 36\lambda + 8)}{105(\lambda+1)^2}\boldsymbol{E} \cdot \boldsymbol{E} \right] + Re^{3/2} \frac{2(5\lambda+2)^2}{9\pi(\lambda+1)^2}(\boldsymbol{A} + \boldsymbol{A}^\dagger) + O(Re^2), \tag{4.39}$$

where we again note that $\boldsymbol{\Gamma} = \boldsymbol{1}_1\boldsymbol{1}_2$ and $\boldsymbol{E} = \frac{1}{2}(\boldsymbol{1}_1\boldsymbol{1}_2 + \boldsymbol{1}_2\boldsymbol{1}_1)$ for simple shear flow; the order of the next correction to the stresslet is also indicated in (4.39). It was noted by Vivek Raja *et al.* (2010) that inertia, at $O(Re)$, only alters the normal stresses in simple shear flow, so that the shear component of the stresslet may be written as

$$S_{12} = \frac{2\pi(5\lambda+2)}{3(\lambda+1)} + Re^{3/2}\frac{2(5\lambda+2)^2}{9\pi(\lambda+1)^2}(A_{12} + A_{21}) + O(Re^2), \tag{4.40}$$

$$= \frac{4\pi}{3} \left[ \frac{(5\lambda+2)}{2(\lambda+1)} + Re^{3/2}\frac{(5\lambda+2)^2}{12\pi^2(\lambda+1)^2}(A_{12} + A_{21}) + O(Re^2) \right]. \tag{4.41}$$

At $O(\phi Re^{3/2})$, the shear viscosity of a dilute emulsion becomes a function of the shear rate.

We now calculate the elements of **A**. This calculation is clearly not a trivial one since the elements $A_{11}$, $A_{21}$ and $A_{33}$ involve five-dimensional integrals, while $A_{12}$ and $A_{22}$ involve four-dimensional ones. The multi-dimensional nature and the infinite intervals involved make a direct numerical approach a difficult one; this may indeed have led to the inaccurate results reported earlier for the $O(Re^{3/2})$ correction to the stresslet (see Lin *et al.* 1970; Stone *et al.* 2000). We therefore first reduce the dimensionality of integration to two by analytical means, before resorting to numerics. To begin with, we reduce the nested characteristic integrals in $A_{11}$, $A_{21}$ and $A_{33}$ to a single integral using an integration by parts. For instance, consider the nested integral in the expressions for $A_{11}$ and $A_{21}$:

$$\left.\begin{array}{l} \displaystyle\int_0^\infty \mathrm{d}s \frac{\left(k^2 + 2k_1 k_2 s + k_1^2 s^2 - 2k_1^2\right) \mathrm{e}^{-(k^2 s + k_1 k_2 s^2 + \frac{1}{3}k_1^2 s^3)}}{\left(k^2 + 2k_1 k_2 s + k_1^2 s^2\right)^2} \\[4mm] \displaystyle\int_0^\infty \mathrm{d}s' \frac{\left(k_2 + k_1(s + s')\right) \mathrm{e}^{-[k^2 s' + k_1 k_2 (s'^2 + 2ss') + \frac{1}{3}k_1^2 (s'^3 + 3ss'^2 + 3s^2 s')]}}{[k^2 + 2k_1 k_2 (s + s') + k_1^2 (s + s')^2]^2}. \end{array}\right\} \qquad (4.42)$$

Defining a variable $s'' = (s + s')$ allows one to combine the two exponentials, and the above integral takes the form

$$\int_0^\infty \mathrm{d}s \frac{\left(k^2 + 2k_1 k_2 s + k_1^2 s^2 - 2k_1^2\right)}{\left(k^2 + 2k_1 k_2 s + k_1^2 s^2\right)^2} \int_s^\infty \mathrm{d}s'' \frac{\left(k_2 + k_1 s''\right) \mathrm{e}^{-[k^2 s'' + k_1 k_2 s''^2 + \frac{1}{3}k_1^2 s''^3]}}{\left[k^2 + 2k_1 k_2 s'' + k_1^2 s''^2\right]^2}. \qquad (4.43)$$

One may now integrate (4.43) by parts. Noting that

$$\int \frac{\left(k^2 + 2k_1 k_2 s + k_1^2 s^2 - 2k_1^2\right)}{\left(k^2 + 2k_1 k_2 s + k_1^2 s^2\right)^2} \mathrm{d}s = \frac{k_3^2}{k_1 \left(k_1^2 + k_3^2\right)^{3/2}} \tan^{-1}\left(\frac{k_2 + k_1 s}{\left(k_1^2 + k_3^2\right)^{1/2}}\right) \\ - \frac{k_1(k_2 + k_1 s)}{\left(k_1^2 + k_3^2\right)\left[k_1^2 + k_3^2 + (k_2 + k_1 s)^2\right]}, \qquad (4.44)$$

one obtains

$$\int_0^\infty \mathrm{d}s \frac{\left(k^2 + 2k_1 k_2 s + k_1^2 s^2 - 2k_1^2\right)}{\left(k^2 + 2k_1 k_2 s + k_1^2 s^2\right)^2} \int_s^\infty \mathrm{d}s'' \frac{\left(k_2 + k_1 s''\right) \mathrm{e}^{-[k^2 s'' + k_1 k_2 s''^2 + \frac{1}{3}k_1^2 s''^3]}}{\left[k^2 + 2k_1 k_2 s'' + k_1^2 s''^2\right]^2} \\ = \int_0^\infty \mathrm{d}s \frac{(k_2 + k_1 s) \mathrm{e}^{-[k^2 s + k_1 k_2 s^2 + \frac{1}{3}k_1^2 s^3]}}{k_1 \left(k^2 + 2k_1 k_2 s + k_1^2 s^2\right)^2} \left[\frac{k_3^2}{k_1 \left(k_1^2 + k_3^2\right)^{3/2}} \left[\tan^{-1}\left(\frac{k_2 + k_1 s}{\left(k_1^2 + k_3^2\right)^{1/2}}\right)\right]\right. \\ \left. - \tan^{-1}\left(\frac{k_2}{\left(k_1^2 + k_3^2\right)^{1/2}}\right) + \frac{k_1^2}{\left(k_1^2 + k_3^2\right)}\left[\frac{k_2}{k^2} - \frac{(k_2 + k_1 s)}{k_1^2 + k_3^2 + (k_2 + k_1 s)^2}\right]\right]. \qquad (4.45)$$

For the nested characteristic integral in $A_{33}$, one similarly obtains

$$\int_0^\infty ds \frac{e^{-[k^2 s + k_1 k_2 s^2 + \frac{1}{3}k_1^2 s^3]}}{\left(k^2 + 2k_1 k_2 s + k_1^2 s^2\right)^2} \int_0^\infty ds' \frac{(k_2 + k_1(s + s'))\, e^{-[k^2 s' + k_1 k_2 (s'^2 + 2s' s) + \frac{1}{3}k_1^2 (s'^3 + 3ss'^2 + 3s^2 s')]}}{\left[k^2 + 2k_1 k_2 (s + s') + k_1^2 (s + s')^2\right]^2}$$

$$= \int_0^\infty ds \frac{(k_2 + k_1 s)\, e^{-[k^2 s + k_1 k_2 s^2 + \frac{1}{3}k_1^2 s^3]}}{\left(k^2 + 2k_1 k_2 s + k_1^2 s^2\right)^2} \left[ \frac{1}{\left(k_1^2 + k_3^2\right)^{1/2}} \left[ \tan^{-1} \left( \frac{k_2}{\left(k_1^2 + k_3^2\right)^{1/2}} \right) \right. \right.$$

$$\left. \left. - \tan^{-1} \left( \frac{(k_2 + k_1 s)}{\left(k_1^2 + k_3^2\right)^{1/2}} \right) \right] + \left[ \frac{k_2}{k^2} - \frac{(k_2 + k_1 s)}{k_1^2 + k_3^2 + (k_2 + k_1 s)^2} \right] \right]. \tag{4.46}$$

Using (4.45) and (4.46), we now write all the non-trivial elements of $\boldsymbol{A}$ as four-dimensional integrals:

$$A_{11} = \int d\boldsymbol{k}\, k_1^4 \left[ \frac{k_2^2}{k^8} - \int_0^\infty ds \frac{(k_2 + sk_1)^2\, e^{-(k^2 s + k_1 k_2 s^2 + \frac{1}{3}k_1^2 s^3)}}{\left(k^2 + 2k_1 k_2 s + k_1^2 s^2\right)^3} \right]$$

$$- \int d\boldsymbol{k} \int_0^\infty ds \frac{(k_2 + k_1 s)\, e^{-[k^2 s + k_1 k_2 s^2 + \frac{1}{3}k_1^2 s^3]}}{\left(k^2 + 2k_1 k_2 s + k_1^2 s^2\right)^2} \left[ \frac{k_1 k_3^2}{\left(k_1^2 + k_3^2\right)^{1/2}} \left[ \tan^{-1} \left( \frac{k_2 + k_1 s}{\left(k_1^2 + k_3^2\right)^{1/2}} \right) \right. \right.$$

$$\left. \left. - \tan^{-1} \left( \frac{k_2}{\left(k_1^2 + k_3^2\right)^{1/2}} \right) \right] + k_1^4 \left[ \frac{k_2}{k^2} - \frac{(k_2 + k_1 s)}{k_1^2 + k_3^2 + (k_2 + k_1 s)^2} \right] \right], \tag{4.47}$$

$$A_{12} = \int d\boldsymbol{k}\, \frac{k_1^3 \left(k_1^2 + k_3^2\right)}{k^2} \int_0^\infty ds \frac{(k_2 + sk_1)\, e^{-(k^2 s + k_1 k_2 s^2 + \frac{1}{3}k_1^2 s^3)}}{\left(k^2 + 2k_1 k_2 s + k_1^2 s^2\right)^2}, \tag{4.48}$$

$$A_{21} = -\int d\boldsymbol{k}\, k_1^3 k_2 \int_0^\infty ds \frac{(k_2 + sk_1)^2\, e^{-(k^2 s + k_1 k_2 s^2 + \frac{1}{3}k_1^2 s^3)}}{\left(k^2 + 2k_1 k_2 s + k_1^2 s^2\right)^3} - \int d\boldsymbol{k}$$

$$\times \int_0^\infty ds \frac{(k_2 + k_1 s)\, e^{-[k^2 s + k_1 k_2 s^2 + \frac{1}{3}k_1^2 s^3]}}{\left(k^2 + 2k_1 k_2 s + k_1^2 s^2\right)^2} \left[ \frac{k_2 k_3^2}{k_1 \left(k_1^2 + k_3^2\right)^{3/2}} \left[ \tan^{-1} \left( \frac{k_2 + k_1 s}{\left(k_1^2 + k_3^2\right)^{1/2}} \right) \right. \right.$$

$$\left. \left. - \tan^{-1} \left( \frac{k_2}{\left(k_1^2 + k_3^2\right)^{1/2}} \right) \right] + k_1^3 k_2 \left[ \frac{k_2}{k^2} - \frac{(k_2 + k_1 s)}{k_1^2 + k_3^2 + (k_2 + k_1 s)^2} \right] \right], \tag{4.49}$$

$$A_{22} = \int d\boldsymbol{k}\, \frac{k_1^2 k_2 \left(k_1^2 + k_3^2\right)}{k^2} \left[ \int_0^\infty ds \frac{(k_2 + sk_1)\, e^{-(k^2 s + k_1 k_2 s^2 + \frac{1}{3}k_1^2 s^3)}}{\left(k^2 + 2k_1 k_2 s + k_1^2 s^2\right)^2} - \frac{k_2}{k^6} \right], \tag{4.50}$$

$$A_{33} = \int d\boldsymbol{k}\, k_1^2 k_3^2 \left[ \frac{k_2^2}{k^8} - \int_0^\infty ds \frac{(k_2 + sk_1)^2\, e^{-(k^2 s + k_1 k_2 s^2 + \frac{1}{3}k_1^2 s^3)}}{\left(k^2 + 2k_1 k_2 s + k_1^2 s^2\right)^3} \right] - 2 \int d\boldsymbol{k}$$

$$\times \int_0^\infty ds \frac{(k_2 + k_1 s)\, e^{-[k^2 s + k_1 k_2 s^2 + \frac{1}{3}k_1^2 s^3]}}{\left(k^2 + 2k_1 k_2 s + k_1^2 s^2\right)^2} \left[ k_1^2 k_3^2 \left(k_1^2 + k_3^2\right)^{1/2} \left[ \tan^{-1} \left( \frac{k_2}{\left(k_1^2 + k_3^2\right)^{1/2}} \right) \right. \right.$$

$$\left. \left. - \tan^{-1} \left( \frac{(k_2 + k_1 s)}{\left(k_1^2 + k_3^2\right)^{1/2}} \right) \right] + k_1^2 k_3^2 \left(k_1^2 + k_3^2\right) \left[ \frac{k_2}{k^2} - \frac{(k_2 + k_1 s)}{k_1^2 + k_3^2 + (k_2 + k_1 s)^2} \right] \right]. \tag{4.51}$$

It becomes convenient now to change spherical coordinates with the polar axis along the gradient direction of simple shear flow. By defining $k_1 = k \sin \theta \cos \phi$, $k_3 = k \sin \theta \sin \phi$ and $k_2 = k \cos \theta$, $\theta$ being the polar angle and $\phi$ being the azimuthal

angle in the $k_1$–$k_3$ plane, the resulting integral over $k$ is of the general form $\int_0^\infty k^2 e^{-ak^2}\,dk$, which is, of course, readily evaluated, giving $\sqrt{\pi}/4a^{3/2}$. Using this result, and the symmetry of simple shear flow, one may now express the elements of $\boldsymbol{A}$ as three-dimensional integrals:

$$
A_{11} = \sqrt{\pi} \int_0^1 dt \int_0^{\pi/2} d\phi \left\{ -(1-t^2)^2 \cos^4\phi \int_0^\infty \frac{ds}{s^{3/2}} \left[ 2t^2 - \frac{\gamma_+ t}{\alpha_+^2 \beta_+^{3/2}} + \frac{\gamma_- t}{\alpha_-^2 \beta_-^{3/2}} \right] \right.
$$
$$
+ (1-t^2)^{3/2} \sin^2\phi \cos^2\phi \int_0^\infty \frac{ds}{s^{3/2}} \left[ \frac{\gamma_+}{\alpha_+^2 \beta_+^{3/2}} \left( \sin^{-1} t - \sin^{-1} \frac{\gamma_+}{\sqrt{\alpha_+}} \right) \right.
$$
$$
\left. \left. + \frac{\gamma_-}{\alpha_-^2 \beta_-^{3/2}} \left( \sin^{-1} t - \sin^{-1} \frac{\gamma_-}{\sqrt{\alpha_-}} \right) \right] \right\}, \tag{4.52}
$$

$$
A_{12} = \sqrt{\pi} \int_0^1 dt \int_0^{\pi/2} d\phi \left\{ -t(1-t^2)^{3/2} \cos^3\phi \int_0^\infty \frac{ds}{s^{3/2}} \left[ \frac{\gamma_- t}{\alpha_-^2 \beta_-^{3/2}} - \frac{\gamma_+ t}{\alpha_+^2 \beta_+^{3/2}} - \right] \right.
$$
$$
+ t(1-t^2) \sin^2\phi \cos\phi \int_0^\infty \frac{ds}{s^{3/2}} \left[ \frac{\gamma_+}{\alpha_+^2 \beta_+^{3/2}} \left( \sin^{-1} t - \sin^{-1} \frac{\gamma_+}{\sqrt{\alpha_+}} \right) \right.
$$
$$
\left. \left. - \frac{\gamma_-}{\alpha_-^2 \beta_-^{3/2}} \left( \sin^{-1} t - \sin^{-1} \frac{\gamma_-}{\sqrt{\alpha_-}} \right) \right] \right\}, \tag{4.53}
$$

$$
A_{21} = \sqrt{\pi} \int_0^1 dt \int_0^{\pi/2} d\phi (1-t^2)^{5/2} \cos^3\phi \int_0^\infty \frac{ds}{s^{3/2}} \left[ \frac{\gamma_+^2}{\alpha_+^2 \beta_+^{3/2}} - \frac{\gamma_-^2}{\alpha_-^2 \beta_-^{3/2}} \right], \tag{4.54}
$$

$$
A_{22} = \sqrt{\pi} \int_0^1 dt \int_0^{\pi/2} d\phi\, t(1-t^2)^2 \cos^2\phi \int_0^\infty \frac{ds}{s^{3/2}} \left[ \frac{\gamma_+^2}{\alpha_+^3 \beta_+^{3/2}} + \frac{\gamma_-^2}{\alpha_-^3 \beta_-^{3/2}} - 2t^2 \right], \tag{4.55}
$$

$$
A_{33} = -\sqrt{\pi} \int_0^1 dt \int_0^{\pi/2} d\phi \sin^2\phi \cos^2\phi \left\{ (1-t^2)^2 \int_0^\infty \frac{ds}{s^{3/2}} \left[ \frac{\gamma_+ t}{\alpha_+^2 \beta_+^{3/2}} + \frac{\gamma_- t}{\alpha_-^2 \beta_-^{3/2}} - 2t^2 \right] \right.
$$
$$
+ (1-t^2)^{3/2} \int_0^\infty \frac{ds}{s^{3/2}} \left[ \frac{\gamma_+}{\alpha_+^2 \beta_+^{3/2}} \left( \sin^{-1} t - \sin^{-1} \frac{\gamma_+}{\sqrt{\alpha_+}} \right) \right.
$$
$$
\left. \left. + \frac{\gamma_-}{\alpha_-^2 \beta_-^{3/2}} \left( \sin^{-1} t - \sin^{-1} \frac{\gamma_-}{\sqrt{\alpha_-}} \right) \right] \right\}, \tag{4.56}
$$

where $t = \cos\theta$, and

$$
\alpha_\pm = 1 \pm 2t\sqrt{1-t^2} \cos\phi\, s + (1-t^2) \cos^2\phi\, s^2, \tag{4.57}
$$
$$
\beta_\pm = 1 \pm 2t\sqrt{1-t^2} \cos\phi\, s + (1-t^2) \cos^2\phi\, \frac{s^2}{3}, \tag{4.58}
$$
$$
\gamma_\pm = t \pm \sqrt{1-t^2} \cos\phi\, s. \tag{4.59}
$$

Note that the arctangents in the earlier expressions have been replaced by arcsines above since this leads to a slight simplification of the argument. Finally, on defining the variable $\hat{s} = \sqrt{1-t^2} \cos\phi\, s$, the integrals over $\phi$ may be expressed in terms of Beta functions (see Gradshteyn & Ryzhik 1965). Using the result

$$
\int_0^{\pi/2} \cos^{(2n+1)/2}\phi\, d\phi = \frac{1}{2} \mathcal{B}\left( \frac{(2n+3)}{4}, \frac{1}{2} \right), \tag{4.60}
$$

and that $\mathscr{B}(p,q) = \Gamma(p)\Gamma(q)/\Gamma(p+q)$, the non-trivial elements of **A** may now be expressed as double integrals in $t$ and $\hat{s}$:

$$A_{11} = \frac{2\sqrt{2}\pi^2}{15\left[\Gamma\left(\frac{1}{4}\right)\right]^2} \int_0^1 dt \left\{7t(1-t^2)^{9/4} J_0(t) + 2(1-t^2)^{7/4} J_{2+}(t)\right\}, \tag{4.61}$$

$$A_{12} = \frac{\left[\Gamma\left(\frac{1}{4}\right)\right]^2}{42\sqrt{2}} \int_0^1 dt \left\{-5t^2(1-t^2)^{7/4} J_{1-}(t) + 2t(1-t^2)^{5/4} J_{2-}(t)\right\}, \tag{4.62}$$

$$A_{21} = \frac{5\left[\Gamma\left(\frac{1}{4}\right)\right]^2}{42\sqrt{2}} \int_0^1 dt(1-t^2)^{11/4} J_{1-}(t), \tag{4.63}$$

$$A_{22} = -\frac{6\sqrt{2}\pi^2}{5\left[\Gamma\left(\frac{1}{4}\right)\right]^2} \int_0^1 dt\, t(1-t^2)^{9/4} J_0(t), \tag{4.64}$$

$$A_{33} = \frac{4\sqrt{2}\pi^2}{15\left[\Gamma\left(\frac{1}{4}\right)\right]^2} \int_0^1 dt \left\{t(1-t^2)^{9/4} J_0(t) - (1-t^2)^{7/4} J_{2+}(t)\right\}, \tag{4.65}$$

where

$$J_0(t) = \int_0^\infty \frac{d\hat{s}}{\hat{s}^{3/2}}$$
$$\times \left[2t - \frac{(t+\hat{s})}{(1+2t\hat{s}+\hat{s}^2)^2 \left(1+t\hat{s}+\frac{\hat{s}^2}{3}\right)^{3/2}} - \frac{(t-\hat{s})}{(1-2t\hat{s}+\hat{s}^2)^2 \left(1-t\hat{s}+\frac{\hat{s}^2}{3}\right)^{3/2}}\right], \tag{4.66}$$

$$J_{1\pm}(t) = \int_0^\infty \frac{d\hat{s}}{\hat{s}^{3/2}}$$
$$\times \left[\frac{(t+\hat{s})}{(1+2t\hat{s}+\hat{s}^2)^2 \left(1+t\hat{s}+\frac{\hat{s}^2}{3}\right)^{3/2}} \pm \frac{(t-\hat{s})}{(1-2t\hat{s}+\hat{s}^2)^2 \left(1-t\hat{s}+\frac{\hat{s}^2}{3}\right)^{3/2}}\right], \tag{4.67}$$

$$J_{2\pm}(t) = \int_0^\infty \frac{d\hat{s}}{\hat{s}^{3/2}} \left[\frac{(t+\hat{s})}{(1+2t\hat{s}+\hat{s}^2)^2 \left(1+t\hat{s}+\frac{\hat{s}^2}{3}\right)^{3/2}} \left(\sin^{-1} t - \sin^{-1}\frac{(t+\hat{s})}{\sqrt{1+2t\hat{s}+\hat{s}^2}}\right)\right.$$
$$\left. \pm \frac{(t-\hat{s})}{(1-2t\hat{s}+\hat{s}^2)^2 \left(1-t\hat{s}+\frac{\hat{s}^2}{3}\right)^{3/2}} \left(\sin^{-1} t - \sin^{-1}\frac{(t-\hat{s})}{\sqrt{1-2t\hat{s}+\hat{s}^2}}\right)\right]. \tag{4.68}$$

The double integrals are readily evaluated using Gaussian quadrature, and the convergence with respect to the upper limit in the inner $s$-integral is verified by combining the numerical estimate for a finite interval in $s$ with an analytical approximation for large $s$. One finds

$$A_{11} = 0.38, \tag{4.69}$$
$$A_{22} = -0.64, \tag{4.70}$$
$$A_{12} = 0.83, \tag{4.71}$$
$$A_{21} = 0.19, \tag{4.72}$$
$$A_{33} = 0.26, \tag{4.73}$$

which, together with (4.39), determine the stresslet to $O(Re^{3/2})$. The values of $A_{ij}$ given by (4.69)–(4.73) show that, in contrast to the imposed simple shear flow, the linear flow at $O(Re^{3/2})$ has a genuine three-dimensional character with vortex stretching. It may be thought of as a superposition of a (non-axisymmetric) bi-axial extension, with the extensional plane making an angle of about $23°$ with the flow-vorticity plane (measured in the anticlockwise sense), and a solid-body rotation with a vorticity vector opposing the ambient vorticity; the principal rates of deformation are $-0.84$, $0.58$ and $0.26$ in a coordinate system aligned with the rate-of-strain tensor.

Using (4.69)–(4.73), the stresslet in simple shear flow, to $O(Re^{3/2})$, is finally given by

$$
\begin{aligned}
\boldsymbol{S} = & \frac{2\pi(5\lambda + 2)}{3(\lambda + 1)}(\mathbf{1}_1\mathbf{1}_2 + \mathbf{1}_2\mathbf{1}_1) - Re\left[\frac{8\pi(3\lambda^2 + 3\lambda + 1)}{27(\lambda + 1)^2}(\mathbf{1}_1\mathbf{1}_1 - \mathbf{1}_2\mathbf{1}_2)\right. \\
& \left. + \frac{\pi(43\lambda^2 + 36\lambda + 8)}{105(\lambda + 1)^2}(\mathbf{1}_1\mathbf{1}_1 + \mathbf{1}_2\mathbf{1}_2)\right] + Re^{3/2}\frac{2(5\lambda + 2)^2}{9\pi(\lambda + 1)^2}[0.76\mathbf{1}_1\mathbf{1}_1 - 1.28\mathbf{1}_2\mathbf{1}_2 \\
& + 1.02(\mathbf{1}_1\mathbf{1}_2 + \mathbf{1}_2\mathbf{1}_1) + 0.52\mathbf{1}_3\mathbf{1}_3] + O(Re^2),
\end{aligned}
\tag{4.74}
$$

and the $O(Re^{3/2})$ stresslet coefficient, in particular, is

$$\boldsymbol{S}^{(2)} = \frac{2(5\lambda + 2)^2}{9\pi(\lambda + 1)^2}[0.76\mathbf{1}_1\mathbf{1}_1 - 1.28\mathbf{1}_2\mathbf{1}_2 + 1.02(\mathbf{1}_1\mathbf{1}_2 + \mathbf{1}_2\mathbf{1}_1) + 0.52\mathbf{1}_3\mathbf{1}_3] \tag{4.75}$$

The components of $\boldsymbol{S}^{(2)}$, in the limit $\lambda \to \infty$, may be compared with the results of earlier calculations. Since the isotropic part of the stresslet is of particular significance in the infinitely dilute limit, the result (4.75) may equivalently be written as $S_{12}^{(2)} = 1.8$, $(S_{11}^{(2)} - S_{22}^{(2)}) = 3.61$ and $(S_{22}^{(2)} - S_{33}^{(2)}) = -3.18$ for $\lambda \to \infty$. The corresponding results of Stone *et al.* (2000) are 1.82, 3.34 and $-1.56$, and the $O(Re^{3/2})$ contribution towards an $N_2$ appears to be in error. A closer examination of the plots given in Mikulencak & Morris (2004), comparing the predictions of Stone *et al.* (2000) for the stresslet components with the numerics, shows a significant overestimation of $(S_{22}-S_{33})$ on the part of the theory in a range of $Re$ where $(S_{11}-S_{22})$ continues to be predicted accurately. On the other hand, all the stresslet components given in Lin *et al.* (1970) appear to be incorrect.

One may also calculate the angular velocity of a rigid particle, to $O(Re^{3/2})$, for $\lambda \to \infty$. The spherical particle must rotate at a rate equal to half the vorticity of the imposed linear flow. The opposing vorticity vectors of the simple shear flow and the linear flow field, at $O(Re^{3/2})$, imply that the particle slows down due to inertia; its

angular velocity being given by

$$\boldsymbol{\Omega}_p = \left[ -\frac{1}{2} + Re^{3/2} \lim_{\lambda \to \infty} \frac{(5\lambda + 2)}{6\pi^2(\lambda + 1)}(A_{12} - A_{21}) \right] \mathbf{1}_3$$

$$= \left[ -\frac{1}{2} + 0.054 Re^{3/2} \right] \mathbf{1}_3. \tag{4.76}$$

The above angular velocity correction was accurately calculated in Stone *et al.* (2000).

## 5. The $O(Re^{3/2})$ contributions to the Reynolds stresses

Here, we present the results for the $O(Re^{3/2})$ contributions to the Reynolds stress integrals in (3.16). The quantities to be calculated naturally separate into two categories: integrals that are a bilinear functional of $\hat{\boldsymbol{u}}^d(\boldsymbol{k})$ and $\hat{\boldsymbol{u}}^*(\boldsymbol{k})$, and those that are quadratic functionals of $\hat{\boldsymbol{u}}^*(\boldsymbol{k})$. Thus, defining

$$\frac{1}{2} \int \{\hat{u}_i^d(\boldsymbol{k})\hat{u}_j^*(\boldsymbol{k}) + \hat{u}_i^*(\boldsymbol{k})\hat{u}_j^d(\boldsymbol{k})\} \, \mathrm{d}\boldsymbol{k} = \frac{(5\lambda + 2)^2}{(\lambda + 1)^2} R_{ij}, \tag{5.1}$$

$$\int \{\hat{u}_i^*(\boldsymbol{k})\hat{u}_j^*(\boldsymbol{k})\} \, \mathrm{d}\boldsymbol{k} = \frac{(5\lambda + 2)^2}{(\lambda + 1)^2} Q_{ij}, \tag{5.2}$$

the direct inertial contributions to the dispersed-phase stress may be written in the form

$$\frac{3}{4\pi} \left( \frac{4\pi}{15} \Gamma_{ik}\Gamma_{jk} + \int_{V_d} \Gamma_{ik}r_k u_j'^{(0)} \, \mathrm{d}\boldsymbol{r} + \int_{V_d} \Gamma_{jk}r_k u_i'^{(0)} \, \mathrm{d}\boldsymbol{r} - \int_{V-V_d} u_i'^{(0)} u_j'^{(0)} \, \mathrm{d}\boldsymbol{r} \right)$$
$$+ \frac{3Re^{3/2}}{32\pi^4} \frac{(5\lambda + 2)^2}{(\lambda + 1)^2}(2R_{ij} + Q_{ij}). \tag{5.3}$$

Employing a sequence of variable transformations similar to those used in the earlier section to simplify the stresslet calculation, the non-trivial elements of $\boldsymbol{R}$ and $\boldsymbol{Q}$, respectively, may be reduced to the following two- and three-dimensional integrals:

$$R_{11} = \frac{128\pi^4}{45 \left[ \Gamma\left(\frac{1}{4}\right) \right]^2} \left[ 3 \int_0^1 \mathrm{d}t \, t^2 (1 - t^2)^{5/4} K_{1-}(t) - \frac{14}{3} \int_0^1 \mathrm{d}t \, t^2 (1 - t^2)^{9/4} K_{1-}(t) \right.$$
$$\left. - 2 \int_0^1 \mathrm{d}t \, t(1 - t^2)^{3/4} K_{2-}(t) + \frac{4}{3} \int_0^1 \mathrm{d}t \, t(1 - t^2)^{7/4} K_{2-}(t) \right], \tag{5.4}$$

$$R_{12} = R_{21} = \frac{16\pi^2 \left[ \Gamma\left(\frac{1}{4}\right) \right]^2}{9} \left[ \frac{5}{42} \int_0^1 \mathrm{d}t \, t(1 - 2t^2)(1 - t^2)^{7/4} K_{1+}(t) \right.$$
$$- \frac{1}{6} \int_0^1 \mathrm{d}t \, t(1 - t^2)^{7/4} K_{1+}(t) + \frac{1}{21} \int_0^1 \mathrm{d}t \, (1 - 2t^2)(1 - t^2)^{5/4} K_{2+}(t)$$
$$\left. + \frac{5}{21} \int_0^1 \mathrm{d}t \, t(1 - t^2)^{11/4} K_{1+}(t) \right], \tag{5.5}$$

$$R_{22} = -\frac{128\pi^4}{15\left[\Gamma\left(\frac{1}{4}\right)\right]^2}\int_0^1 dt(1-t^2)^{9/4}(1-2t^2)K_{1-}(t), \tag{5.6}$$

$$R_{33} = -\frac{512\pi^4}{135\left[\Gamma\left(\frac{1}{4}\right)\right]^2}\left[\int_0^1 dt\, t^2(1-t^2)^{9/4}K_{1-}(t) + \int_0^1 dt\, t(1-t^2)^{7/4}K_{2-}(t)\right], \tag{5.7}$$

and

$$Q_{11} = -\frac{512\pi^4}{135\left[\Gamma\left(\frac{1}{4}\right)\right]^2}\left[4\int_0^1 dt(1-t^2)^{5/4}L_{3+}(t) + 4\int_0^1 dt\, t(1-t^2)^{7/4}L_{2+}(t)\right.$$
$$\left. + 7\int_0^1 dt\, t^2(1-t^2)^{9/4}L_{1+}(t)\right], \tag{5.8}$$

$$Q_{12} = Q_{21} = \frac{64\pi^2\left[\Gamma\left(\frac{1}{4}\right)\right]^2}{189}\left[5\int_0^1 dt\, t(1-t^2)^{11/4}L_{1-}(t) + 2\int_0^1 dt\,(1-t^2)^{9/4}L_{2-}(t)\right], \tag{5.9}$$

$$Q_{22} = -\frac{512\pi^4}{15\left[\Gamma\left(\frac{1}{4}\right)\right]^2}\int_0^1 dt\,(1-t^2)^{13/4}L_{1+}(t), \tag{5.10}$$

$$Q_{33} = -\frac{1024\pi^4}{135\left[\Gamma\left(\frac{1}{4}\right)\right]^2}\left[\int_0^1 dt(1-t^2)^{5/4}L_{3+}(t) - 2\int_0^1 dt\, t(1-t^2)^{7/4}L_{2+}(t)\right.$$
$$\left. + \int_0^1 dt\, t^2(1-t^2)^{9/4}L_{1+}(t)\right]. \tag{5.11}$$

The following integrals appear in the above simplified expressions for the Reynolds stresses:

$$K_{1\pm}(t) = \int_0^\infty \frac{d\hat{s}}{\hat{s}^{1/2}}$$

$$\times\left[\frac{(t+\hat{s})}{(1+2t\hat{s}+\hat{s}^2)^2\left(1+t\hat{s}+\frac{\hat{s}^2}{3}\right)^{1/2}} \pm \frac{(t-\hat{s})}{(1-2t\hat{s}+\hat{s}^2)^2\left(1-t\hat{s}+\frac{\hat{s}^2}{3}\right)^{1/2}}\right], \tag{5.12}$$

$$K_{2\pm}(t) = \int_0^\infty \frac{d\hat{s}}{\hat{s}^{1/2}}\left[\frac{(t+\hat{s})}{(1+2t\hat{s}+\hat{s}^2)^2\left(1+t\hat{s}+\frac{\hat{s}^2}{3}\right)^{1/2}}\left(\sin^{-1}t - \sin^{-1}\frac{(t+\hat{s})}{\sqrt{1+2t\hat{s}+\hat{s}^2}}\right)\right.$$

$$\left. \pm \frac{(t-\hat{s})}{(1-2t\hat{s}+\hat{s}^2)^2\left(1-t\hat{s}+\frac{\hat{s}^2}{3}\right)^{1/2}}\left(\sin^{-1}t - \sin^{-1}\frac{(t-\hat{s})}{\sqrt{1-2t\hat{s}+\hat{s}^2}}\right)\right], \tag{5.13}$$

$$L_{1\pm}(t) = \int_0^\infty \int_0^\infty d\hat{s}\, d\hat{s}' \left[ \frac{(t+\hat{s})(t+\hat{s}')}{(1+2t\hat{s}+\hat{s}^2)^2(1+2t\hat{s}'+\hat{s}'^2)^2\left(\hat{s}+t\hat{s}^2+\dfrac{\hat{s}^3}{3}+\hat{s}'+t\hat{s}'^2+\dfrac{\hat{s}'^2}{3}\right)^{1/2}} \right.$$

$$\left. \pm \frac{(t-\hat{s})(t-\hat{s}')}{(1-2t\hat{s}+\hat{s}^2)^2(1-2t\hat{s}'+\hat{s}'^2)^2\left(\hat{s}-t\hat{s}^2+\dfrac{\hat{s}^3}{3}+\hat{s}'-t\hat{s}'^2+\dfrac{\hat{s}'^2}{3}\right)^{1/2}} \right], \tag{5.14}$$

$$L_{2\pm}(t) = \int_0^\infty \int_0^\infty d\hat{s}\, d\hat{s}'$$

$$\times \left[ \frac{(t+\hat{s})(t+\hat{s}')\left(\sin^{-1}\dfrac{(t+\hat{s}')}{\sqrt{1+2t\hat{s}'+\hat{s}'^2}}-\sin^{-1}t\right)}{(1+2t\hat{s}+\hat{s}^2)^2(1+2t\hat{s}'+\hat{s}'^2)^2\left(\hat{s}+t\hat{s}^2+\dfrac{\hat{s}^3}{3}+\hat{s}'+t\hat{s}'^2+\dfrac{\hat{s}'^2}{3}\right)^{1/2}} \right.$$

$$\left. \pm \frac{(t-\hat{s})(t-\hat{s}')\left(\sin^{-1}\dfrac{(t-\hat{s}')}{\sqrt{1-2t\hat{s}'+\hat{s}'^2}}-\sin^{-1}t\right)}{(1-2t\hat{s}+\hat{s}^2)^2(1-2t\hat{s}'+\hat{s}'^2)^2\left(\hat{s}-t\hat{s}^2+\dfrac{\hat{s}^3}{3}+\hat{s}'-t\hat{s}'^2+\dfrac{\hat{s}'^2}{3}\right)^{1/2}} \right], \tag{5.15}$$

$$L_{3\pm}(t) = \int_0^\infty \int_0^\infty d\hat{s}\, d\hat{s}'$$

$$\times \left[ \frac{(t+\hat{s})(t+\hat{s}')\left(\sin^{-1}\dfrac{(t+\hat{s})}{\sqrt{1+2t\hat{s}+\hat{s}^2}}-\sin^{-1}t\right)\left(\sin^{-1}\dfrac{(t+\hat{s}')}{\sqrt{1+2t\hat{s}'+\hat{s}'^2}}-\sin^{-1}t\right)}{(1+2t\hat{s}+\hat{s}^2)^2(1+2t\hat{s}'+\hat{s}'^2)^2\left(\hat{s}+t\hat{s}^2+\dfrac{\hat{s}^3}{3}+\hat{s}'+t\hat{s}'^2+\dfrac{\hat{s}'^2}{3}\right)^{1/2}} \right.$$

$$\left. \pm \frac{(t-\hat{s})(t-\hat{s}')\left(\sin^{-1}\dfrac{(t-\hat{s})}{\sqrt{1-2t\hat{s}+\hat{s}^2}}-\sin^{-1}t\right)\left(\sin^{-1}\dfrac{(t-\hat{s}')}{\sqrt{1-2t\hat{s}'+\hat{s}'^2}}-\sin^{-1}t\right)}{(1-2t\hat{s}+\hat{s}^2)^2(1-2t\hat{s}'+\hat{s}'^2)^2\left(\hat{s}-t\hat{s}^2+\dfrac{\hat{s}^3}{3}+\hat{s}'-t\hat{s}'^2+\dfrac{\hat{s}'^2}{3}\right)^{1/2}} \right]. \tag{5.16}$$

Again, we use Gaussian quadrature to evaluate the elements of $\boldsymbol{R}$ and $\boldsymbol{Q}$ to find

$$R_{11} = -15.21, \tag{5.17}$$
$$R_{12} = R_{21} = -1.56, \tag{5.18}$$
$$R_{22} = -21.83, \tag{5.19}$$
$$R_{33} = -4.64, \tag{5.20}$$

and

$$Q_{11} = -11.16, \tag{5.21}$$
$$Q_{12} = Q_{21} = 10.52, \tag{5.22}$$

$$Q_{22} = -31.08, \tag{5.23}$$

$$Q_{33} = -8.76. \tag{5.24}$$

Using (3.8) and the above results in (5.3), the expression for the direct inertial contributions, to $O(Re^{3/2})$, is given by

$$-\frac{Re}{4}\left(\frac{2(5\lambda+2)^2}{35(\lambda+1)^2} - \frac{2\lambda(5\lambda+2)}{35(\lambda+1)^2} + \frac{3\lambda^2}{35(\lambda+1)^2}\right)(\mathbf{1}_1\mathbf{1}_1 + \mathbf{1}_2\mathbf{1}_2) + \frac{3Re^{3/2}}{32\pi^4}$$

$$\times\frac{(5\lambda+2)^2}{(\lambda+1)^2}\{-41.58\mathbf{1}_1\mathbf{1}_1 - 74.74\mathbf{1}_2\mathbf{1}_2 + 7.4(\mathbf{1}_1\mathbf{1}_2 + \mathbf{1}_2\mathbf{1}_1) - 18.04\mathbf{1}_3\mathbf{1}_3\} + O(Re^2). \tag{5.25}$$

It must be emphasized that while the stresslet contribution at $O(Re^{3/2})$ has been calculated before, albeit incorrectly, for a suspension of rigid particles, the Reynolds stress contributions at the same order have gone unnoticed. The latter contribute significantly to the normal stress differences at $O(\phi Re^{3/2})$.

## 6. Comparison of theory and numerics

Before proceeding to a comparison both with earlier bulk stress computations for a dilute emulsion (Li & Sarkar 2005) and with new results for the stresslet coefficient alone presented later in this section, we summarize the results of the preceding analysis with a discussion of its predictions. Using (4.38) for the stresslet coefficient, and (5.3) for the direct inertial contributions, the dispersed-phase stress in an infinitely dilute emulsion may be written as

$$\Sigma_{ij}^{(d)} = \phi\left[\frac{(5\lambda+2)}{(\lambda+1)}E_{ij} - Re\left(\frac{4(3\lambda^2+3\lambda+1)}{9(\lambda+1)^2}\left(\Omega_{ik}E_{kj} - E_{ik}\Omega_{kj}\right) - \frac{8\lambda}{35(\lambda+1)^2}E_{ik}E_{kj}\right)\right.$$

$$\left. + Re^{3/2}\frac{(5\lambda+2)^2}{(\lambda+1)^2}\left(\frac{1}{6\pi^2}(A_{ij}+A_{ji}) + \frac{3}{32\pi^4}\left(2R_{ij}+Q_{ij}\right)\right)\right] + O(\phi Re^2). \tag{6.1}$$

Furthermore, using the numerical results for the $O(Re^{3/2})$ stresslet and the Reynolds stress coefficients in §§ 4 (see (4.75)) and 5 (see (5.25)), the dispersed-phase stress tensor in simple shear flow, to $O(\phi Re^{3/2})$, is given by

$$\mathbf{\Sigma}^{(d)} = \phi\left[\frac{(5\lambda+2)}{2(\lambda+1)}(\mathbf{1}_1\mathbf{1}_2 + \mathbf{1}_2\mathbf{1}_1) - Re\left(\frac{2(3\lambda^2+3\lambda+1)}{9(\lambda+1)^2}(\mathbf{1}_1\mathbf{1}_1 - \mathbf{1}_2\mathbf{1}_2)\right.\right.$$

$$\left. - \frac{2\lambda}{35(\lambda+1)^2}(\mathbf{1}_1\mathbf{1}_1 + \mathbf{1}_2\mathbf{1}_2)\right) + Re^{3/2}\frac{(5\lambda+2)^2}{(\lambda+1)^2}\left(\frac{1}{6\pi^2}\{0.76\mathbf{1}_1\mathbf{1}_1 - 1.28\mathbf{1}_2\mathbf{1}_2\right.$$

$$+ 1.02(\mathbf{1}_1\mathbf{1}_2 + \mathbf{1}_2\mathbf{1}_1) + 0.52\mathbf{1}_3\mathbf{1}_3\} + \frac{3}{32\pi^4}\{-41.58\mathbf{1}_1\mathbf{1}_1 - 74.74\mathbf{1}_2\mathbf{1}_2$$

$$\left.\left. + 7.4(\mathbf{1}_1\mathbf{1}_2 + \mathbf{1}_2\mathbf{1}_1) - 18.04\mathbf{1}_3\mathbf{1}_3\}\right)\right] + O(\phi Re^2). \tag{6.2}$$

The shear viscosity and the first and second normal stress differences, to $O(\phi Re^{3/2})$, are respectively

$$\mu_e = 1 + \phi\left[\frac{(5\lambda+2)}{2(\lambda+1)} + 0.024Re^{3/2}\frac{(5\lambda+2)^2}{(\lambda+1)^2}\right] + O(\phi Re^2), \tag{6.3}$$

$$N_1 = \phi \left[ -Re \frac{4(3\lambda^2 + 3\lambda + 1)}{9(\lambda + 1)^2} + 0.066 Re^{3/2} \frac{(5\lambda + 2)^2}{(\lambda + 1)^2} \right] + O(\phi Re^2), \tag{6.4}$$

$$N_2 = \phi \left[ Re \frac{2(105\lambda^2 + 96\lambda + 35)}{315(\lambda + 1)^2} - 0.085 Re^{3/2} \frac{(5\lambda + 2)^2}{(\lambda + 1)^2} \right] + O(\phi Re^2). \tag{6.5}$$

From (6.4) and (6.5), we note that the $O(Re)$ and $O(Re^{3/2})$ contributions to the normal stress differences have opposing signs, and a balance leads to critical Reynolds numbers:

$$\bar{Re}_c^{N1} = 45.34 \frac{(3\lambda^2 + 3\lambda + 1)^2}{(5\lambda + 2)^4}, \tag{6.6}$$

$$\bar{Re}_c^{N2} = 5.58 \times 10^{-3} \frac{(105\lambda^2 + 96\lambda + 35)^2}{(5\lambda + 2)^4}, \tag{6.7}$$

for reversals in sign of $N_1$ and $N_2$, respectively. Of course, not knowing the numerical pre-factors in the $O(Re^2)$ contributions renders the relevance of the above critical Reynolds numbers questionable. Nevertheless, it is worth noting that $\bar{Re}_c^{N2}$ increases from about 0.1, in the limit $\lambda \to \infty$, to only about 0.42 for $\lambda = 0$ (the corresponding values of $\bar{Re}_c^{N1}$ are 0.65 and 2.83), and a reversal in sign of $N_2$ thus appears probable for large $\lambda$. The possibility of a sign reversal, of course, hinges on the range of validity of a small-$Re$ asymptotic expansion. Earlier computations do not offer definitive evidence in this regard, however. The theoretical predictions for the diagonal components of the rigid particle stresslet compare well with the results of Mikulencak & Morris (2004) up until $Re \approx 0.5$, a range that includes $\bar{Re}_c^{N2}$. However, the diagonal components of the bulk stress also include contributions from the Reynolds stress integrals. While the stresslet, at $O(Re^{3/2})$, is determined only by the limiting form of the velocity field in the matching region, the Reynolds stress integrals at this order depend on the full form of the outer velocity field. The range of validity of a finite-$Re$ result is expected to depend on the region where the dominant contributions arise, and agreement between theory and numerics for the stresslet components, over a significant range in $Re$, does not therefore guarantee a similar agreement for corresponding components of the Reynolds stresses. In fact, in our own computations, the results for the Reynolds stresses were found to be very sensitive to the size of the computational domain. The resulting domain size dependence, particularly at small $Re$, has led to our presenting numerical results only for the stresslet components (see §6.2); similar problems were encountered by Mikulencak & Morris (2004).

The recent lattice Boltzmann simulations of Kulkarni & Morris (2008) for an inertial suspension in a bounded domain indicate no signs of either a saturation or a reversal in the normal stress differences even at the smallest volume fraction ($\phi = 0.05$) simulated. However, $\phi = 0.05$ may already be outside the range of an infinitely dilute approximation. The comparison between the present analysis and simulations will be quantitative only if the $O(\phi Re^{3/2})$ contribution calculated here is much larger than the $O(\phi^2)$ contribution arising from pair interactions. The resulting restriction, $\phi \ll Re^{3/2}$, implies $Re \gtrsim 0.4$ for $\phi = 0.05$; the assumption $Re \ll 1$ then being a little untenable. Thus, in the interests of an unambiguous comparison with theory, there is clearly a need for simulating an infinitely dilute (single drop) scenario, in the limit $Re \ll 1$, over a range of viscosity ratios. This is partly addressed in §6.2, where we extend the results of Mikulencak & Morris (2004) by presenting results for the drop stresslet over a range of viscosity ratios.

The speculated reversal in sign above, for the normal stress differences (especially $N_2$), should occur even for $Ca = 0$, being solely a consequence of micro-scale inertia; here, $Ca = \mu a \dot{\gamma} / \sigma$ is the Capillary number, $\sigma$ being the coefficient of interfacial tension, and measures the relative importance of viscous and interfacial tension forces. On the other hand, Vivek Raja *et al.* (2010) predicted reversals in the signs of $N_1$ and $N_2$, specific to a dilute emulsion, arising from the competing effects of inertial and viscous stresses on drop deformation. The associated critical Reynolds numbers were $O(Ca)$, given by

$$Re_c^{N1} = \frac{9(19\lambda + 16)^2}{160(3\lambda^2 + 3\lambda + 1)} Ca, \tag{6.8}$$

$$Re_c^{N2} = \frac{9(551\lambda^3 + 1623\lambda^2 + 1926\lambda + 800)}{16(\lambda + 1)(105\lambda^2 + 96\lambda + 35)} Ca. \tag{6.9}$$

The dependence of the viscometric coefficients on both $Re$ and $Ca$, and the related sign reversals, may be analysed by combining the known $O(\phi Ca)$ contributions (see Schowalter *et al.* 1968; Frankel & Acrivos 1970) with the inertial contributions summarized in (6.3)–(6.5); one obtains

$$\mu_e = 1 + \phi \left[ \frac{(5\lambda + 2)}{2(\lambda + 1)} + 0.024 Re^{3/2} \frac{(5\lambda + 2)^2}{(\lambda + 1)^2} + O(Re^2, ReCa, Ca^2) \right], \tag{6.10}$$

$$N_1 = \phi \left[ Ca \frac{(19\lambda + 16)^2}{40(\lambda + 1)^2} - Re \frac{4(3\lambda^2 + 3\lambda + 1)}{9(\lambda + 1)^2} + 0.066 Re^{3/2} \frac{(5\lambda + 2)^2}{(\lambda + 1)^2} \right.$$
$$\left. + O(Re^2, ReCa, Ca^2) \right], \tag{6.11}$$

$$N_2 = \phi \left[ -Ca \frac{(551\lambda^3 + 1623\lambda^2 + 1926\lambda + 800)}{280(\lambda + 1)^3} + Re \frac{2(105\lambda^2 + 96\lambda + 35)}{315(\lambda + 1)^2} \right.$$
$$\left. - 0.085 Re^{3/2} \frac{(5\lambda + 2)^2}{(\lambda + 1)^2} + O(Re^2, ReCa, Ca^2) \right]. \tag{6.12}$$

The above superposition is valid to $O(ReCa)$, which is when the contributions due to finite $Re$ and $Ca$ couple. For the range of $Re$ and $Ca$ under consideration, the $O(ReCa)$ contributions are, however, much smaller than those included in (6.10)–(6.12). A shear-thinning contribution, at $O(\phi Ca^2)$, has also been neglected in (6.10), since it is again expected to be much smaller than the $O(\phi Re^{3/2})$ shear-thickening contribution.

To examine the possibility of sign reversals for $N_2$, we equate (6.12) to zero, leading to a cubic equation in $Re^{1/2}$. Provided $0 < Ca < Ca_c$ with

$$Ca_c = 1.49 \times 10^{-3} \frac{(105\lambda^2 + 96\lambda + 35)^3(\lambda + 1)}{(5\lambda + 2)^4(551\lambda^3 + 1623\lambda^2 + 1926\lambda + 800)}, \tag{6.13}$$

this equation has a pair of positive roots. The corresponding critical Reynolds numbers are given by

$$Re_1^{N2} = \frac{\alpha_1^2}{9} \left[ 2\cos\left( \frac{\cos^{-1}\left[ \frac{(27\alpha_2 + 2\alpha_1^3)}{2\alpha_1^3} \right] + 4\pi}{3} \right) - 1 \right]^2, \tag{6.14}$$

$$Re_2^{N2} = \frac{\alpha_1^2}{9} \left[ 2\cos \left( \frac{\cos^{-1} \left[ \frac{(27\alpha_2 + 2\alpha_1^3)}{2\alpha_1^3} \right] + 2\pi}{3} \right) - 1 \right]^2, \qquad (6.15)$$

where

$$\alpha_1 = -0.075 \frac{(105\lambda^2 + 96\lambda + 35)}{(5\lambda + 2)^2}, \qquad (6.16)$$

$$\alpha_2 = 0.042 Ca \frac{(551\lambda^3 + 1623\lambda^2 + 1926\lambda + 800)}{(5\lambda + 2)^2(\lambda + 1)}, \qquad (6.17)$$

and the range of interest corresponds to $0 < \cos^{-1}[(27/\alpha_2 + 2\alpha_1^3)/2\alpha_1^3] < \pi$. The second normal stress difference must undergo a sign reversal at each of $Re_1^{N2}$ and $Re_2^{N2}$. With increasing $Re$, $N_2$ first changes from negative to positive at $Re = Re_1^{N2}$, and then becomes negative when $Re > Re_2^{N2}$ due to the eventual dominance of the $O(Re^{3/2})$ inertial correction. For $Ca \ll 1$, $Re_1^{N2} \approx Re_c^{N2} \sim O(Ca)$, while $Re_2^{N2}$ remains small but finite for all $\lambda$, being well approximated by $\bar{Re}_c^{N2}$ obtained above from a balance of the inertial terms alone (see (6.7)). Vivek Raja *et al.* (2010) neglected the $O(Re^{3/2})$ correction, and only found the first sign reversal at $Re_1^{N2} \approx Re_c^{N2}$. Next, equating $N_1$ to zero again yields a cubic equation. The critical Reynolds number obtained in this case, from equating the $O(Re)$ and $O(Re^{3/2})$ terms, remains of order unity or larger for all $\lambda$ (see (6.6)). As a result, the two positive roots of the cubic equation are well separated in the limit $Ca \ll 1$, and a general solution serves little purpose. The smaller of the two roots is well approximated by $Re_c^{N1}$ while the larger approaches $\bar{Re}_c^{N1}$. It is likely that $N_1$ changes from positive to negative at $Re = Re_c^{N1} \approx O(Ca)$ (the sign reversal found by Vivek Raja *et al.* 2010). The second sign reversal predicted at $Re = \bar{Re}_c^{N1}$ may, however, be outside the range of validity of the theory. For $Ca$ larger than the threshold value given by (6.13), the interval of sign reversal vanishes, and $N_2$ must always remain negative while continuing to exhibit a non-monotonic dependence on $Re$; a similar threshold for $N_1$ and the resulting non-monotonic behaviour may be outside the range of validity of the theory.

### 6.1. *Comparison with previous simulations of the rheology of dilute emulsions of slightly deformable drops*

With the above theoretical scenario in mind, we now compare (6.10)–(6.12), for $\lambda = 1$, with the viscometric coefficients obtained by Li & Sarkar (2005). The authors studied the effect of inertia on single drop deformation, and the implied steady shear rheology of a dilute emulsion, for a viscosity ratio of unity. A dilute emulsion undergoing simple shear flow was simulated by positioning a single drop between infinite parallel plates moving in opposite directions with periodic boundary conditions in the horizontal coordinates. The Navier–Stokes equations were solved using a front-tracking finite-difference method with the singular interfacial tension forces being distributed over a thin layer surrounding the drop. Figures 1 and 2 compare the theoretical predictions for $N_1$ and $N_2$ (normalized by $\phi$) with those obtained from simulations, and figure 3 presents a similar comparison for the shear viscosity. The theory being valid only for small $Re$, the comparison is restricted to $Re \leqslant 1$, although the simulation results are available for $Re$ up to 3.

In figures 1 and 2, we note that $Ca = 0.02$ is already large enough for there to be no sign reversal either for $N_1$ or $N_2$. Furthermore, the $O(\phi Re^{3/2})$ correction for $N_2$
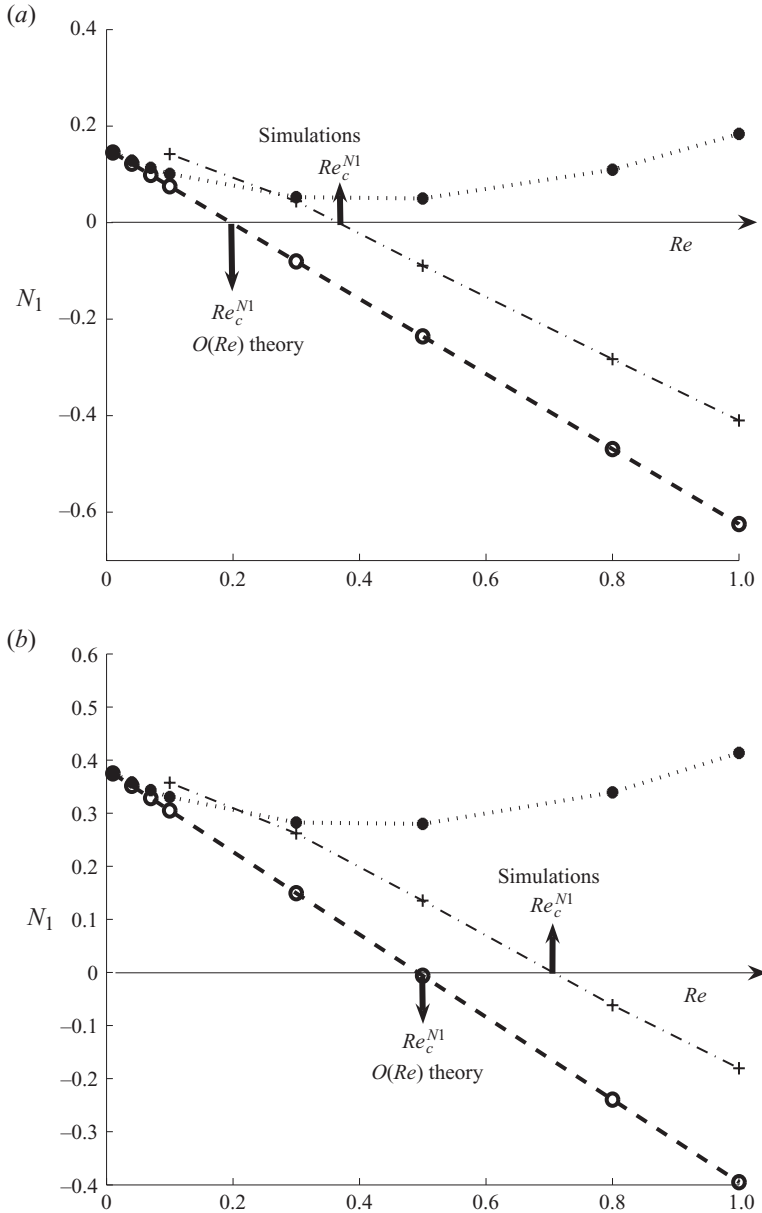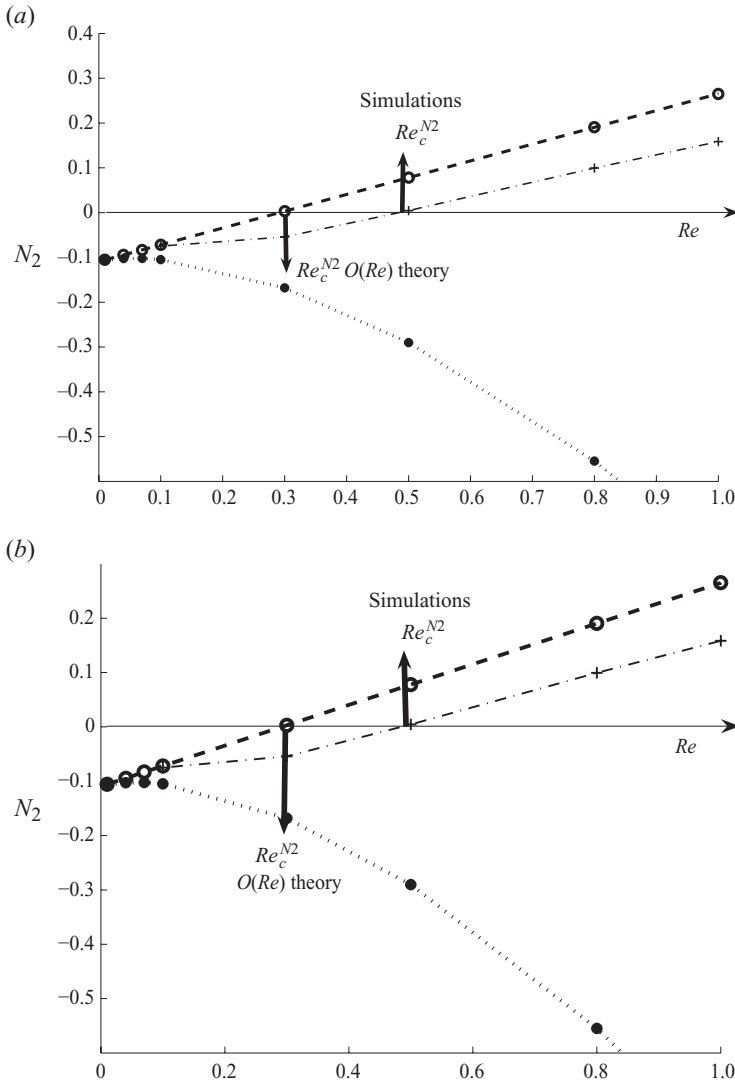
FIGURE 1. ($a, b$) The variation of the first normal stress difference including inertial corrections to $O(Re)$ (bold dashed line) and $O(Re^{3/2})$ (bold dotted line) from (6.11) as a function of $Re$ for $Ca = 0.02$ and $Ca = 0.05$; $\lambda = 1$. The dash-dotted lines in both figures denote the simulation results.

becomes dominant at a much smaller $Re$, and thus, while there is a significant region of non-monotonic variation for the theoretical $N_1$ curve, that for $N_2$ is restricted to $Re < 0.1$ (the smallest $Re$ in the simulations). One could find smaller values of $Ca$ at which both $N_1$ and $N_2$ exhibit intervals of reversed sign, but their relevance appears in doubt since the numerical results, even for $N_2$, are significantly different. The dependence of the computed normal stress differences on $Re$ is, in all cases,

(a)



(b)



FIGURE 2. (a, b) The variation of the second normal stress difference including inertial corrections to $O(Re)$ (bold dashed line) and $O(Re^{3/2})$ (bold dotted line) from (6.12) as a function of $Re$ for $Ca = 0.02$ and $Ca = 0.05$; $\lambda = 1$. The bold dash-dotted lines in both figures denote the simulation results.

monotonic, and the $O(\phi Re)$ theory of Vivek Raja *et al.* (2010) fares much better in comparison to the $O(\phi Re^{3/2})$ results derived here. For $N_1$, the latter theory appears to agree a little better with numerics for $Re \leqslant 0.3$, but for $N_2$, the $O(\phi Re)$ theory leads to a more accurate prediction over the entire range of $Re$ and $Ca$ examined. Moreover, the predictions of the $O(\phi Re^{3/2})$ theory rapidly worsen for $Re \geqslant 0.5$, being both of the wrong sign and slope in this range. It is also important to note that both the $O(\phi Re)$ and $O(\phi Re^{3/2})$ theories do not approach the computed results even at the smallest $Re$, a discrepancy already noted by Vivek Raja *et al.* (2010). Notwithstanding this last observation, it is tempting to attribute the deviations to the asymptotic nature of the perturbation expansion; in which case, the $O(Re^{3/2})$ corrections, while making the
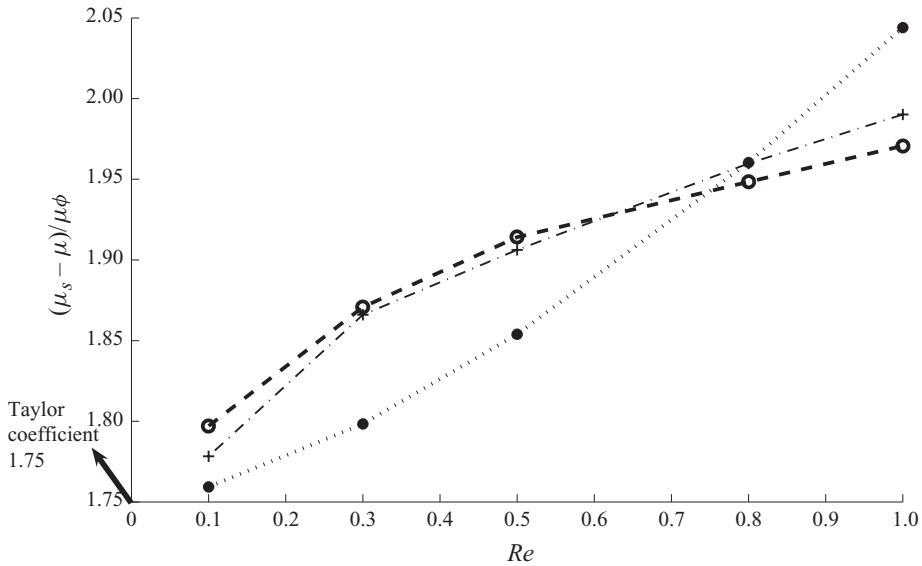
FIGURE 3. The variation of the $O(\phi)$ correction to the shear viscosity of the suspending fluid, as a function of $Re$, from both theory ((6.10), dotted line) and simulation. The dashed and dash-dotted lines denote the simulation results for $Ca = 0.02$ and $Ca = 0.05$, respectively.

expansion more accurate for small $Re$, do not extend its range of validity. Thus, the predicted sign reversals of $N_2$, and perhaps, even the non-monotonic dependence for either $N_2$ or $N_1$, are in a range of $Re$ where higher-order inertial corrections become equally important.

Figure 3 for the shear viscosity does raise some questions about the accuracy of the simulations, however. The significant discrepancy between theory and numerics even at $Re = 0.1$ is not unexpected; for instance, the comparison given in Mikulencak & Morris (2004) for the shear component of the rigid particle stresslet $(\lambda \to \infty)$ reveals a significant discrepancy between theory and numerics at the same $Re$ (this comparison is more relevant than that for normal stresses, since the stresslet contribution provides a reasonable approximation to the total shear viscosity to $O(Re^{3/2})$). More troubling is the qualitative difference between theory and computation. While the former predicts a viscosity enhancement of $O(Re^{3/2})$, the computed viscosity only shows a sub-linear growth with increasing $Re$. The near coincidence of the $Ca = 0.02$ and $Ca = 0.05$ curves at the smaller values of $Re$ implies that this difference is not related to drop deformation (the two curves do depart at higher $Re$, perhaps due to the coupled effects of inertia and drop deformation not included in the theory). An examination of the corresponding plot in Mikulencak & Morris (2004) shows that the suspension shear viscosity (the stresslet contribution) exhibits a faster-than-linear growth up until $Re \approx 1$. Also, in contrast to figure 3, the computed suspension viscosity is smaller than the corresponding theoretical prediction at any finite $Re$. In fact, for $Re = 0.1$, the computed enhancement in the suspension viscosity appears to be smaller than that computed for an emulsion with $\lambda = 1$ (and $Ca = 0.02$). This is again surprising since the theory predicts that the effect of the viscosity ratio on the inertial correction at $O(Re^{3/2})$ is entirely contained in the factor $[(5\lambda + 2)/(\lambda + 1)]^2$, which increases from 12.25 at $\lambda = 1$ to 25 for $\lambda \to \infty$. Thus, for sufficiently small $Ca$ (the case here),

the viscosity enhancement of an emulsion of unit viscosity ratio must be significantly smaller than that for a suspension.

### 6.2. *Finite volume simulation of the stresslet of non-deformable drops at finite Reynolds numbers*

The discrepancies revealed in §6.1, from the detailed comparison of the $O(\phi Re^{3/2})$ theory with available numerical results, have highlighted the need for an accurate simulation of an infinitely dilute emulsion, over a range of viscosity ratios, particularly for small $Re$. Towards this end, we now report results obtained by simulating an isolated neutrally buoyant spherical drop of variable viscosity, over a range of $Re$, subjected to a simple shear flow. Enforcing a spherical shape implies that, unlike Li & Sarkar (2005), our computations do not explicitly include drop deformation, and thereby, only help evaluate the theoretical estimates for the inertial contributions to the bulk stress. Ideally, one would want accurate estimates for both the stresslet and Reynolds stress contributions. However, the numerical calculation of the Reynolds stress integrals at small $Re$ is a delicate task with the dominant contributions arising at large distances of $O(Re^{-1/2})$; our computations confirm this difficulty and the results for the Reynolds stresses proved to be very sensitive to the size of the computational domain. The results included here are therefore restricted to the stresslet components obtained by substituting the computed velocity and stress fields on the drop surface in the first term in (3.2).

The equation of continuity and the steady Navier–Stokes equations are solved in dimensionless form both inside and outside the drop using a control volume formulation with the SIMPLE algorithm (see Mao & Chen 1997); the Reynolds numbers are defined in the same way as in §2. Preservation of a spherical shape demands a vanishing normal velocity component at the drop surface ($r = 1$). One needs to additionally implement equality of the interior and exterior tangential velocity and stress components at $r = 1$; the required interfacial jump in normal stress is balanced by a slight deformation (that is not explicitly calculated). The far-field boundary condition of simple shear flow is applied on a distant spherical boundary of radius $R_{inf}$. The grid for all computations consists of 30 and 60 uniform nodes in the $\theta$ and $\phi$ directions, respectively; here, $\theta$ is the polar angle with the vorticity axis of the ambient simple shear and $\phi$ is the dihedral angle between the gradient-vorticity plane and the plane containing the position ($\boldsymbol{r}$) and ambient vorticity vectors. For $Re \leqslant 1$, the exterior domain has 135 nodes in the radial direction; the region near the drop surface is finely resolved with the 10 modes closest to the surface having a spacing of $\Delta r = 2.5 \times 10^{-3}$. An additional 20 nodes are used inside the drop with the 5 nodes nearest the surface again having a spacing of $\Delta r = 2.5 \times 10^{-3}$. The computations for larger $Re$ begin to exhibit an insensitivity to domain size at smaller values of $R_{inf}$, and the total number of nodes in the radial direction therefore decreases in general with increasing $Re$.

Figure 4 depicts the variation of the stresslet contributions to the viscometric coefficients, suitably scaled, with $Re$, for different values of $R_{inf}$ and for $\lambda = 1$ and $\lambda = \infty$ (the surface boundary condition in this latter case is one of rigid rotation consistent with a zero-torque condition, and only the exterior fields need to be solved for; see Mikulencak & Morris 2004). The plots show that, in the range $Re \leqslant 1$, the computed values become insensitive to the domain size once $R_{inf}$ exceeds 64.6. The increasing insensitivity to domain size for the larger values of $Re$ is already evident, and is confirmed later in figure 13 for larger $Re$.
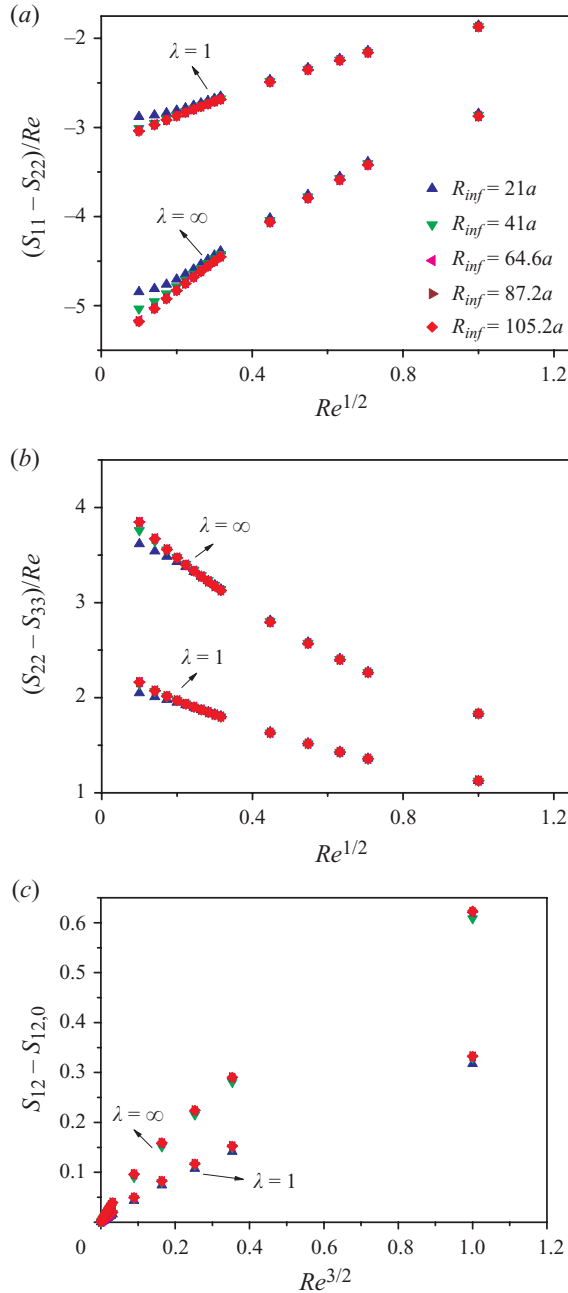
FIGURE 4. (Colour online) Variation of $(a, b)$ the first and second normal stresslet differences and $(c)$ the shear component of the stresslet, with $Re$, for different values of $R_{inf}$.

Figure 5 compares the computed diagonal stresslet components $(R_{inf} = 105.2)$ with the analytical results for different viscosity ratios. The first and second normal stress differences, normalized by $Re$, and plotted as a function of $Re^{1/2}$, show good agreement with the theoretical predictions for small $Re$; the nearly linear variation in this range confirms the $Re^{3/2}$ scaling. In the range $0.01 < Re < 0.1$, the slopes and intercepts
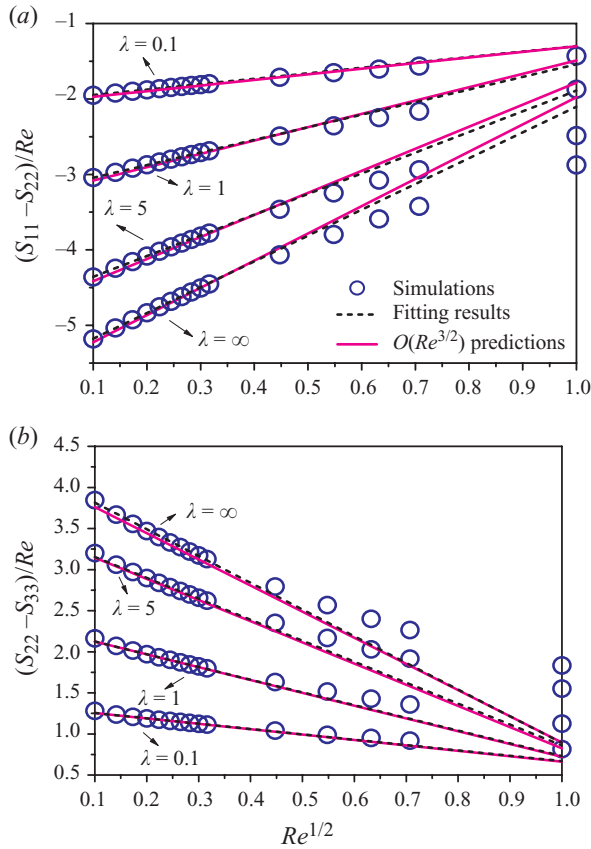
FIGURE 5. (Colour online) $(a,b)$ Plots of $(S_{11}-S_{22})/Re$ and $(S_{22}-S_{33})/Re$ as a function of $Re^{1/2}$.

obtained by fitting the computed curves for $(S_{11} - S_{22})/Re$ and $(S_{22} - S_{33})/Re$ versus $Re^{1/2}$ are respectively $0.72, -2.02$ and $-0.65, 1.32$ for $\lambda = 0.1$, which are close to the corresponding analytical values of $0.75, -2.05$ and $-0.66, 1.32$. Similar results for other values of $\lambda$ are shown in table 1.

Figure 6 plots, as a function of $Re^{3/2}$, the difference between the shear component of the stresslet and its extrapolated value $(S_{12,0})$ for $Re = 0$. The difference rather than the absolute value is used since $S_{12,0}$ deviates slightly from the classical Taylor coefficient primarily due to the finite computational domain; for instance, with $\lambda = 0.1$ and $Re = 10^{-6}$, $S_{12,0} \approx 4.746$, while the corresponding analytical value for $Re = 0$ is 4.76. In contrast to the diagonal components, the numerical results for $(S_{12}-S_{12,0})$ depart significantly from the analytical asymptotes even in the range $0.01 < Re < 0.1$, implying a greater sensitivity to higher-order inertial effects not included in the theory. A similar behaviour was found earlier for a rigid particle (see Mikulencak & Morris 2004). The validation of the theoretical prediction for the shear component evidently requires smaller values of $Re$, and hence, larger domain sizes. To avoid an unrealistically large computational domain, we account for the systematic dependence of the numerical results on $R_{inf}$ (this dependence being stronger than that for the diagonal components), and the extrapolated value obtained in the limit of an infinite domain is then used for comparison with theory. Thus, figure 7($a$) shows the shear

| $\lambda$ | Simulation fit $(0.01 < Re < 0.1)$ | Theory |
|---|---|---|
| 0.1 | $(S_{11} - S_{22})/Re = 0.72Re^{1/2} - 2.01$ | $(S_{11} - S_{22})/Re = 0.75Re^{1/2} - 2.05$ |
|  | $(S_{22} - S_{33})/Re = -0.65Re^{1/2} + 1.32$ | $(S_{22} - S_{33})/Re = -0.66Re^{1/2} + 1.32$ |
| 1 | $(S_{11} - S_{22})/Re = 1.67Re^{1/2} - 3.21$ | $(S_{11} - S_{22})/Re = 1.77Re^{1/2} - 3.26$ |
|  | $(S_{22} - S_{33})/Re = -1.55Re^{1/2} + 2.28$ | $(S_{22} - S_{33})/Re = -1.56Re^{1/2} + 2.28$ |
| 5 | $(S_{11} - S_{22})/Re = 2.74Re^{1/2} - 4.63$ | $(S_{11} - S_{22})/Re = 2.92Re^{1/2} - 4.71$ |
|  | $(S_{22} - S_{33})/Re = -2.55Re^{1/2} + 3.41$ | $(S_{22} - S_{33})/Re = -2.58Re^{1/2} + 3.40$ |
| $\infty$ | $(S_{11} - S_{22})/Re = 3.42Re^{1/2} - 5.52$ | $(S_{11} - S_{22})/Re = 3.61Re^{1/2} - 5.59$ |
|  | $(S_{22} - S_{33})/Re = -3.25Re^{1/2} + 4.14$ | $(S_{22} - S_{33})/Re = -3.18Re^{1/2} + 4.08$ |

TABLE 1. Comparison of the normal stress differences (the stresslet contributions) between simulations and theory.
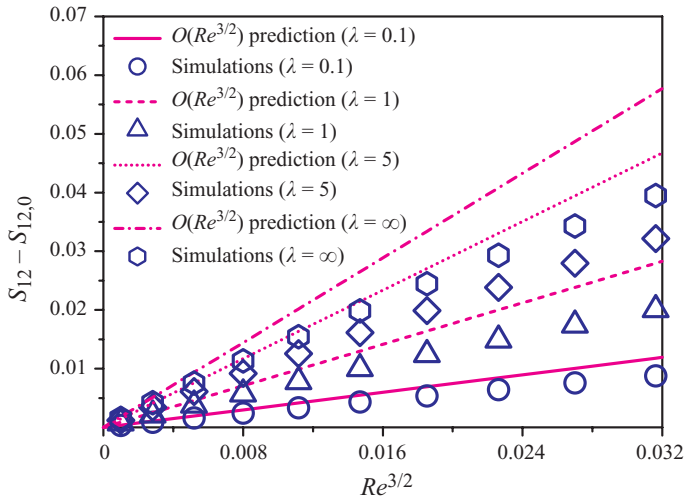


FIGURE 6. (Colour online) Plot of $(S_{12}-S_{12,0})$ as a function of $Re^{3/2}$; here, $S_{12,0}$ is the stresslet coefficient for $Re = 0$.

component of the rigid particle stresslet, again as a function of $Re^{3/2}$, but in the range $0.0005 < Re < 0.01$ with $R_{inf} = 64.6$, 87.2, 105.2 and 153. The data for each $R_{inf}$ are fitted well by a straight line passing through the origin, confirming the proportionality to $Re^{3/2}$ in the limit $Re \to 0$. Figure 7(b) includes a plot of the slopes of these straight line fits against $1/R_{inf}$. The plot yields an extrapolated slope of 1.79 in the limit $R_{inf} \to \infty$, which is very close to the analytical value of 1.80 (see (4.75)). A similar trend is observed for $\lambda = 5$ and the corresponding plots appear in figures 8(a) and 8(b).

The plots in figures 9–12 show the computed stresslet components for intermediate $Re$ $(1 \leqslant Re \leqslant 10)$, for different values of $\lambda$, when the theoretical predictions no longer hold. These computations were carried out for $R_{inf} = 28$, and figure 13 shows that the results are already representative of those of an infinite domain. For this range of $Re$, the computations for a rigid particle failed to converge beyond a critical ($Re$-dependent) $R_{inf}$, which is related to the failure of the iteration needed to approach a torque-free condition. This critical value was much smaller than that found for large but finite viscosity ratios, and as a result, the converged results for a rigid particle
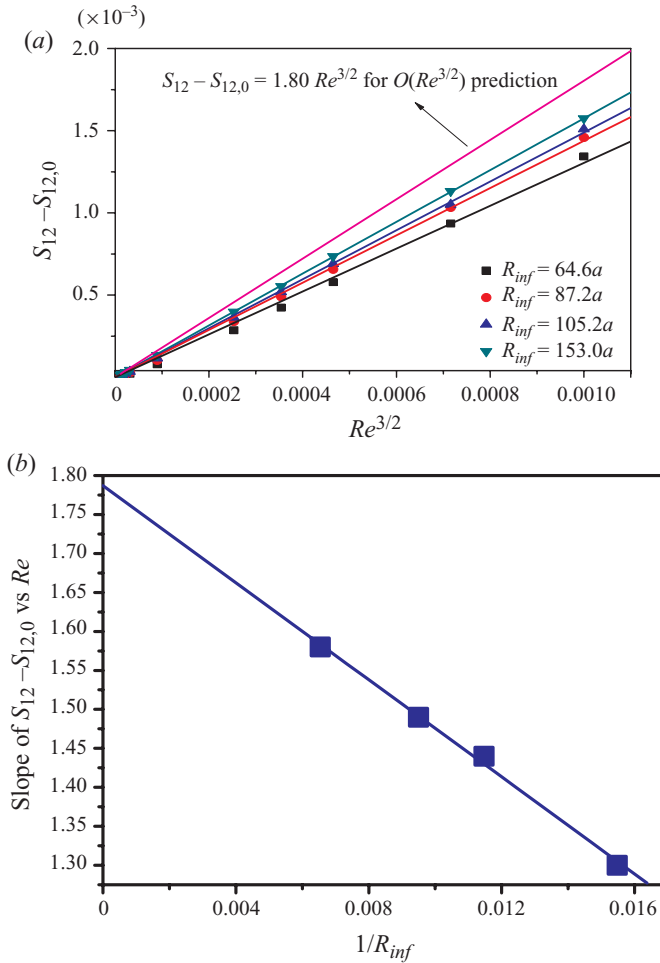
FIGURE 7. (Colour online) (*a*) Plots of $(S_{12} - S_{12,0})$ versus $Re^{3/2}$ for different values of $R_{inf}$ for $\lambda = \infty$. (*b*) The straight line slopes, obtained from the plot of $(S_{12} - S_{12,0})$ versus $Re^{3/2}$ in (*a*), plotted against $1/R_{inf}$.

continued to exhibit a domain-size dependence. To circumvent this difficulty, we obtained the viscometric coefficients for a rigid particle by extrapolating the results for drops of high viscosity. Figure 14 shows the variation of the three viscometric coefficients with $\lambda$ for $Re = 10$ (which exhibited the greatest sensitivity to domain size for $Re \geqslant 1$) and with $R_{inf} = 28$; a similar calculation for $R_{inf} = 56$ gave nearly coincident results. The large value of $\lambda$ needed for attainment of the $\lambda \to \infty$ plateau differs from one viscometric coefficient to the other. Nevertheless, regression fits show that the values for $\lambda = 20$ are already within 3 % of the corresponding values for a rigid particle for $Re = 10$. Results obtained from computations of rigid particles are consistent with the large $\lambda$ limits found in the above manner, although minor differences persist due to the restriction to smaller domain sizes in these cases.

It is seen from figures 9–12 that the three viscometric coefficients exhibit a near-linear variation in the range $1 \leqslant Re \leqslant 10$. The linearity appears consistent with the expected $O(\rho\dot{\gamma}^2 a^2)$ scaling for the stresses at moderate $Re$. This seems reasonable for the diagonal components which are $O(Re)$ in the limit $Re \to 0$. The $O(Re^{3/2})$ scaling
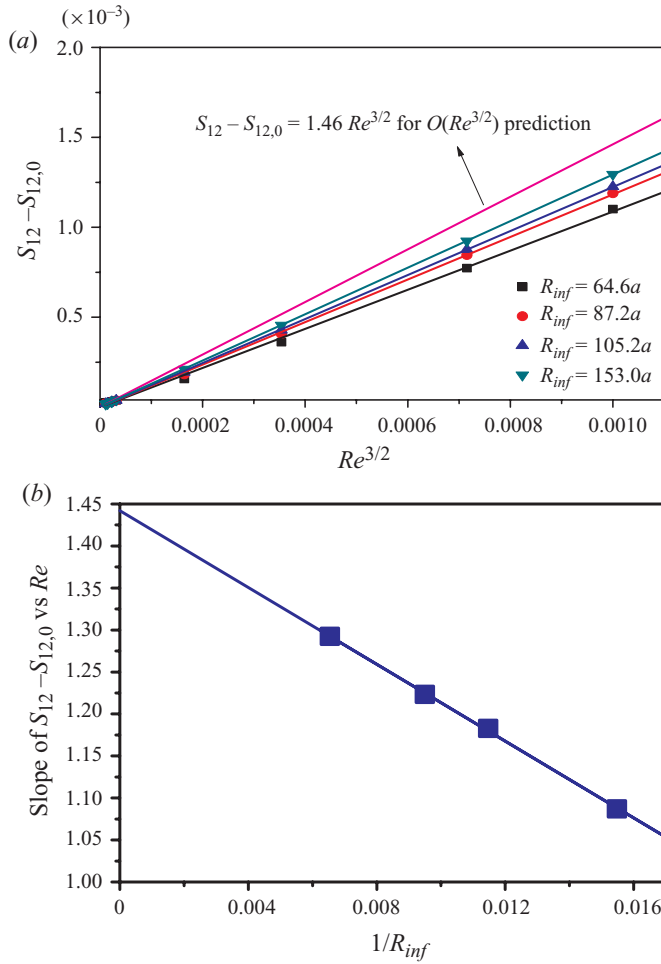
FIGURE 8. (Colour online) (a) Plots of $(S_{12} - S_{12,0})$ versus $Re^{3/2}$ for different values of $R_{inf}$ for $\lambda = 5$. (b) The straight line slopes, obtained from the plot of $(S_{12} - S_{12,0})$ versus $Re^{3/2}$ in (a), plotted against $1/R_{inf}$.

for the shear component arises from the fractional ($O(Re^{-1/2})$) scaling for the inertial screening length for small $Re$; since the screening length is $O(a)$ for $Re$ of $O(1)$ or larger, an $O(Re)$ scaling for moderate $Re$ continues to be reasonable in this case. The moderate-$Re$ results may therefore be fitted by an expression of the form

$$\frac{S}{Re} = P_1 + \frac{P_2}{Re}, \qquad (6.18)$$

where $S$ is any one of $S_{11} - S_{22}$, $S_{22} - S_{33}$ or $S_{12} - S_{12,0}$. On the other hand, taking the analysis of earlier sections into account, $S$ must reduce to the form

$$\frac{S}{Re} = \hat{P}_1 + \hat{P}_2 Re^{1/2}, \qquad (6.19)$$

in the limit $Re \to 0$; here, the coefficients $\hat{P}_i$ may be obtained from the predictions for the viscometric coefficients (see (6.3)–(6.5)). A simple empirical fit, applicable to the
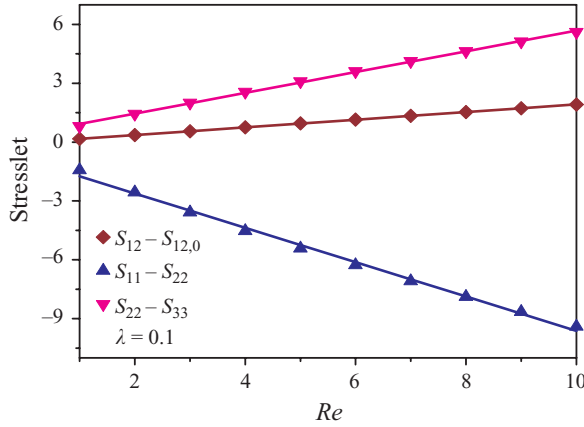
FIGURE 9. (Colour online) The plots of $S_{11} - S_{22}$, $S_{22} - S_{33}$ and $S_{12} - S_{12,0}$ as a function of $Re$ for $\lambda = 0.1$; $R_{inf} = 28$.
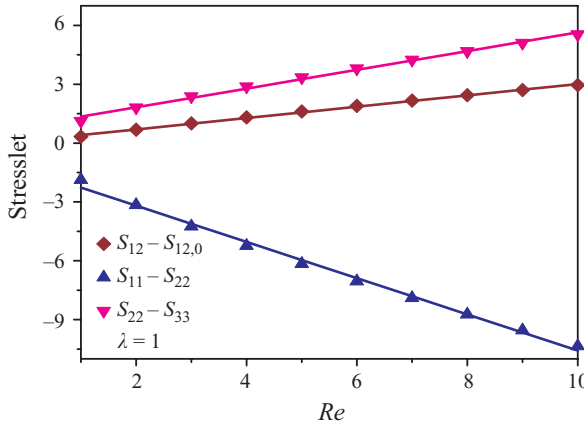


FIGURE 10. (Colour online) The plots of $S_{11} - S_{22}$, $S_{22} - S_{33}$ and $S_{12} - S_{12,0}$ as a function of $Re$ for $\lambda = 1$; $R_{inf} = 28$.
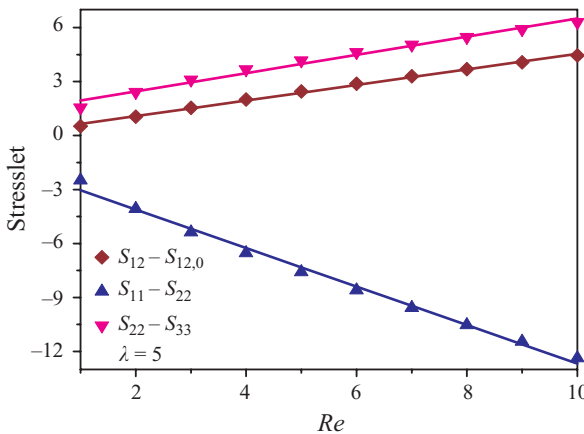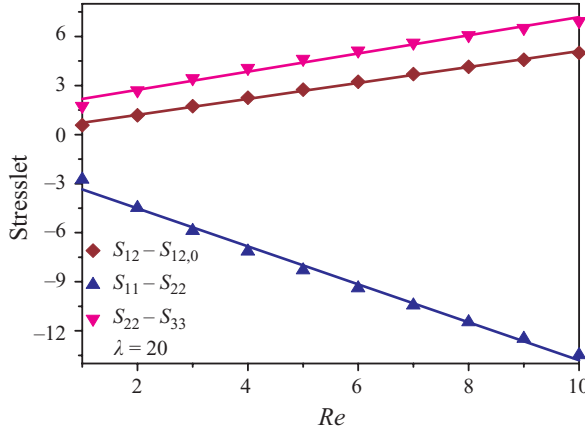


FIGURE 11. (Colour online) The plots of $S_{11} - S_{22}$, $S_{22} - S_{33}$ and $S_{12} - S_{12,0}$ as a function of $Re$ for $\lambda = 5$; $R_{inf} = 28$.

FIGURE 12. (Colour online) The plots of $S_{11} - S_{22}$, $S_{22} - S_{33}$ and $S_{12} - S_{12,0}$ as a function of $Re$ for $\lambda = 20$; $R_{inf} = 28$.

whole range of $Re$ under consideration, may therefore be taken as

$$\frac{S}{Re} = \hat{P}_1 \frac{1 + q_1 Re^{1/2} + p_1 Re}{1 + q_2 Re^{1/2} + p_2 Re}. \tag{6.20}$$

The undetermined parameters $(p_1, p_2, q_1, q_2)$ may be determined by enforcing the analytical form in the limit $Re \to 0$, and in addition, using the computed values for large $Re$. Equation (6.20) is, however, only applicable to the normal stress differences. The shear component, $S_{12} - S_{12,0}$, is $O(Re^{3/2})$ for small $Re$, and hence, $\hat{P}_1 = 0$ in (6.19) for this case. Thus, the empirical fit appropriate for $S_{12} - S_{12,0}$ must be of the form

$$\frac{S}{Re} = \hat{P}_2 \frac{Re^{1/2} + p_1 Re}{1 + q_2 Re^{1/2} + p_2 Re}, \tag{6.21}$$

where the unknown parameters may be determined in the manner described above. The values of these parameters for different $\lambda$ are shown in table 2. The accuracy of the derived empirical fits for $Re \leqslant 10$ is highlighted in figures 15–18, where the fits appear together with the predictions of the small-$Re$ theoretical analysis and the computed values in the intermediate range of $Re$.

In summary, the computations presented in this section confirm the analytical predictions for the stresslet components, to $O(Re^{3/2})$. In addition, the empirical fits derived from the computed stresslet values extend up to a Reynolds number of 10 over a wide range of viscosity ratios.

## 7. Conclusions and discussion

In this paper, we have determined the dispersed-phase stress tensor for a dilute emulsion in simple shear flow which, to $O(\phi Re^{3/2})$, is given by

$$\boldsymbol{\Sigma}^{(d)} = \phi \left[ \frac{(5\lambda + 2)}{2(\lambda + 1)}(\mathbf{1}_1\mathbf{1}_2 + \mathbf{1}_2\mathbf{1}_1) - Re \left( \frac{2(3\lambda^2 + 3\lambda + 1)}{9(\lambda + 1)^2}(\mathbf{1}_1\mathbf{1}_1 - \mathbf{1}_2\mathbf{1}_2) \right. \right.$$
$$\left. - \frac{2\lambda}{35(\lambda + 1)^2}(\mathbf{1}_1\mathbf{1}_1 + \mathbf{1}_2\mathbf{1}_2) \right) + Re^{3/2} \frac{(5\lambda + 2)^2}{(\lambda + 1)^2} \left( \frac{1}{6\pi^2}\{0.76\mathbf{1}_1\mathbf{1}_1 - 1.28\mathbf{1}_2\mathbf{1}_2 \right.$$
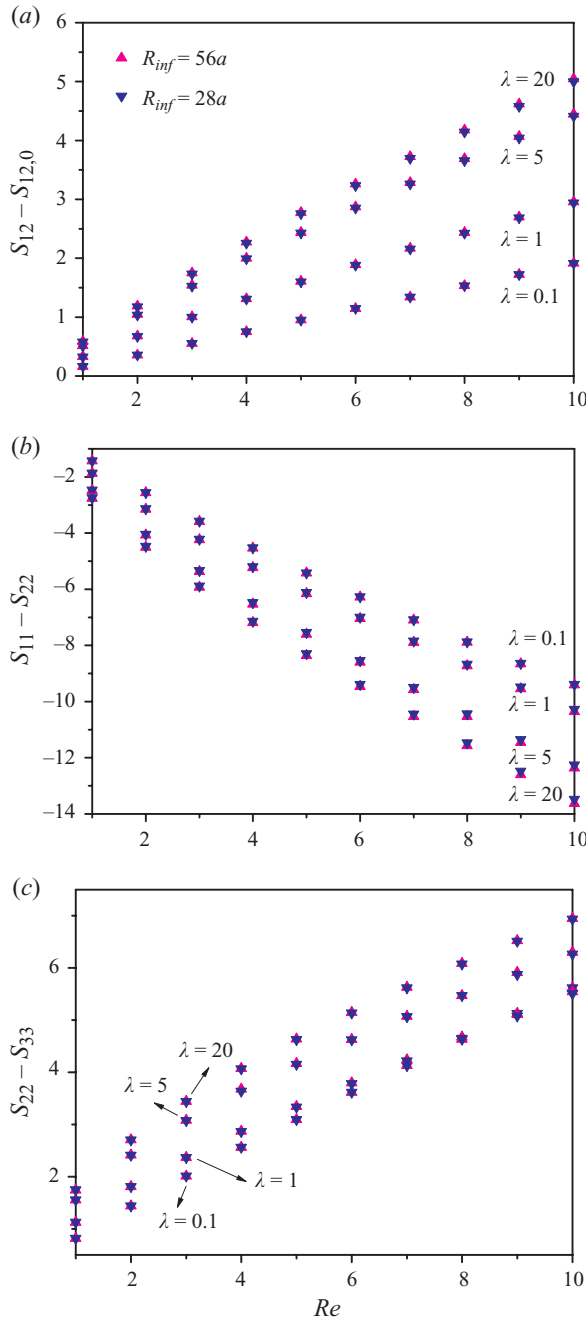
FIGURE 13. (Colour online) (*a–c*) The plots of $S_{12} - S_{12,0}$, $S_{11} - S_{22}$ and $S_{22} - S_{33}$ as a function of $Re$ for $\lambda = 0.1$, 1, 5 and 20; $R_{inf} = 28$ and 56.

$$+ 1.02(\mathbf{1}_1\mathbf{1}_2 + \mathbf{1}_2\mathbf{1}_1) + 0.52\mathbf{1}_3\mathbf{1}_3\} + \frac{3}{32\pi^4}\{-41.58\mathbf{1}_1\mathbf{1}_1 - 74.74\mathbf{1}_2\mathbf{1}_2$$

$$+ 7.4(\mathbf{1}_1\mathbf{1}_2 + \mathbf{1}_2\mathbf{1}_1) - 18.04\mathbf{1}_3\mathbf{1}_3\}\bigg)\bigg] + O(\phi Re^2, \phi^2). \tag{7.1}$$

| $\lambda$ | Stresslet component | Pre-factor | Parameters in the fitting expressions | | | |
|---|---|---|---|---|---|---|
| | | | $q_1$ | $p_1$ | $q_2$ | $p_2$ |
| 0.1 | $S_{11} - S_{22}$ | $\hat{P}_1 = -2.05$ | 0.27 | 0.69 | 0.64 | 1.60 |
| | $S_{22} - S_{33}$ | $\hat{P}_1 = 1.32$ | 0.33 | 0.97 | 0.83 | 2.41 |
| | $S_{12} - S_{12,0}$ | $\hat{P}_2 = 0.37$ | – | 4.15 | 1.91 | 7.92 |
| 1 | $S_{11} - S_{22}$ | $\hat{P}_1 = -3.26$ | 0.21 | 0.55 | 0.76 | 1.94 |
| | $S_{22} - S_{33}$ | $\hat{P}_1 = 2.28$ | 0.18 | 0.47 | 0.87 | 2.26 |
| | $S_{12} - S_{12,0}$ | $\hat{P}_2 = 0.88$ | – | 15.88 | 3.05 | 48.47 |
| 5 | $S_{11} - S_{22}$ | $\hat{P}_1 = -4.71$ | 0.18 | 0.46 | 0.80 | 2.01 |
| | $S_{22} - S_{33}$ | $\hat{P}_1 = 3.40$ | 0.13 | 0.32 | 0.89 | 2.14 |
| | $S_{12} - S_{12,0}$ | $\hat{P}_2 = 1.46$ | – | 19.31 | 3.37 | 65.06 |
| 20 | $S_{11} - S_{22}$ | $\hat{P}_1 = -5.32$ | 0.18 | 0.45 | 0.82 | 2.07 |
| | $S_{22} - S_{33}$ | $\hat{P}_1 = 3.88$ | 0.13 | 0.31 | 0.90 | 2.17 |
| | $S_{12} - S_{12,0}$ | $\hat{P}_2 = 1.70$ | – | 24.09 | 3.49 | 84.09 |

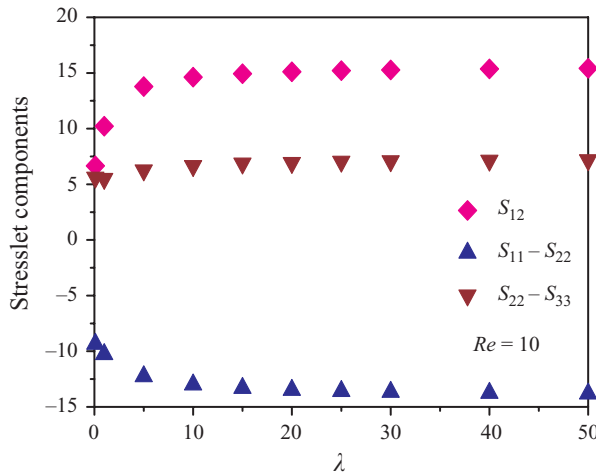TABLE 2. Coefficients of the fitting expressions for the components for $Re \leqslant 10$.



FIGURE 14. (Colour online) The plots of $S_{11} - S_{22}$, $S_{22} - S_{33}$ and $S_{12}$ as a function of $\lambda$ for $Re = 10$; the results shown are for $R_{inf} = 28$.

The separate contributions of the stresslet and the Reynolds stresses, to this order, are given by

$$\frac{(5\lambda + 2)}{2(\lambda + 1)}(\mathbf{1}_1\mathbf{1}_2 + \mathbf{1}_2\mathbf{1}_1) - Re\left[\frac{2(3\lambda^2 + 3\lambda + 1)}{9(\lambda + 1)^2}(\mathbf{1}_1\mathbf{1}_1 - \mathbf{1}_2\mathbf{1}_2) + \frac{(43\lambda^2 + 36\lambda + 8)}{140(\lambda + 1)^2}\right.$$

$$\left.\times (\mathbf{1}_1\mathbf{1}_1 + \mathbf{1}_2\mathbf{1}_2)\right] + Re^{3/2}\frac{(5\lambda + 2)^2}{6\pi^2(\lambda + 1)^2}[0.76\mathbf{1}_1\mathbf{1}_1 - 1.28\mathbf{1}_2\mathbf{1}_2 + 1.02(\mathbf{1}_1\mathbf{1}_2 + \mathbf{1}_2\mathbf{1}_1)$$

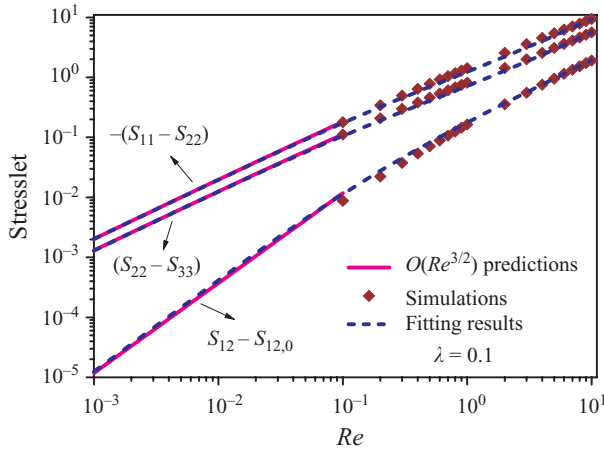$$+ 0.52\mathbf{1}_3\mathbf{1}_3], \tag{7.2}$$

FIGURE 15. (Colour online) Variation of stresslet components with *Re* for $\lambda = 0.1$.
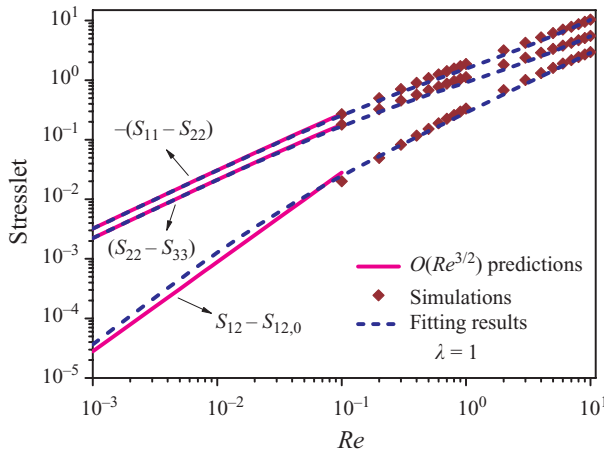


FIGURE 16. (Colour online) Variation of stresslet components with *Re* for $\lambda = 1$.
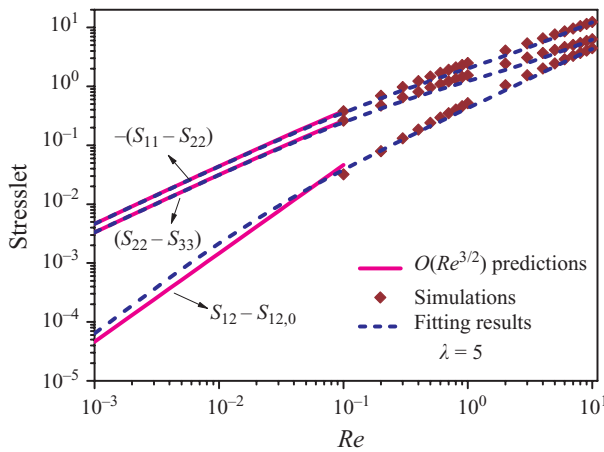


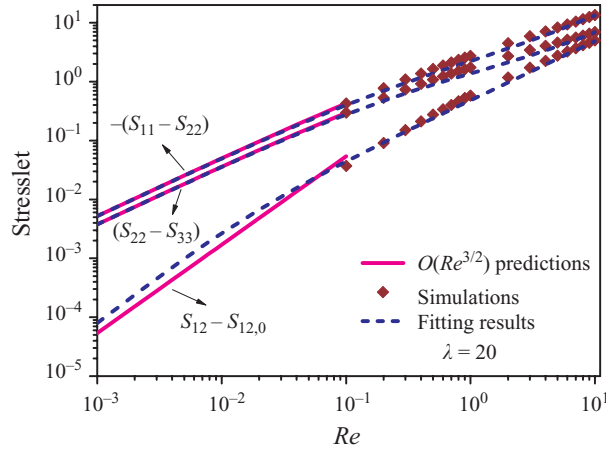FIGURE 17. (Colour online) Variation of stresslet components with *Re* for $\lambda = 5$.

FIGURE 18. (Colour online) Variation of stresslet components with $Re$ for $\lambda = 20$.

and

$$-\frac{Re}{4}\left(\frac{2(5\lambda+2)^2}{35(\lambda+1)^2} - \frac{2\lambda(5\lambda+2)}{35(\lambda+1)^2} + \frac{3\lambda^2}{35(\lambda+1)^2}\right)(\mathbf{1_1 1_1} + \mathbf{1_2 1_2})$$

$$+\frac{3Re^{3/2}}{32\pi^4}\{-41.58\mathbf{1_1 1_1} - 74.74\mathbf{1_2 1_2} + 7.4(\mathbf{1_1 1_2} + \mathbf{1_2 1_1}) - 18.04\mathbf{1_3 1_3}\}, \tag{7.3}$$

respectively. The resulting shear viscosity and the first and second normal stress differences are respectively

$$\mu_e = 1 + \phi\left[\frac{(5\lambda+2)}{2(\lambda+1)} + 0.024Re^{3/2}\frac{(5\lambda+2)^2}{(\lambda+1)^2}\right] + O(\phi Re^2, \phi^2), \tag{7.4}$$

$$N_1 = \phi\left[-Re\frac{4(3\lambda^2+3\lambda+1)}{9(\lambda+1)^2} + 0.066Re^{3/2}\frac{(5\lambda+2)^2}{(\lambda+1)^2}\right] + O(\phi Re^2, \phi^2), \tag{7.5}$$

$$N_2 = \phi\left[Re\frac{2(105\lambda^2+96\lambda+35)}{315(\lambda+1)^2} - 0.085Re^{3/2}\frac{(5\lambda+2)^2}{(\lambda+1)^2}\right] + O(\phi Re^2, \phi^2). \tag{7.6}$$

The analytical predictions for the stresslet components are in agreement with the computations for small $Re$ and over a range of viscosity ratios. The numerical results presented are based on a control volume formulation for a spherical drop, and extend up to $Re = 10$. These results show that the predicted shear-thickening of the viscosity, for small $Re$, becomes milder for Reynolds number of order unity or larger; a similar change in the scaling of the normal stress differences is much weaker. The analytical and numerical results together allow the development of empirical fits for each viscometric coefficient valid for $Re \leqslant 10$. The fits are shown in figures 15–18 and capture the above transition in the shear-thickening behaviour. In the limit $\lambda \to \infty$, both the analysis and the numerical results agree with the earlier computations of the rigid particle stresslet by Mikulencak & Morris (2004). The only available numerical estimates for the Reynolds stress contributions are those of Li & Sarkar (2005) for a dilute emulsion with a viscosity ratio of unity. A comparison of the theory and numerics, however, shows a significant discrepancy even at the smallest $Re$. It is not clear if the disagreement arises due to the neglect of higher-order inertial corrections in the theoretical analysis, or due to the known sensitivity of the Reynolds stress integrals, particularly at small $Re$, to the size of the computational domain.

From the theoretical expressions for the viscometric coefficients, we note that the Reynolds stress integrals contribute significantly to the two normal stress differences (48 % of the total $N_1$ and 64 % of the total $N_2$), but a partial cancellation on account of the opposing signs of $(R_{12} + R_{21})$ and $Q_{12}$ leads to a smaller contribution (less than 30 %) to the shear viscosity at $O(\phi Re^{3/2})$. The earlier estimate of Stone et al. (2000) for the inertial corrections to the suspension stress, which omitted the contributions due to the Reynolds stresses, underpredicts the shear viscosity by about 29 %. The relative dominance of the shear component of the stresslet implies, however, that a large part of the shear-thickening owes its origin to the linear flow set up in the matching region by the outer velocity field (the elements of whose velocity gradient tensor are, within a proportionality factor, given by (4.69)–(4.73)). This flow reinforces the extensional character of the ambient simple shear in the 12th quadrant; the drop is thus stretched further along the 45° direction in this quadrant. The amplitude of the former flow is $O(Re^{3/2})$, a nonlinear function of the shear rate, leading to the shear-rate-dependent increase in the viscosity.

The inertial shear-thickening for a suspension in an ambient linear flow (not just simple shear) may, in fact, be deduced without a detailed calculation. The argument is easiest for an extensional flow, in which case the particle angular velocity is identically zero by symmetry, and both the Stokes and inertial velocity fields satisfy the same boundary conditions. As pointed out by Ryskin (1980), it follows immediately from Helmholtz's minimum dissipation theorem (see Batchelor 1967; Kim & Karrila 1991) that the inertial correction to the dissipation must be positive definite. Note that the theorem only predicts the dissipation at finite $Re$ to be greater than that at $Re = 0$, and the extensional viscosity could, in principle, have a non-monotonic dependence on $Re$ (without dipping below the Stokes value). The first effects of inertia must nevertheless lead to an extension-thickening. For linear flows with vorticity, the particle angular velocity, and therefore the velocity boundary conditions, are a function of $Re$. Although a direct application of Helmholtz's theorem is not possible as a result, one is led to the same conclusion starting from the following expression for the average (non-dimensional) dissipation in a representative microscopic volume:

$$2\mu_s \boldsymbol{E} : \boldsymbol{E} = 2 \left[ (1 + \phi) \boldsymbol{E} : \boldsymbol{E} + \frac{3\phi}{4\pi} \int_{V - V_p} \boldsymbol{e} : \boldsymbol{e} \, \mathrm{d}V \right], \qquad (7.7)$$

where $\mu_s$ denotes the suspension viscosity and $(V - V_p)$ denotes the unbounded fluid domain. In (7.7), the excess dissipation due to the particulate phase is divided into two parts: a kinematic enhancement that arises because the rate of strain in the suspending fluid has to increase in order to conform to the specified average rate of strain ($\boldsymbol{E}$) in the suspension; and an additional integral, over the fluid domain, of a quadratic functional of the perturbation strain rate ($\boldsymbol{e}$) induced by the particle. If $\boldsymbol{e}^{(0)}$ denotes the corresponding perturbation strain rate at $Re = 0$, one may write (7.7) in the form

$$2\mu_s \boldsymbol{E} : \boldsymbol{E} = 2 \left[ (1 + \phi) \boldsymbol{E} : \boldsymbol{E} + \frac{3\phi}{4\pi} \left( \int_{V - V_p} \boldsymbol{e}^{(0)} : \boldsymbol{e}^{(0)} \, \mathrm{d}V \right. \right.$$
$$\left. \left. + \int_{V - V_p} (\boldsymbol{e} - \boldsymbol{e}^{(0)}) : (\boldsymbol{e} - \boldsymbol{e}^{(0)}) \, \mathrm{d}V + 2 \int_{V - V_p} \boldsymbol{e}^{(0)} : (\boldsymbol{e} - \boldsymbol{e}^{(0)}) \, \mathrm{d}V \right) \right], \quad (7.8)$$

where the second integral is positive definite. Applying the divergence theorem to the third integral, and noting that the first integral combines with the $O(\phi)$ contribution in the first term contribution to give the Einstein coefficient ($5\phi/2$), one obtains

$$2\mu_s \boldsymbol{E} : \boldsymbol{E} = 2\left[\left(1 + \frac{5}{2}\phi\right)\boldsymbol{E} : \boldsymbol{E} + \frac{3\phi}{4\pi}\left(\int_{V-V_p}(\boldsymbol{e} - \boldsymbol{e}^{(0)}):(\boldsymbol{e} - \boldsymbol{e}^{(0)})\,\mathrm{d}V\right.\right.$$
$$\left.\left. - \int_{S_p}(\boldsymbol{u} - \boldsymbol{u}^{(0)})\cdot(\boldsymbol{\sigma}^{(0)}\cdot\boldsymbol{n})\,\mathrm{d}S\right)\right], \quad (7.9)$$

where $\boldsymbol{\sigma}^{(0)}\cdot\boldsymbol{n}$ denotes the Stokesian surface force density. Since $(\boldsymbol{u} - \boldsymbol{u}^{(0)})$ on the surface of the particle is a rigid-body rotation and $\boldsymbol{\sigma}^{(0)}$ is a linear functional of $\boldsymbol{E}$, it is readily shown that the third integral must finally involve a contraction between symmetric $(\boldsymbol{E})$ and antisymmetric $(\boldsymbol{\epsilon})$ tensors, and is therefore identically zero. Thus, the average dissipation at finite $Re$ may be written as

$$2\mu_s \boldsymbol{E} : \boldsymbol{E} = 2\left[\left(1 + \frac{5}{2}\phi\right)\boldsymbol{E} : \boldsymbol{E} + \frac{3\phi}{4\pi}\int_{V-V_p}(\boldsymbol{e} - \boldsymbol{e}^{(0)}):(\boldsymbol{e} - \boldsymbol{e}^{(0)})\,\mathrm{d}V\right], \quad (7.10)$$

for a rigid particle suspension, clearly pointing to a shear-thickening rheology. However, the above simplistic argument does not hold for a dilute emulsion, since the difference between the Stokes velocity field and the one at finite $Re$, on the surface of a finite viscosity drop, is no longer a rigid-body rotation.

While the bulk stress calculation in this paper has primarily relied on the Fourier-transformed velocity field (the spatial structure was only examined in the region of overlap $(a \ll r \ll aRe^{-1/2})$, this being needed to derive the stresslet to $O(Re^{3/2})$), it is nevertheless of interest to further examine the disturbance velocity field due to a drop (particle) at finite $Re$, with the intent of characterizing its structure in physical space in the outer region. Such a solution would have the usual importance attached to solutions of the linearized Navier–Stokes equations in other situations. For instance, in the simpler case of a drop (particle) translating in a quiescent fluid, the solution in the outer region, obtained for small $Re$, remains relevant even for $Re \sim O(1)$ or larger in a region where the disturbance velocity field becomes small, and the linearization accurate. In the limit $Re \ll 1$, this, of course, happens for distances greater than $O(aRe^{-1})$ with $Re = aU/\nu$, $U$ being the translational velocity. However, for any $Re$ (notwithstanding a wake instability), the far-field velocity disturbance induced by a translating particle has the same source-wake structure as that contained in the small-$Re$ solution originally derived by Oseen (see Batchelor 1967). Such a structure is typical for a point source of momentum in an ambient uniform flow. One may attribute a similar significance to a solution of the linearized Navier–Stokes equations for a point force or force dipole in simple shear flow. The axisymmetry of the uniform flow problem ensures that there is no added difficulty in obtaining a solution in three dimensions, and the structure of the far-field velocity disturbance due to a translating sphere mirrors that of a translating cylinder. This may no longer be the case in simple shear flow, and one expects the dynamics of the vorticity field to be quite different in two and three dimensions. The two-dimensional problem has already been analysed by Robertson & Acrivos (1970), who examined the simple shear flow past a torque-free neutrally buoyant cylinder at small but finite $Re$. Since the ambient flow is homogeneous, the axial vorticity field in the outer region, at leading order, behaves as a passive scalar and satisfies a convection–diffusion equation. The solution in two dimensions is thus readily obtained by analogy with a passive scalar (see Bretherton 1962; Elrick 1962; Foister & Van de Ven 1980). On the other hand, the general form for the three-dimensional disturbance vorticity field in physical space, associated with a point-force dipole in simple shear flow, at finite $Re$ (a Reynolds

number in these cases may be defined using the length scale based on the magnitude of the dipole $(D/\mu\Gamma)^{1/2}$), remains unknown; the case of a point force has recently been examined by Asmolov & Feuillebois (2010). Unlike the two-dimensional case, the ambient flow now stretches and tilts the disturbance vorticity field in addition to convecting it, and the ambient vorticity is in turn stretched and tilted by the disturbance velocity field. The two-way coupling implies that the equation for the disturbance vorticity field also involves the velocity field and may be written as

$$\frac{\partial \boldsymbol{\omega}'}{\partial t} + (\boldsymbol{\Gamma} \cdot \boldsymbol{r}) \cdot \nabla \boldsymbol{\omega}' - \boldsymbol{\omega}' \cdot \boldsymbol{\Gamma}^{\dagger} = \boldsymbol{\omega}^{\infty} \cdot \nabla \boldsymbol{u}' + \nabla^2 \boldsymbol{\omega}' + (\boldsymbol{E} \cdot \nabla) \wedge \nabla \delta(\boldsymbol{x}). \qquad (7.11)$$

One may, of course, still obtain a closed equation for the vorticity alone by taking a curl of (7.11). The fundamental solution of the resulting system of equations would yield the analogue of the Green's function of a passive scalar, but now for a three-dimensional solenoidal vector field.

The aforementioned distinction between two and three dimensions for a simple shear flow has already been highlighted in the nearly inviscid limit. For instance, Lighthill (1956) analysed the inviscid translation of a sphere in a simple shear flow and showed that the bending of the vortex lines of the ambient field around the sphere into horseshoe-shaped configurations provides a natural means for the production of streamwise vorticity; the latter is an important ingredient for generating a lift on a translating particle immersed in an inviscid rotational flow (see Auton 1987; Auton, Hunt & Prud'homme 1988). The inviscid limit does retain some similarity with the vorticity dynamics in the outer region at small *Re*. However, the viscous scenario appears more complicated since the ambient simple shear flow may now be regarded as acting on the more complicated vorticity field associated with the Stokes field for a force dipole. The vorticity field in this case consists of twin families of vortex rings generated as the curves of intersection of the one-parameter family of rectangular hyperbolae $(x_1 x_2 = \text{constant})$ with a second family of elliptic cylinders $((x_1 \pm x_2)^2 + x_3^2 = \text{constant})$. In fact, the differences between two and three dimensions at small *Re*, for the flow field near a torque-free spherical particle $(r \sim O(a))$, have already been highlighted previously; a small amount of inertia was found to eliminate the region of closed streamlines that envelopes a freely rotating sphere at $Re = 0$, and the resulting spiralling streamlines have a profound effect on the rates of heat and mass transfer (see Subramanian & Koch 2006). However, the differences in the far-field behaviour, for distances of the order of the inertial screening length, remain to be elucidated.

Finally, although the significance of micro-scale inertia in rheological context has been highlighted in the Introduction, its study remains important for reasons other than their rheological relevance. There have been recent experiments, both with single spherical particles (see Bottin, Dauchot & Daviaud 1997; Bottin et al. 1998) and a dilute suspension of such particles (see Matas, Morris & Guazzelli 2008), in an attempt to understand the nature of the transition to turbulence in shearing flows and the effect of particles on the same. It is a well-known fact that the simplest shearing flows, including plane Couette flow (simple shear flow in a bounded domain) and pipe flow, transition to turbulence beyond a certain threshold value of the Reynolds number despite being linearly stable for all Reynolds numbers (see Schmid & Henningson 2001). The threshold Reynolds number values for plane Couette and pipe flows are approximately 325 and 2000, respectively (these are now the macro-scale Reynolds numbers based on the gap width and pipe diameter, respectively). The variance with the predictions of the linear-stability analysis is attributed to the subcritical nature

of the laminar–turbulent transition (Darbyshire & Mullin 1995; Dauchot & Daviaud 1995). The dynamical systems point of view of the turbulent dynamics, at least for relatively modest values of the macro-scale Reynolds number corresponding to the transitional regime, is that the turbulent state is essentially a wandering trajectory in an appropriately defined state space comprising occasional close visitations of equilibria connected by transient interludes (see Halcrow *et al.* 2009). These equilibria are exact three-dimensional solutions, either stationary or time-periodic, of the Navier–Stokes equations (Nagata 1990; Clever & Busse 1997). Despite being unstable (saddle-like), the union of such equilibria, together with the heteroclinic connections between them, forms a scaffold that helps organize a turbulent trajectory, and helps explain the dynamics in shear flows. Such unstable equilibria are captured numerically via a continuous deformation approach by first considering a modified problem with known solutions, and deforming it progressively to recover the original problem with the originally stable solutions being mapped onto the unstable solutions of interest (see Cherhabili & Ehrenstein 1995). The easiest experimental equivalent of such an approach would be a slight alteration of the geometry. For plane Couette flow, Bottin *et al.* (1997) accomplished this by the insertion of both a thin wire and a spherical bead in the central plane of the flow. The underlying idea in all the above cases, either experimental or computational, is that the modification in either the geometry or forcing serves to stabilize the otherwise unstable equilibria; a finite-amplitude perturbation then accesses the resulting non-trivial basin of attraction in the modified state. The recurring structures in almost all of the non-trivial equilibria, occurring in the transitional range, are streamwise vortices and streaks. Indeed, Bottin *et al.* (1997) found, for both the wire and the bead, the appearance of elongated streamwise vortices, organized along the spanwise coordinate, beyond a threshold value of the macro-scale Reynolds number. The disturbance due to the wire or the bead remains localized (as inferred from the length of the streamwise vortices) below this threshold. Interestingly, the threshold Reynolds number remains finite even as the radius of the wire becomes vanishingly small, suggesting that the velocity field in the outer region (characterized by the inertial screening length, $(\nu/\dot{\gamma})^{1/2}$), and therefore, independent of the wire diameter) may play an important role in the emergence of such structures. The physical mechanism involving the stabilization is likely to be either on account of a topological correspondence between the micro-scale flow in the outer region and the structure of the emerging unstable equilibrium, or perhaps, via an instability of the former. The experiments of Matas *et al.* (2003), examining the transition to turbulence in pipe flow of a dilute suspension of density matched particles, lend credence to the crucial role of micro-scale inertia in such a coupling between the particle–scale flow field. The authors found the critical macro-scale Reynolds number for a suspension to increase with an increase in $\phi$ for the smallest particles (diameter $\sim 40\,\mu$m), as one would expect in the inertialess limit when the particles enhance the effective viscosity in proportion to their volume fraction. On the other hand, the transition Reynolds number decreased with increasing $\phi$ for larger-sized particles. For small enough $\phi$, this decrease appears to be linear in $\phi$, and it is likely that each particle acts independently in facilitating the appearance of streamwise vorticity on the macro-scale, thereby promoting the onset of intermittent dynamics. The particle size at which the decrease in the transition Reynolds number first occurs corresponds to a micro-scale Reynolds number close to unity. It is of interest to note that an inertial suspension, for small values of the micro-scale Reynolds numbers, exhibits a shear-thickening rheology on the macro-scale, thereby leading to a reduced macro-scale Reynolds number. On the other hand, for values of the micro-scale

Reynolds number of order unity, when an inner region, in the usual sense (that is, a region in the vicinity of the particle where inertial forces are negligible), ceases to exist, the effect at the macro-scale mimics that of an increased macro-scale Reynolds number.

## REFERENCES

ASMOLOV, E. S. & FEUILLEBOIS, F. 2010 Far-field disturbance flow induced by a small non-neutrally buoyant sphere in a linear shear flow. *J. Fluid Mech.* **643**, 449–470.

AUTON, T. R. 1987 The lift force on a spherical body in a rotational flow. *J. Fluid Mech.* **183**, 199–218.

AUTON, T. R., HUNT, J. C. R. & PRUD'HOMME M. 1988 The force exerted on a body in inviscid unsteady non-uniform rotational flow. *J. Fluid Mech.* **197**, 241–257.

BATCHELOR, G. K. 1967 *Introduction to Fluid Dynamics*, p. 348. Cambridge University Press.

BOTTIN, S., DAUCHOT, O. & DAVIAUD, F. 1997 Intermittency in a locally forced plane Couette flow. *Phys. Rev. Lett.* **79** (22), 4377–4380.

BOTTIN, S., DAUCHOT, O., DAVIAUD, F. & MANNEVILLE, P. 1998 Experimental evidence of streamwise vortices as finite amplitude solutions in transitional plane Couette flow. *Phys. Fluids* **10** (10), 2597–2607.

BRADY, J. F. & MORRIS, J. F. 1997 Microstructure of strongly sheared suspensions and its impact on rheology and diffusion. *J. Fluid Mech.* **348**, 103–139.

BRETHERTON, F. P. 1962 Slow viscous motion round a cylinder in a simple shear. *J. Fluid Mech.* **12**, 591–613.

CHERHABILI, A. & EHRENSTEIN, U. 1995 Spatially localized two-dimensional finite amplitude states in plane Couette flow. *Eur. J. Mech.* B/*Fluids* **14**, 677–696.

CLEVER, R. & BUSSE, F. 1997 Tertiary and quaternary solutions for plane Couette flow. *J. Fluid Mech.* **344**, 137–153.

DARBYSHIRE, A. G. & MULLIN, T. 1995 Transition to turbulence in constant-mass-flux pipe flow. *J. Fluid Mech.* **289**, 83–114.

DAUCHOT, O. & DAVIAUD, F. 1995 Finite amplitude perturbation and spots growth mechanism in plane Couette flow. *Phys. Fluids* **7** (2), 335–343.

DING, E. J. & AIDUN, C. K. 2000 The dynamics and scaling law for particles suspended in shear flow with inertia. *J. Fluid Mech.* **423**, 317–344.

ELRICK, D. E. 1962 Source functions for diffusion in uniform shear flow. *Austral. J. Phys.* **15**, 283–288.

FOISTER, R. T. & VAN DE VEN, T. G. M. 1980 Diffusion of Brownian particles in shear flows. *J. Fluid Mech.* **96**, 105–132.

FRANKEL, N. A. & ACRIVOS, A. 1970 The constitutive equation for a dilute emulsion. *J. Fluid Mech.* **44**, 65–78.

GRADSHTEYN, I. S. & RYZHIK, I. M. 1965 *Table of Integrals, Series and Products.* Academic Press.

HALCROW, J., GIBSON, J. F., CVITANOVIC, P. & VISWANANTH D. 2009 Heteroclinic connections in plane Couette flow. *J. Fluid Mech.* **621**, 365–376.

HAPPEL, J. & BRENNER, H. 1973 *Low Reynolds Number Hydrodynamics.* Noordhoff.

KIM, S. & KARRILA, S. J. 1991 *Microhydrodynamics: Principles and Selected Applications.* Butterworth-Heinemann.

KOSSACK, C. A. & ACRIVOS, A. 1974 Steady simple shear flow past a circular cylinder at moderate Reynolds number: a numerical solution. *J. Fluid Mech.* **66**, 353–376.

KULKARNI, M. P. & MORRIS, J. F. 2008 Suspension properties at finite Reynolds number from simulated shear flow. *Phys. Fluids* **20**, 040602.

LEAL, L. G. 1992 *Laminar Flow and Convective Transport Processes.* Butterworth-Heinemann.

Li, X. & Sarkar, K. 2005 Effects of inertia on the rheology of a dilute emulsion of viscous drops in steady shear. *J. Rheol.* **49**, 1377–1394.

Lighthill, M. J. 1956 Drift. *J. Fluid Mech.* **1**, 31–53.

Lin, C. J., Peery, J. H. & Schowalter, W. R. 1970 Simple shear flow around a rigid sphere: inertial effects and suspension rheology. *J. Fluid Mech.* **44**, 1–17.

Mao, Z. S. & Chen, J. Y. 1997 Numerical solution of viscous flow past a solid sphere with the control volume formulation. *Chin. J. Chem. Engng* **5** (2), 105.

Matas, J. P., Morris, J. F. & Guazzelli, E. 2003 Transition to turbulence in particular pipe flow. *Phys. Rev. Lett.* **90** (1), 014501-1.

Mikulencak, D. R. & Morris, J. F. 2004 Stationary shear flow around fixed and free bodies at finite Reynolds number. *J. Fluid Mech.* **520**, 215–242.

Nagata, M. 1990 Three-dimensional finite-amplitude solutions in plane Couette flow: bifurcation from infinity. *J. Fluid Mech.* **217**, 519–527.

Proudman, I. & Pearson, J. R. A. 1957 Expansions at small Reynolds numbers for the flow past a sphere and a circular cylinder. *J. Fluid Mech.* **2**, 237–262.

Roberston, C. R. & Acrivos, A. 1970 Low-Reynolds-number shear flow past a rotating circular cylinder. Part 1. Momentum transfer. *J. Fluid Mech.* **40**, 685–703.

Ryskin, G. 1980 The extensional viscosity of a dilute suspension of spherical particles at intermediate microscale Reynolds numbers. *J. Fluid Mech.* **99**, 513–529.

Saffman, P. G. 1965 The lift on a small sphere in a slow shear flow. *J. Fluid Mech.* **22**, 385–400.

Schmid, P. J. & Henningson, D. S. 2001 *Stability and Transition in Shear Flows*. Springer.

Schowalter, W. R., Chaffey, C. E. & Brenner, H. 1968 Rheological behaviour of a dilute emulsion. *J. Colloid Interface Sci.* **26**, 152–160.

Stone, H. A., Brady, J. F. & Lovalenti, P. M. 2000 Inertial effects on the rheology of suspensions and on the motion of individual particles (unpublished).

Subramanian, G. & Koch, D. L. 2006 Inertial effects on the transfer of heat or mass from neutrally buoyant spheres in a steady linear velocity field. *Phys. Fluids* **18**, 073302.

Taylor, G. I. 1932 The viscosity of a fluid containing small drops of another fluid. *Proc. R. Soc. Lond.* A **146** (501), 41–48.

Vivek Raja, R., Subramanian, G. & Koch, D. L. 2010 Inertial effects on the rheology of a dilute emulsion. *J. Fluid Mech.* **646**, 255–296.

Wang, L. Y., Yin, X., Koch, D. L. & Cohen, C. 2009 Hydrodynamic diffusion and mass transfer across a sheared suspension of neutrally buoyant particles. *Phys. Fluids* **21**, 033303.